THE UNIVERSITY OF HULL

Simulated Marine Plastics Pollution Weathering: A Novel Laboratory System for Weathering Plastics.

being a Thesis submitted for the Degree of

Masters by Research in Environmental Science

at the University of Hull

by

Richard McCumskay, BSc

February 2021

Abstract

Over the last three years there has been a call for more environmentally relevant laboratory weathering experiments. These experiments would require well-defined reaction conditions and standardised reporting of both the rate of degradation and methods used. Several new designs have been proposed, however, no design has yet been developed that meets these requirements. This thesis critically reviews the current plastic weathering methodologies and presents a novel method that produces well-defined conditions, omitted by other works. The method presented here aims to implement irradiance of ultraviolet radiation (UVR), temperature and saltwater parameters in a standardised way, as the three most influential variables of marine plastic weathering. In doing so, the practice of reporting single irradiance values is questioned due to its shortfall when comparing studies. The performance of the proposed method was assessed by weathering five plastics for 18 days before the experiment was stopped due to the Covid-19 Pandemic. The degradation of the plastics was measured using a trio of FTIR interfaces (ATR, Diffuse and Specular). A novel introduction of saltwater to the plastic samples provides stable simulated marine conditions to replicate marine weathering. The weathering characteristics from this method were found to be similar to those reported in outdoor weathering studies, showing that the laboratory method presented here is able to simulate environmental weathering. Despite promising results, the performance of the system could still be improved. The ultraviolet irradiance spectrum produced by the weather-o-meter, failed to match solar irradiance over the UVR range from 310 nm – 350 nm, despite having an overall irradiance which matched solar levels. Given the wavelength specific nature of plastic degradation, future work should aim to report the spectrum used, alongside the total irradiance.

Acknowledgments

This work was supported through the Energy and Environment Institute (EEI) at the University of Hull. Thanks, are given to my supervisors Professor Mike Rogerson [a]; Dr. Rodney Forster [b]; Dr. Cath Waller [b] and colleagues in the Plastic in the Environment Research Group (PERG) within the EEI. Agilent Technologies and Ocean Insights are also acknowledged for their help and support with equipment needs during the research. Special thanks are also given to Dr. Alex Iles [b] and Nigel parkin [b] who crafted the plastics samples used in this work in the Chemistry workshop at the University of Hull. Finally, my partner Marek Slánička deserves thanks for his support and patience throughout the write-up period of this thesis.

[a] University of Northumbria, 2 Sandyford Rd, Newcastle upon Tyne, UK. NE1 8QH.

[b] University of Hull, Cottingham Rd, Hull, UK. HU6 7R

Table of Contents

1. Literature Review

1.1 The plastic problem

It is now widely accepted that plastic fragments are ubiquitous in both terrestrial (Wong *et al.*, 2020; Wang *et al.*, 2020) and marine environments as waste (Hahladakis, 2020; Mohamed Nor & Obbard, 2014; Pelegrini *et al.*, 2019). Over 62% of all waste in the oceans is plastic (Hahladakis, 2020), with an estimated 20 million tons of additional plastic entering marine environments every year (Urbanek, Rymowicz & Mirończuk, 2018). Attempts to start to remove the plastic waste from the environment are underway in the Great Pacific Garbage Patch (GPGP) (Morrison *et al.*, 2019), which is reported to contain and estimated average of 79 thousand tons of plastic waste, ranging from 45 – 129 (Lebreton *et al.*, 2018). The main constituents of marine plastic waste in the GPGP are: High density Polyethylene (HDPE) and Polypropylene (PP) (Pelegrini *et al.*, 2019), both of which have a specific gravity less than that of saltwater. This means that they are found as floating objects (i.e. neustonic). These plastics have also been shown to stay afloat even after environmental weathering (Zhu *et al.*, 2020; Enders *et al.*, 2015). Several other polymer species can also be found in the marine environment in high quantities; Polystyrene (PS), Polyethylene terephthalate (PET) and Polyvinyl-Chloride (PVC) also enter the environment, however, they settle in the sediments due to their higher densities with respect to saltwater (Hahladakis, 2020). Polyamide (PA, Nylon) has also been reported in high amounts due to its extensive use in fishing nets and ropes, washing up on shorelines (Xu *et al.*, 2020; Welden & Cowie, 2017). These plastics are known to affect a wide array of marine organisms, with the list getting longer every year as more studies are done (Markic *et al.*, 2020; Franco *et al.*, 2019; Moore, 2008), with publications being published on the topic since the 1970's (Carpenter *et al.*, 1972).

1.2 Current research

The effect of plastic on the environment is as much a concern for researchers globally today, as it was in the 1970's (Carpenter & Smith, 1972; Wong, Green & Cretney, 1974). Even recently, Jahnke *et al.* (2017) highlighted that the number 1 research priority regarding plastic waste research was, '*to improve our understanding of the multiple biotic and abiotic factors influencing the weathering process*', showing that much more research on the topic is required. Weathering and/or ageing of a material is the process of physical and chemical change over time, caused due to the exposure to environmental stressors. In the case of plastic weathering, ultraviolet radiation (UVR), temperature, salinity, oxygen availability, mechanical stress, biofilm formation and digestion all constitute weathering processes that can change the chemical and physical properties. Weathering is a complex process, and to understand it, the individual processes caused by each environmental factor must be understood. There is already excellent knowledge of the basic weathering processes from industrial engineering and materials chemistry research. These industrial research questions focus on how polymers oxidise, shorten and simplify under idealised and accelerated conditions in the laboratory or in the built environment. These experiments often study how to either prolong or shorten the service life of the polymer for consumer goods. However, current research is challenged to apply this knowledge and novel approaches to constrain weathering experiments to environmentally relevant conditions in terrestrial, estuarine and marine systems. Here, conditions are more complex, more variable and less likely to remain constant through the lifetime of a plastic object. Recent research emphasises a pressing need for environmentally relevant experiments (Chamas *et al.*, 2020; Liu *et al.*, 2020; Biber, Foggo & Thompson, 2019; Tian *et al.*, 2019; Andrade *et al.*, 2019), which looks at evaluating the relevance of each single environmental process and parameter (Zhu *et al.*, 2020; Potthoff *et al.*, 2017). An example being that researchers must match the environmental levels of solar radiation (Cai *et al.*, 2018)

and by using daylight pass filters on the light sources (Ward *et al.*, 2019; Gijsman, Meijers & Vitarelli, 1999), rather than exposing plastics to high doses of UVC that would not be present in the environment (Hebner & Maurer-Jones, 2020). Liu, Mandelis & Huan (2018) highlights deficiencies in the metrics and the experimental conditions used in plastics degradation research, calling for a more standardised approach to plastics degradation and weathering research. Environmental parameters need to be matched to those naturally found in the target environment for comparisons between laboratory experiments and naturally weathered plastics to be at all possible. Differences in the weathering methods have been shown to cause different pathways of degradation in LDPE over a 4 month period by Hirsch *et al.* (2017) between accelerated laboratory weathering and natural weathering conditions. Differences in the two treatments, namely, differences in UVR, temperature and humidity are likely causes for the differences seen in the weathered plastics. The ability to reproduce a solar spectrum in the laboratory is a known challenge, summarised by, highlighting the few options of either specific fluorescent tubes or metal halides.

1.2.1 Ultraviolet Radiation

Ultraviolet radiation (UVR) is defined as the portion of the electromagnetic spectrum between 100 nanometres (nm) and 400 nm. UVR is classified by wavelength into three regions by the ISO standard ISO-21348 (information is provided courtesy of Space Environment Technologies): UVA, Ultraviolet radiation in the range 320nm to 400nm, UVB, 280nm to 320nm and UVC, 100nm to 280nm. Highly energetic UVC photons are extremely deleterious to organic compounds, however environmental levels are almost zero as these wavelengths do not reach the earth's surface due to absorption in the atmosphere by ozone. Ultraviolet Radiation (UVR) is known to be the main cause of weathering, causing oxidation of plastics in the environment, termed photo-oxidative degradation (Arias Villamizar & Vázquez Morillas, 2018; Gewert, Plassmann & MacLeod, 2015). UVB has been shown to be the main UVR region

to cause photo-oxidative degradation (Andrady, 2011; Ktimpf, Sommer & Zirngiebl, 1990). It has been shown that the absorption of UVR is wavelength dependent by Vaskuri *et al.* (2017), producing an action spectra for polystyrene. An action spectra illustrates the relative effectiveness of a wavelength to excite and change chemical bonds within a material. It is therefore important to select relevant wavelengths used to study the weathering of plastics. The choice of lamp used in the studies can often be questionable when attempting to relate weathering to the environment, especially when rigs have been custom designed (Gewert *et al.*, 2018). Both the presence of UVC and the irradiance levels needs to be environmentally relevant. The development of new techniques must therefore be scrutinised to prevent errors being carried out by other scientists following new methodologies (Rummel *et al.*, 2019).

Baker & Smith (1982) and Calkins (1982) showed that UVR is not only limited to surface waters and can penetrate below the ocean surface with Fleischmann (1989) quantifying the UVR penetration in measurable quantities to a depth of 25 meters below the water surface. The attenuation of light in water is a function of scattering and absorption. Quantum flux was shown to fall as a reciprocal power function of depth (Fleischmann, 1989). Badji *et al.* (2018) also suggests that the increased refractive index of saltwater reduces the utilisation rate of UVR by plastic in comparison to ultrapure water. The influence of UVR is therefore mainly limited to surface waters of coastal regions in which light attenuation is strongest due to suspended particulates and plankton causing decrease water clarity but may penetrate further in clearer offshore waters. UVR at the wavelength of 310 nm has been shown to decrease to 10% of that the surface irradiance in as little as 50 cm of water, but has also been seen reaching 10% at 4.4 meters in the German bight (Franklin & Forster, 1997). This highlights the importance of particulates in the water that can limit penetration of light. A reduction to 10% irradiance has been seen as deep as 12.8 meters in the middle of the gulf of Mexico using the same 310 nm wavelength (Franklin & Forster, 1997).

1.2.2 Temperature

Temperature has been found to be the second most important factor in the weathering of plastics, both in the environment (Rajakumar *et al.,* 2009) and in the lab. The world ocean maintains a relatively constant temperature, with a global average of 16.1±℃. Consequently, the effects of thermal degradation will be negligible in the environment as the temperatures required to initiate the thermal degradation in common plastic waste, such as HDPE, PP, PS, PA and PET, are much higher (Singh *et al.*, 2020; Min, Cuiffi & Mathers, 2020; Shen *et al.*, 2019). Temperature therefore plays a role in controlling chemical and biological rates of reaction involved in weathering as shown by Satoto *et al.* (1997). In the marine environment, saltwater is known to cool plastic (Biber, Foggo & Thompson, 2019; Kalogerakis *et al.*, 2017; Leonas, 1993). Weathering, as seen by the production of carbonyl groups, also seemed to be correlated with the variation of temperature rather than directly by solar radiation alone in dry treatments (Satoto *et al.*, 1997). This has also been shown by using Principal Component Analysis (PCA) with five degradation characteristics by Lv *et al.*, (2017). It has been approximated that photochemical oxidation in PS increased by 25% for every 10℃ increase in water temperature (Ward *et al.*, 2019). In the marine environment the presence of water is therefore a key factor affecting the rate of photochemical degradation. Due to its high heat capacity, water has to absorb 4,184 Joules of heat energy for the temperature of one kilogram of water to increase 1°C. Coupled with the high density of water, this means that saltwater has a fast thermal diffusivity. Thermal diffusivity is a measure of how quickly a material can absorb heat from its surroundings, i.e. from plastic floating in the water. Thus, the plastic remains much cooler in water than in air because any heat diffuses from the plastic into the water very quickly.

1.2.3 Water

Within the marine environment, the presence of water determines the temperature, salinity and density, oxygen availability and the irradiance any plastic waste will receive. The presence of water can also lead to hydrolysis of certain plastics, however, this mechanism of degradation is very slow in comparison to photo-oxidative degradation (Chamas *et al.*, 2020). The importance of water to degrade plastics has been shown by Tian *et al.* (2019), with saltwater having a greater effect of the breakdown of plastics than freshwater (Arias Villamizar & Vázquez Morillas, 2018). The cooling effect of water during weathering experiments has been shown to reduce photodegradation (Ward *et al.*, 2019; Kalogerakis *et al.*, 2017; Leonas, 1993; Pegram & Andrady, 1989). On the other hand, the mechanical stress caused by water, such as wave and tide action, has been shown to cause significant degradation of plastics in the ocean. Mechanical degradation is known to lead to the formation of both microplastics (Hebner & Maurer-Jones, 2020; Chen *et al.*, 2019; Biber, Foggo & Thompson, 2019; Julienne, Delorme & Lagarde, 2019) and nano plastics (Tian *et al.*, 2019; Shen *et al.*, 2019). This process is usually amplified by the reduction in tensile strength and brittleness caused by photodegradation (Biber, Foggo & Thompson, 2019; Arias Villamizar & Vázquez Morillas, 2018; Biesinger, Corcoran & Walzak, 2011).

1.2.4 Salinity and Oxygen

At the surface of the ocean, where neustonic plastics accumulate, the availability of oxygen and salts, coupled with the UVR from solar radiation leads to potentially perfect conditions for photo-oxidative degradation. Most grades of plastics are unsaturated polymer chains. Carbonyl compounds form as a result of the thermo-mechanical degradation that the polymer experiences during processing (Valadez-Gonzalez, Cervantes-Uc & Veleva, 1999). It is also known that plastics can adsorb metal ions from salt water (Wang *et al.*, 2019, 2018; Brennecke *et al.*, 2016; Biesinger, Corcoran & Walzak, 2011) The UV energy is then absorbed by the carbonyl compounds and metal complexes (releasing the metal ions), which then act as oxidation catalysts helping to break the polymer chains. However it has been observed that the photodegradation of PVC and the release of organotin compounds (OTCs) were both inhibited in high salinity conditions, probably due to the enhanced re-adsorption of OTCs on PVC microplastics and the formation of halogen radicals that were less reactive toward neutral OTCs (Chen *et al.*, 2019). When studying the degradation of neustonic plastic waste in the ocean, it is clear that the presence of saltwater represents an environmentally relevant variable that affects photodegradation.

Zhu *et al.* (2020) used natural seawater that was pre-treated by sterilising the water with UVC and gravity filtering it before use. This highlights a novel way of controlling contaminants while maintaining natural saltwater parameters in weathering experiments. Many researchers have also employed multiple methods to incorporate saltwater into the experimental design. Natural saltwater has been used in several degradation studies (Chamas *et al.*, 2020; Welden & Cowie, 2017; Kalogerakis *et al.*, 2017), including taking plastic samples that have been naturally weathered straight from the environment (ter Halle *et al.*, 2017; Ioakeimidis *et al.*, 2016), with other publications using Artificial Seawater (Ward *et al.*, 2019; Rummel *et al.*, 2019; Andrade *et al.*, 2019; Gewert *et al.*, 2018). Some plastic degradation experiments have

also shown increased degradation in the saltwater environment due to oxidation catalysts (auto oxidising metal salts) in the saltwater (Leonas, 1993). However, plastic weathered in saltwater has also been shown to have reduced photodegradation (Tian *et al.*, 2019; Biesinger, Corcoran & Walzak, 2011; Andrady, 2011; Pegram & Andrady, 1989).

The presence of saltwater in weathering experiments also affects the oxygen availability of the samples. It has been shown that the rate of production of carbonyl groups, a product of thermo-oxidative and photo-oxidative degradation, in PP plastic increases with increased oxygen pressure by Richaud *et al.* (2006). It has been suggested by Andrady (2011) that the relatively low oxygen availability in saltwater and low temperatures in the oceans retard photo-oxidative degradation. Oxygen concentrations at depth have also been suggested to be a limiting factor in the photo-oxidative degradation pathway by Gewert, Plassmann & MacLeod (2015). Well-oxygenated surface water only contains around 8 mg O_2/l, while the air contains 210 mg O_2/l which is only 3.8% of that in air (Fondriest Environmental, Inc., 2013). This is balanced by the influence of mechanical stress such as wave action and collision with other objects, with fracturing and fragmentation increasing total surface area, impeding 'armouring' of surfaces by oxidised residues and increasing the ability of oxygen to penetrate into the material of the plastic object, increase surface area to volume ratio (Hebner & Maurer-Jones, 2020; Biber, Foggo & Thompson, 2019; Julienne, Delorme & Lagarde, 2019). Indeed, plastics exposed for longer periods of time on beaches where the temperature, oxygen availability and UV exposure are all much higher, and mechanical stress is at its greatest, show strongly increased degradation (Pelegrini *et al.*, 2019; Kalogerakis *et al.*, 2017; Biesinger, Corcoran & Walzak, 2011; Corcoran, Biesinger & Grifi, 2009). Given that the presence of saltwater can both increase plastic degradation through sorption of salts and mechanical stress and decrease polymer degradation through cooling the plastics and limiting oxygen, environmentally analogous salinities, temperatures, depths and exposures should be used in weathering studies.

1.2.5 Biotic degradation

It is a known issue that when designing experiments that weather plastics in the marine environment, bacterial and biotic degradation will occur. Arias Villamizar & Vázquez Morillas (2018) found that biofilm formation was higher for plastics exposed in the marine environment, where crustaceans, algae, and other species were observed. Plastics degrading in the surface waters have been shown to develop larger microbial communities than those found at deeper levels (Tu *et al.*, 2020). Bacterial community structure also changes with time, rather than a colonisation followed by growth of the initial bacteria, the species of bacteria present changes as the biofilm community matures (Tu *et al.*, 2020). The community of microorganisms which colonise on plastic has been termed the 'Plastisphere' (Erni-Cassola *et al.*, 2020), being coined in 2011 and published in 2013 by Zettler *et al.* (2011) and Zettler, Mincer & Amaral-Zettler (2013), respectively. This plastisphere is known to exert mechanical, chemical and enzymatic stress, eroding the surface, increasing the degradation of the plastics (Sangeetha Devi *et al.*, 2015; Shah *et al.*, 2008; Gu, 2003). Microorganisms such as bacteria excrete extracellular enzymes. These enzymes attach to the polymeric surfaces of the plastic and cleave the polymer chains. Water soluble intermediates are then produced during this depolymerization and are assimilated into the bacterial cell for use as a carbon source in aerobic conditions (Shah *et al.*, 2008). After a biofilm has had time to degrade the polymer, the end state is a mineralised polymer surface. This mineralised surface will respond to UVR differently than a virgin polymer surface (Chamas *et al.*, 2020; Albertsson & Karlsson, 1990). However, research looking at this bio-mineralised plastic degradation is in its infancy. Microorganisms, through the process of bioerosion, may be removing degraded layers of the polymer caused by photooxidation. Pelegrini *et al.* (2019) observed a reduction of the carbonyl index (CI) measurements from the surface of some samples. The formation and presence of a biofilm layer can however reduce the photodegradation of the plastic by acting as a protective layer against

UVR (Tu *et al.*, 2020; Yin *et al.*, 2019; Arias Villamizar & Vázquez Morillas, 2018). It is for this reason that the control of bacteria within weathering experiments is important when looking at the effects of photodegradation in the marine environment. Researchers have added UVC sterilisation to saltwater before experimentation to prevent sample contamination by biofilms and organic contaminants (Zhu *et al.*, 2020). Biotic degradation is not only bacteria. It has also been shown that some species of green algae can produce enzymes that break down plastics. Kim *et al.* (2020) showed that *Chlamydomonas reinhardtii,* a freshwater species of microalgae, can produce PETase for the enzymatic-degradation of polyethylene terephthalate. After only 4 weeks, terephthalic acid (TPA), the fully degraded form of PET, was detected by high performance liquid chromatography analysis (HPLC-MS). Dents and holes on the surface could also be seen with scanning electron microscopy (SEM) much like those made by bacteria. The *Chlamydomonas reinhardtii* was however genetically modified in this experiment to produce PETase and so environmental occurrence of PETase production is unlikely. It has been observed that Polyamide (Nylon) 4 bio-degraded in seawater by protobacteria that belong to the family *Alteromonadaceae* without genetic modification of the bacteria (Yamano *et al.*, 2019). In both environmental and laboratory experiments, degradation occurs, as measured by net weight loss and biochemical oxygen demand. The availability of microorganisms within the water determined the rate of degradation as locations with fewer microorganisms degraded the plastics at a slower rate (Yamano *et al.*, 2019). Some plastics, during photodegradation can release co-leachates into the environment during weathering which have been observed to inhibit microbial growth (Zhu *et al.*, 2020). Short-oxidized chains generated from photooxidative weathering has been hypothesised as an immediate food source for newly colonising bacteria, however once these intermediates have been assimilated, the viability of the plastic as a carbon source decreases and bacterial colony size decreases after as short a period as 2 days (Erni-Cassola *et al.*, 2020). As described above, this bacterial layer might now

protect the plastic from further photooxidative weathering which would release more short-oxidized chains, causing the plastisphere colony to be short lived. As bacterial biofilms and other biotic degradation can alter the degradation pathways of plastics, control of biodegradation effects (e.g. removing the variable) needs to be undertaken to understand the effect of photodegradation in the marine environment alone.

1.3 Weathering Studies

1.3.1 Industrial / Polymer material Science

Experimentation on plastics has been extensively conducted for industrial plastics to either extend their lifespan or to improve the understanding of their breakdown rates (Table 1). Tests have been done to assess how the plastic performs when additives are introduced to the plastic matrix to prevent photodegradation (Chen *et al.*, 2020; Peng *et al.*, 2020; Ahmed, 2016) or to increase the degradation through the addition of photocatalysts to increase degradation rates (Liu *et al.*, 2012; Shang, Chai & Zhu, 2003; Ho & Pometto III, 1999). Many weathering experiments also look at material coating, many of which will enter the marine environment (Lankone *et al.*, 2020; Caron *et al.*, 2018).

Industrial experiments usually focus on the early stages of degradation, corresponding to the lifespan of the product and negate the effect of saltwater weathering entirely (Fiorio *et al.*, 2020; Al-Salem *et al.*, 2019; Manfredi, Barberis & Marengo, 2017; Ahmed, 2016; Arrieta *et al.*, 2013; Gulmine *et al.*, 2003). Most of these products do not come into contact with saltwater until the end of their service life, e.g. after being disposed of. Therefore, industrial weathering research with marine conditions are rarely assessed, with only a few examples to the contrary (Patti & Acierno, 2019). As can be seen in Table 1, most of the industrial weathering research is conducted in dry conditions. This makes drawing any similarities with environmental plastic and industrially weathered plastics unfeasible, despite the wealth of

findings from these experiments. Also accelerated weathering in industrial weathering experiments often involves the use of UVC to exaggerate the photodegradation (Matsui *et al.*, 2016; Liu *et al.*, 2012; Waldman & De Paoli, 2008; Shang, Chai & Zhu, 2003). In the same effort, temperature is also increased to accelerate weathering, with experiments usually being carried out at 50 - 60 ℃. Due to the accelerated nature of these experiments, most are over a relatively short amount of time, usually lasting no longer than 3 months (≲2232 hours). Due to the nature of the industry, higher radiation intensities, temperatures and humidity achieve rapid degradation in a conveniently short time frame (Philip & Al-Azzawi, 2018). Experiments that utilised UVC have been conducted within 30 hours (Waldman & De Paoli, 2008).

Almost all of the industrial experiments highlighted in Table 1 used FTIR to measure the chemical bond changes during weathering, and due to the large size of the plastics being tested the measurements using FTIR can be made quickly and reliably (Käppler *et al.*, 2016). In order to look at the fate of plastics in the environment, there has been a recent call for more environmentally relevant weathering studies (Chamas *et al.*, 2020; Liu *et al.*, 2020; Biber, Foggo & Thompson, 2019; Andrade *et al.*, 2019).

Table 1: A selection of studies that illustrate the utilisation of commercially available weather-o-meters to provide the source of ultraviolet radiation and industrial plastic degradation experiments for material science studies.

Industrial							
Polymer	Form	Treatment	Irradiance	Temp °C	Duration	Measurement	Reference
LDPE	Custom	Air	Sunlight	-	-	Tensile strength (TS), Cure Characteristics and Equilibrium Swelling	Ahmed, 2016
LDPE and polyolefins	Film	Air and Freshwater	QUA UVA-340	50 - 60	5.5 - 15 days	FTIR-ATR, Scanning electron microscopy (SEM), Differential scanning calorimetry (DSC) and Thermo gravimetric analysis (TGA)	Al-Salem *et al.*, 2019
PET and PP-66	Fibre	Air	Sunlight	-	6 months	FTIR-ATR, TS, X-ray diffraction, (XRD) and (DSC)	Arrieta *et al.*, 2013
PU	Coatings	Air	QUA UVA-340	55	28 days	Scratch Test	Chang *et al.*, 2018
PET	Fibre	Air and Freshwater	Xeon Arc Lamp	18 - 31.5	300 hours	FTIR-ATR, TS, XRD, DSC, UV–Visible Spectrophotometry, Viscometery and Optical Birefringence	Fashandi, Zadhoush & Haghighat, 2008
ABS	Custom	Air	QUA UVA-340	50	360 hours	FTIR-ATR, SEM, TS, Colorimetric and Thermal-oxidative Resistance	Fiorio *et al.*, 2020
HDPE and LDPE	Custom	Air	Xeon Lamp	50 - 60	1600 hours	FTIR-ATR, SEM, Density, Hardness and DSC	Gulmine *et al.*, 2003
Cu-Phthalo cyanine	Coatings	Air	Xeon Lamp	90	3 months	FTIR-ATR, Nano release protocol, Colour and gloss measurements, Laser scanning confocal microscopy (LSCM) and Inductively coupled plasma mass spectrometry (ICP-MS)	Lankone *et al.*, 2020
HDPE	Film	Air	254 nm & > 365 nm Ultra-violet Lamps	25	300 hours	FTIR-ATR, Raman, XPS, PSA, XRD and Nitrogen Isothermal Adsorption	Liu *et al.*, 2012
PP and PC	Custom	Air	Xeon Lamp	35	800 hours	FTIR-ATR	Manfredi, Barberis & Marengo, 2017

PS (HIPS)	Film	Air	Xe-Hg Lamp (280 - 450 nm)	60	12 hours	Thermal Evolved Gas Analyzer / Mass Spectrometer (EGA-MS)	Matsui *et al.*, 2016
PET and PU	Custom, Fibre	Air	UV Bulb Lamp (300 - 600 nm)	35	8 days	FTIR-ATR, SEM and Puncture Strength.	Patti & Acierno, 2019
PP and Wood flour	Custom	Air and Freshwater	QUA UVA-340	50 - 60	960 hours	FTIR-ATR, SEM, TS, Surface Colour and Unnotched Impact Tests, Water Absorption Properties	Peng *et al.*, 2020
PS	Film	Air	8w Ultraviolet Lamps y=254	24.85	-	FTIR-ATR, SEM, XPS and GPC	Shang, Chai & Zhu, 2003
HDPE	Pellet	Air and Freshwater	Xeon Lamp	-	2000 hours	FTIR-ATR, SEM and TS	Stark & Matuana, 2004
LDPE	Film	Air	Xeon lamp	56	100 hours	FTIR-ATR, SEM and TS	Tuasikal *et al.*, 2014
LDPE	Film	Air	Sunlight	25 - 45	90 days	FTIR-ATR, SEM and TS	Tuasikal *et al.*, 2014
HDPE	Film	Air	QUA UVA-313	50 - 60	1333 hours	FTIR-ATR, DSC, Molecular Weight	Valadez-Gonzalez, Cervantes-Uc & Veleva, 1999
PP and PS	Fibre	Air	UVC, 15 W High-borax ultraviolet TUV 15 W/G15 T8 light	-	110 mins - 1800 mins	FTIR-ATR and SEM	Waldman & De Paoli, 2008

1.3.2 Outdoor weathering

To generate more environmentally relevant data on the degradation of polymers within the environment, many researchers have turned to natural weathering, using the sun as the light source and placing the plastics into the environment. Outdoor weathering experiments are usually much longer experiments than those conducted in the laboratory, however they can be inexpensive in comparison to laboratory based experiments (Capanescu & Cincu, 2003). Outdoor experiments usually have a minimum exposure time of 3 months and examples can be found weathering for as long as 4 - 22 years (Satoto *et al.*, 1997; Ioakeimidis *et al.*, 2016). The advantages of outdoor weathering experiments is that they provide the most realistic conditions in real time (Philip & Al-Azzawi, 2018). The UVR energy levels, temperature, salinity, mechanical stress and biotic interactions will all be regulated by the environment. Weathering data generated in this fashion can accurately assess the fate of plastics within the given environment. However, to independently assess the impact that each variable is having, can be difficult, as each covariate affects the others. To make sense of the weathering experiments in the outdoor environment, two or more experimental treatments are often compared to keep all but one variable different, i.e. with and without solar radiation. (Biber, Foggo & Thompson, 2019; Philip & Al-Azzawi, 2018; Brandon, Goldstein & Ohman, 2016). Table 2 highlights papers that have implemented outdoor weathering, highlighting the key methodology parameters.

Although outdoor weathering provides realistic weathering, Arias Villamizar & Vázquez Morillas (2018) first subjected the samples to artificial weathering for 96 hours, using eight xenon arc lamps to induce degradation before weathering in the environment for a minimum of 150 days. The result showed that fragmentation occurred after 30 days in the air, while only after 120 and 180 day in the marine and freshwater environments, respectively.

These samples were reported to be weathered by UV radiation, salinity, turbulence, previous weathering, as well as by biofilms in the aquatic environments.

Table 2: A selection of studies that illustrate the utilisation of the sun to provide the source of ultraviolet radiation during plastic degradation experiments.

Outdoors						
Polymer	Form	Treatment	Temp °C	Duration	Measurement	Reference
HDPE	Film	Freshwater, Saltwater	30 - 35 26 - 34	150 - 180 days	FTIR-ATR, Tensile strength (TS)	Arias Villamizar & Vázquez Morillas, 2018
PP	Custom	Air, Freshwater	44743	1 year	FTIR-ATR, TS, DSC Spectro-colorimetry, Spectro-photo-goniometry and Confocal rugosimetric measurement	Badji *et al.*, 2018
PET, HDPE and PS	Film	Air, Saltwater	11.8	600 days	FTIR-ATR	Biber, Foggo & Thompson, 2019
HDPE	Pellet	Saltwater, Other			FTIR-ATR, Time-of-Flight Secondary Ion Mass Spectrometry (TOF-SIMS)	Biesinger, Corcoran & Walzak, 2011
PET, HDPE, PVC, LDPE, PP and PS	Pellet	Air, Saltwater		36 months	FTIR-ATR	Brandon, Goldstein & Ohman, 2016
HDPE	Custom	Saltwater	22 +- 1	21 days	FTIR-ATR	Bråte *et al.*, 2018
LDPE	Film	Air		600 hours	FTIR-ATR, DSC	Hirsch *et al.*, 2017
PET	Custom	Saltwater		6 years - 22 years	FTIR-ATR	Ioakeimidis *et al.*, 2016
HDPE	Film	Air, Freshwater, Saltwater, Other		6 months	FTIR-ATR, TS, Molecular Weight (Melt Index) and Image Analysis	Kalogerakis *et al.*, 2017
PP	Custom	Air	15 - 32	18 months	FTIR-ATR	Lv *et al.*, 2017
HDPE and PP	Custom	Saltwater			FTIR-ATR, SEM	Pelegrini *et al.*, 2019
LDPE, PP and Rubber	Film and Custom	Air, Saltwater	4.4 - 30.5, -7.9 - 37.7	12 months	TS	Pegram & Andrady, 1989
PET	Custom	Air, Freshwater	33	13000 hours	Impact Strength, Gloss and Colour	Philip & Al-Azzawi, 2018
PP	Film	Air, Freshwater	Average >27.5	50 - 80 days	FTIR-ATR, SEM and TS	Rajakumar *et al.*, 2009
PS	Custom	Air, Freshwater, saltwater	4 - 34	14 days / 180 days	LC-MS and Custom Quantitative Extraction of Leachates	Rani *et al.*, 2017
HDPE	Film	Air		4 years	FTIR-ATR	Satoto *et al.*, 1997
HDPE, PP and PA	Fibre	Saltwater	5.7 - 17.9	12 months	TS, Chlorophyll Extraction and weight of Attached Biomass.	Welden & Cowie, 2017

Comparison between outdoor weathering and laboratory experiments were conducted by Badji *et al.* (2018) and Philip & Al-Azzawi (2018). Samples in the outdoor weathering were fixed to south facing racks at an angle of 45° degrees. Laboratory weathering implemented the QUV-340 lamps and spray apparatus to simulate rain. Natural weathering shows similarities with artificial weathering in the lab, however, a direct comparison is not an accurate representation of one another (Badji *et al.*, 2018). It was found that the degradation caused by 25 days of artificial weathering was the equivalent of 1 year of outdoor weathering (Philip & Al-Azzawi, 2018). It should be noted that there was considerable difference in the temperature between the two treatments, with the artificial laboratory experiment being carried out at 50°C in comparison to 11.8℃ in the outdoor weathering by Badji *et al.* (2018) and 40 - 60℃ in comparison to -1 - 32℃ by Philip & Al-Azzawi (2018). The finding highlighted that artificial weathering degraded the plastics more than outdoor exposure. Comparison made between outdoor and laboratory weathering have also been conducted by Hirsch *et al.* (2017). They found that the Norrish-I mechanism of degradation was more dominant than the Norish-II in the laboratory weathering, using the same QUV-340 lamps as Badji *et al.* (2018), whereas the opposite was seen for outdoor weathering in sunlight. However, it must be highlighted that there was the same temperature disparity seen between the outdoor and laboratory experiment, with the laboratory experiment being conducted at 60℃. Badji *et al.* (2018) also highlighted when samples were subjected to the same cumulative UVR energy, in each treatment (laboratory and outdoor weathering), weathering occurred faster in the laboratory treatment. Therefore, the assumed reciprocity law, which states 'that if the same energy is given in each experiment, the resulting change should be the same', did not hold true. This has also been observed by other authors (Yang *et al.*, 2017). Biber, Foggo & Thompson (2019) subjected plastic films in the ocean at 1m depth and found that the saltwater cooled the plastic, shielded it for UVR and limited the oxygen availability for photooxidative degradation. A simple rig

design to hold strips of plastic film, held together by wooden beams, was a low-cost design which yielded informative results when compared to a control and air treatment. Polystyrene showed the most rapid rate of degradation.

Several studies have been conducted by sampling plastic waste from the environment. Pelegrini *et al.* (2019) sampled PE and PP samples from the GPGP and found that the plastics were still identifiable and different pathways of degradation had occurred between the two plastic types after marine outdoor weathering. Ioakeimidis *et al.* (2016) used PET bottles that were collected from commercial fishing trawls to assess the environmental weathering of the PET bottles. This experiment generated data based on the sell by date of the plastic bottles rather than setting up a temporal experiment. In applying this approach, they were able to get data from bottles that were 22 years old, something that would otherwise be unachievable if starting from scratch. By using FTIR-ATR and SEM they found that the PET bottles remain unchanged for 15 years, supporting Pelegrini *et al.* (2019) observations. This is due to the presence of saltwater significantly reducing the rate of degradation (Pegram & Andrady, 1989). After this time, there is a significant decrease in the, native functional groups with some even disappearing, or the formation of new functional groups that are not typical for PETs (Ioakeimidis *et al.*, 2016). PET has a specific gravity of 1.34 and so the plastic bottles would have likely spent most of their time on the bottom of the sea. However, the exact life history of the plastic bottle isn't known and so the pathways of degradation can only be suggested. By comparing the spectra of known plastics articles, such as unused LEGO™ to weathered counterparts from the environment by (Turner, Arnold & Williams, 2020), the degradation patterns can be recorded in much the same way.

As the environment subjects the plastics to multiple degradation factors simultaneously, some researchers have attempted to control or limit the variables at play while still subjecting the plastic to solar radiation in outdoor, laboratory style experiments. Exposure in experimental

tanks removed the accumulation of soil and debris on the samples while continuing to provide clear, biologically active sea water (Pegram & Andrady, 1989). Enclosed systems have also been implemented outdoors to look at leachates produced during weathering by exposing tanks filled with saltwater under solar radiation (Rani *et al.*, 2017). It was found that hazardous hexabromocyclododecanes (HBCDDs) were released from expanded polystyrene used in aquaculture (Rani *et al.*, 2017). Kalogerakis *et al.* (2017) weathered plastic bags (films) in artificial beach and surface seawater treatments under natural solar radiation. This allowed for control of the experimental parameters while subjecting the plastic to natural solar radiation levels. Accurate temperature and luminance exposure (lux*d) was logged throughout. They found that after 5 months and luminance exposure of 5500000 of exposure, the plastic films showed the onset of fragmentation after applying mild stress. At 6 months and 7500000 luminance exposure the film has fragmented into almost invisible microplastics after the same mild stress. By utilising solar radiation and logging the luminance throughout, Kalogerakis *et al.* (2017) reports the degradation rate and lifetime prediction of plastic in the marine environment based on energy and time. Similar lifetime predictions have been made by Lv *et al.* (2017) on plastic weather outdoors in China. A Principal component analysis (PCA) was used to establish an integral ageing degree (IAD) based on 5 degradation characteristics. These samples were again mounted to rigs at an angle of 45° degrees and south facing in air. From this data it was found that temperature was the most dominant weathering factor during outdoor weathering of the isotactic polypropylene (iPP) under study (Lv *et al.*, 2017). The constantly changing environmental conditions pose a huge reproducibility challenge and so this method of weathering can be preferred as it provides realistic conditions in real time. However, being able to select and control the weathering factors that are acting on the plastics can allow the effect of each variable to be observed, therefore many researchers implement laboratory weathering experiments.

1.3.3 Laboratory weathering

1.3.3.1 Artificial weathering

Artificial weathering can accelerate weathering at unrealistic artificial levels or simulated realistic levels. Here, the artificial weathering with accelerated weathering parameters such as increased UVR, including UVC and extreme temperatures are reviewed. As described earlier, UVB radiation has more energy than UVA radiation. Both UVA and UVB are found in solar radiation. UVC however, is blocked by the atmosphere and is not responsible for any environment weathering. To increase the rate of degradation, many researchers used wavelengths in the UVC range below 280 nm. Gewert *et al.* (2018) were able to identify 22 degradation products over only 5 days in saltwater. Hebner & Maurer-Jones (2020) showed that more microplastics were produced under 254 nm UVC irradiance than 300 nm UVB due to slower kinetics. Microplastic formation occurred within 72 hours under a 254 nm light source which was noted to be between 4 to 9 times stronger than solar energy. Tian *et al.* (2019) also used a 254 nm wavelength light and observed weathering after only 48 hour with X-ray photoelectron spectroscopy (XPS) before significant changes were seen by FTIR. UVC was reported present in the work conducted by Song *et al.* (2017), however they reported this fell within the natural solar radiation range. The plastic was also weathered for 24 hours a day, with no diurnal cycle, to decrease the overall weathering time. They calculated that 365 days in the weathering chamber was the equivalent to 4.2 years in the environment. This was much less than Badji *et al.* (2018) who calculated an equivalent 105 days to 4.2 years.

Extracting microplastic from organisms taken from the environment requires the tissue to be removed. This usually takes place through the use of enzymes (Courtene-Jones *et al.*, 2017) and agent digestion to break down the organic matter (Thiele, Hudson & Russell, 2019). During this process, there is the potential to adversely affect the microplastic samples under study. Cai *et al.* (2019) weathered both semi-synthetic and natural celluloses in microplastic using H_2O_2

and KOH. Laboratory experiments allow for the use of chemicals not present in the environment to understand the weathering characteristics of plastics during alternative conditions. In order to make laboratory experiments to understand the environmental fate of plastic, experiments that can replicate solar radiation are needed (Cai *et al.*, 2019).

1.3.3.2 Simulated weathering.

Most laboratory experiments aim to replicate natural weathering through simulated environmental conditions. The most difficult environmental parameter to simulate in laboratory experiments is solar radiation (Andrade *et al.*, 2019). A selection of papers that utilise laboratory experiment to simulate solar weathering is shown in Table 3.

There are two common light sources used in laboratory weathering studies, the xenon arc lamps (Julienne, Delorme & Lagarde, 2019; Arias Villamizar & Vázquez Morillas, 2018; Gijsman, Meijers & Vitarelli, 1999) and the QUV UVA-340 fluorescent tubes (Zhu *et al.*, 2020; Lizárraga-Laborín *et al.*, 2018; Hirsch *et al.*, 2017). The xenon arc lamps are utilised by the Suntest instruments (Atlas Material Testing Technology, Illinois, USA). The implementation of lamps to weather the plastic is highlighted in Table 4. The Atlas Suntest is designed to comply with industrial weathering standards, subjecting samples to UVR in a sealed, temperature controlled, weathering chamber. Freshwater can also be introduced through spraying and flooding (Atlas-mts, 2020). Gijsman, Meijers & Vitarelli (1999) implimented the Suntest instrument to determine the degradation pathways of plastics based on the concentrations of chromophores present. They found that PP had the highest oxygen uptake followed by PA6 and then PE. Oxygen uptake was found to be linear with degradation time. Julienne, Delorme & Lagarde (2019) compared the degradation of LDPE between air and freshwater treatments also using the Suntest instrument. Their results show that weathering causes the introduction of oxygenated groups, chain scission and the rearrangement of the surface layer of the LDPE films. The chemical changes lead to a change in mechanical

properties causing increased fragmentation when external stress was applied, as seen in the water treatment (Julienne, Delorme & Lagarde, 2019). Despite the Suntest being able to provide freshwater spray to the plastic sample, a single Suntest was used for both treatments and water was added into a glass bottle (Julienne, Delorme & Lagarde, 2019). Due to the costs of commercially available weather-o-meters some adjustments do need to be made to make them suitable to use for certain experiments (Ward *et al.*, 2019). PS was found to have the fastest rate of photooxidative degradation by Ward *et al.* (2019) using the Atlas Suntest XLS+, in agreement with the outdoor experiment conducted by Biber, Foggo & Thompson (2019). The Atlas Suntest weathering chamber is limited by space and the use of a single lamp in the design. This makes simulating environmental conditions difficult to achieve despite having a desirable solar spectra.

The second preferred lamp type was the QUV-340 lamp used in the Q-Lab QUV range of weathering chambers (Q-LAB, Bolton, England). The QUV chambers were also designed to comply with industrial test standards (Q-LAB, 2020). These fluorescent lamps replicate the irradiance of solar radiation, which is crucial for simulated experiments, however, the chambers are usually run between 40°C - 60°C to accelerate the weathering (Table 3). These temperatures are set by industry standards for industrial weathering applications and so are pre-programmed in the instrument (D20 Committee, 2013). The QUV chambers are also incapable of supplying saltwater to the system due to its corrosive properties and so the marine environment cannot be simulated without modifying the design of the chamber. One advantage of the Q-Lab QUV chamber is that the fluorescent tubes can weather a much larger area than the Atlas Suntest, potentially explaining their wide usage (Table 3). The Suntest implements a single xenon arc lamp whereas the QUV chambers utilise multiple long fluorescent tube lamps.

Arias Villamizar & Vázquez Morillas (2018), Badji *et al.* (2018), Philip & Al-Azzawi (2018) and Hirsch *et al.* (2017) conducted laboratory experiments alongside outdoor weathering as

described in paragraph 1.3.2. Badji *et al.* (2018), Philip & Al-Azzawi (2018) and Hirsch *et al.* (2017) all used the QUV chamber for their laboratory study. Philip & Al-Azzawi (2018) suggest that the ability of the QUV chamber to actively adjust the irradiance through the use of the Solar Eye Irradiance Controller provided the best possible simulation of sunlight (Quill & Fowler, n.d.). Hirsch *et al.* (2017) used the Q-Lab QUV chamber to critically assess measurement techniques for early stage degradation of LDPE. Their results show that Carbonyl index (CI) lacked sensitivity in determining surface changes to the plastic. Contact Angle (CA), based on the hydrophobicity of the surface, performed much better at early stages of weathering. Zhu *et al.* (2020) utilised the QUV Q-Panel chamber to report that simulated sunlight can remove plastics from the sea surface. In order to use seawater in the QUV chamber, quartz glass bottles were used to separate the seawater with the plastic samples inside. The main by-product from the photodegradation was dissolved organic carbon (DOC) which was expected to be utilised by marine bacteria to 'remove it' from the seawater (Zhu *et al.*, 2020). However, Romera-Castillo *et al.* (2018) artificially weathered plastics and found that, of the 60% of the DOC that was available to microbes within 5 days, DOCs that were exposed to UVR became less liable to utilisation.

Commercially available artificial weathering chambers such as the Atlas Suntest and Q-LAB QUV chambers offer a fixed set of constrained environmental parameters that are highly reproducible, constant and defined. However, the relevance of artificial weathering to environmental conditions in several studies can be questioned as the instruments used are designed to test industrial materials at increased irradiance and temperature. So, in order to fine tune these experimental procedures to simulate environmental conditions, custom ad-hoc designs are starting to emerge.

Table 3: A selection of studies that illustrate simulated solar irradiance.

Laboratory Artificial / Simulated Environment							
Polymer	Form	Treatment	Source Irradiance	Temp °C	Duration	Measurement	Reference
PP, PS and PA66	Pellet	Air, Saltwater and Sand	Powerstar HQI-TS 250W/NDL Bulb x2	23 - 28	10 weeks	FTIR-ATR	Andrade *et al.*, 2019
HDPE	Film	Air	Xeon Arc Lamp	57 ±1	96 Days	FTIR-ATR and TS	Arias Villamizar & Vázquez Morillas, 2018
PP	Custom	Air, Freshwater	QUV UVA-340 lamp.	50	100 hours	FTIR-ATR, TS, DSC, Spectro-colorimetry, Spectro-photo goniometry and Confocal rugosimetric measurement	Badji *et al.*, 2018
PVC	Custom	Saltwater	UVA 365 Lamp.	Room Temp.	56 hours	SEM and GC-MS	Chen *et al.*, 2019
HDPE, PP, PA6 and PBT	Film	Air and Freshwater	Xeon Lamp (Daylight filtered)	40 - 50	566 hours	FTIR-ATR and Oxygen Uptake	Gijsman, Meijers & Vitarelli, 1999
LDPE	film	Air	QUA UVA-340	60	3000 hours	FTIR-ATR and DSC	Hirsch *et al.*, 2017
LDPE	film	Air	QUA UVA-340	60	288 hours	FTIR-ATR, TS and DSC	Hirsch, Barel & Segal, 2019
LDPE	Film	Air and Freshwater	Xeon Lamp.	32 - 44	25 weeks	FTIR-ATR	Julienne, Delorme & Lagarde, 2019
HDPE, PLA	Film	Air, Condensation and Freshwater	QUA UVA-340	40 - 60	200 hours	FTIR-ATR, SEM, Tensile loading, DSC and thermo-gravimetric analysis (TGA)	Lizárraga-Laborín *et al.*, 2018
PET	Custom	Air and Freshwater	QUA UVA-340	40 - 60	13000 hours	Impact Strength, Gloss and Colour	Philip & Al-Azzawi, 2018
PP	Custom	Freshwater	Powerstar HQI-TS 250W/NDL, x2 and QUV UVA-340 x2	23	6 days	Bioavailability of DOC	Romera-Castillo *et al.*, 2018
PS	Pellet	Air, Freshwater and Saltwater	Long-arc Xeon Lamp (+ daylight filter)	25 - 35	6 -72 hours	Radiocarbon and Stable Carbon Isotope Conservative Tracer and Elemental Analysis	Ward *et al.*, 2019

HDPE, PP, and PS	Pellet	Air and Saltwater	QUA UVA-340	25 - 30	68 days	FTIR-ATR, SEM, DOC, Elemental analyse, Bioassays and Flow Cytometry	Zhu *et al.*, 2020

Table 4: A selection of studies that illustrate the use of artificial solar radiation which fails to simulate.

Laboratory Artificial / Accelerated							
Polymer	Form	Treatment	Source Irradiance	Temp °C	Duration	Measurement	Reference
8 semi-synthetic textiles	Fibre	Air, Freshwater, H_2O_2 and KOH	UVB 302 nm	-	7 days	FTIR-ATR, XPS	Cai *et al.*, 201)
HDPE	Film	Air	400 W, Mercury lamps. (Borosilicate envelope filters wavelengths below 300 nm)	60	280 - 360 hours	FTIR-ATR	Gardette *et al.*, 2013
PET, HDPE, PP and PS	Pellet	Freshwater	UV lamp (HTC 400-241 SUPRATEC HTC/HTT	~35	5 days	Ultra hight performance liquid chromatography–High resolution mass spectrometry (UHPLC−HRMS).	Gewert *et al.*, 2018
PET, HDPE and PP	Film	Air, Saltwater	254 nm / 300 nm	32 - 35	72 hours / 7 days	FTIR, DSC and UV-visible spectroscopy	Hebner & Maurer-Jones, 2020
HDPE, PP and PS	Pellet	Air, Sand	Metal Halide lamp containing UVC, 0.04 W/m2	43 - 45	360 days	FTIR-ATR, SEM, Density Separation and Mechanical Abrasion	Song *et al.*, 2017
PS	Pellet	Air and Freshwater	UV lamps (254 nm, GPH436T5L)	-	48 hours	FTIR-ATR, SEM, 3-D Fluorescence Spectroscopy, HPLC-C^{14}-LSC and GPC-C^{14}-LSC analyses	Tian *et al.*, 2019

1.3.4 Custom designs

There are no 'off the shelf' commercially available devices that can simulate both photo-oxidative and saltwater stress simultaneously and so researchers are starting to develop custom solutions to tackle this problem. Many of the commercially available weathering chambers were also not designed to environmentally weather plastic samples (Andrade *et al.*, 2019), rather, subjecting the materials to accelerated weathering conditions for industrial applications i.e. material coating (Lankone *et al.*, 2020). In the marine environment, saltwater is known to cool plastic affecting the rate of degradation (Biber, Foggo & Thompson, 2019; Kalogerakis *et al.*, 2017; Leonas, 1993), surrounds the plastic with water throughout weathering, making it impossible to use any current commercial weathering chambers which can't replicate these environmental conditions. Most laboratory weathering experiments requiring saltwater use custom designed weathering chambers for this reason. It should also be noted that the type of plastic used in commercial weather-o-meter tend to be films of plastic (Table 3). Custom designs are able to weather plastic that resembles those found in the environment as waste, such as pellet and meso sized plastic pieces (Table 5) rather than films alone. The temperature at which homemade designs can be run at is also more environmentally relevant in custom designs, however, standardisation of experimental temperature between different authors is lost (Table 5) compared to the predefined settings of the commercial units.

Due to the realistic simulation of the solar radiation that both the Xenon Arc lamps and QUV-340 fluorescent tubes offer, some researchers have utilised them in custom chamber designs. Cai *et al.* (2018) were able to weather plastic pellets (nurdles) in three treatments (Air, Fresh and Saltwater) under the simulated solar radiation in this way using the QUV-340 lamps. They found that hydroxyl groups and carboxyl groups formed in the air and freshwater treatments, whereas only carbonyl groups formed in the seawater treatment, as measured with FTIR. By utilising the QUV lamps, researchers are free to customise the chamber design and

cut down on the cost of premade industrial units.

Gewert *et al.* (2018) demonstrated how plastic leachate could be collected from saltwater after weathering plastics using Ultra-Violet Radiation (UVR), proposing the first attempt at developing a custom made laboratory weathering system with both saltwater and UVR, with other scientists following the design (Rummel *et al.*, 2019). Gardette *et al.* (2013) had used a similar rotating carousel design to irradiated PE films, this design omitted saltwater, instead focusing on thermal degradation. This design was built upon by Gewert *et al.* (2018). Andrade *et al.* (2019) developed a low cost weathering solution using Pyrex measuring cylinders in radial positions around a UVR light source, similar to Gewert *et al.* (2018). This design added mechanical sand aberration as a degradation factor. Studies in the past have attempted to understand the effects of the two competing mechanisms by subjecting the plastic samples to radiation and mechanical stress sequentially (Hebner & Maurer-Jones, 2020; Song *et al.*, 2017). This however raises questions about the environmental relevance of the finding. Andrade *et al.*, (2019) design potentially solves this issue.

There is a real pitfall when trying to accelerate the weathering process in polymers, the physical and chemical changes witnessed during custom weather-o-meter experiments might not correspond to environmental degradation patterns. Waldman & De Paoli (2008) used 'homemade' equipment using a UVC lamp with a maximum peak at 254 nm. The custom equipment was designed for industrial purposes to assess the photodegradation of PP and PS blends. They found that blends of the polymers form carbonyl groups faster than the homopolymers with the PS acting as a radiation trap. This highlights that custom designs allow for any experimental conditions and can be built to test any hypothesis. However, this freedom to create any type of weathering system highlights the need for a standard set of weathering parameters or ranges which will be considered environmentally appropriate.

Table 5: A selection of studies that illustrate the use of custom designed experiments to weather plastic.

Custom designs							
Polymer	Form	Treatment	Source Irradiance	Temp °C	Duration	Measurement	Reference
PP, PS and PA-66	Pellet	Air, Saltwater and Sand	Powerstar HQI-TS 250W/NDL Osram Bulbs	23 - 28	10 weeks	FTIR-ATR	Andrade *et al.*, 2019
Cellophane and Natural polymers	Fibre	Air, Freshwater, H2O2 and KOH	UVB (302 nm)	-	7 days	FTIR-ATR and Microscope	Cai *et al.*, 2019
PP and PS	Pellet	Air, Freshwater and Saltwater	QUA UVA-340	-	3 months	FTIR-ATR and Raman	Cai *et al.*, 2018
PVC	Pellet	Saltwater	UVA (365 NM)	Room Temperature	56 hours	SEM and GC-MS	Chen *et al.*, 2019
PET, HDPE, PP and PS	Pellet	Freshwater	UV Lamp (HTC 400-241 SUPRATEC HTC/HTT)	Around 35	5 days	Ultra hight performance liquid chromatography–High resolution mass spectrometry (UHPLC−HRMS)	Gewert *et al.*, 2018
HDPE	Film	Air, Freshwater, Saltwater and Sand	Sunlight	4.9 - 33, 1 - 66.5, 5.4 - 28.6, 2.6 - 39.8	6 Months	FTIR-ATR, Molecular Weight, Fragmentation and TS	Kalogerakis *et al.*, 2017
LDPE, 2% ECO, 10% ECO, PE + Graft, PS and PE + CS	Film	Air, Freshwater and Saltwater	QUA UVA-340	24 ± 4	240 hours	TS, elongation, and energy at break	Leonas, 1993
PET, HDPE, PP and PS	Pellet	Saltwater	UV Lamp (HTC 400-241 SUPRATEC HTC/HTT)	23 - 30	96 hours	LC-HRMS and Cell Bioassays	Rummel *et al.*, 2019
PP and PS	Fibre	Air	UVC, High-borax Ultraviolet TUV 15 W/G15 Light	-	110 minutes		Waldman & De Paoli, 2008

1.4 Analytical approaches to characterising changes in polymers

Characterisation of polymers is possible using a range of molecular spectroscopy techniques, however Fourier Transform Infra-Red Spectroscopy (FTIR) and Raman spectroscopy (Munno *et al.*, 2020; Zada *et al.*, 2018) are the most widely used, often in combination (Käppler *et al.*, 2016; Cai *et al.*, 2018; Liu *et al.*, 2012). FTIR by far the most widely used technique, being almost ubiquitous in the weathering literature (Table 1 - 5). Käppler *et al.* (2016) highlights that larger sized plastic particles can be measured with FTIR quickly and reliably, giving it practical advantages over Raman spectroscopy where many measurements are required.

1.4.1 Infra-red

Infrared light (IR) is electromagnetic radiation in the wavenumber range of 12800 ~ 10 cm^{-1} and can be divided into near-infrared region (12800 ~ 4000 cm^{-1}), mid-infrared region (4000 ~ 200 cm^{-1}) and far-infrared region (50 ~ 1000 cm^{-1}). IR spectroscopy is the technique that measures the interactions of IR light radiation with molecules when electromagnetic waves travel through the medium. The mid-infrared region is widely used because the absorption of most organic compounds and inorganic bonds is within this region. IR energy is absorbed and causes the bonds within the material to vibrate. There are many vibrational modes for each bond type including; stretching or bending of the molecular bonds, examples of which are shown in figure 1. It is for this reason that IR spectroscopy can also be referred to as Vibrational Spectroscopy (Déniel *et al.*, 2020). Molecules selectively absorb radiation of specific wavenumbers (1/Wavelength) of IR energy, causing a change in the dipole moment of the molecules. For IR spectroscopy, it is therefore essential that there is an electric dipole moment during the IR induced vibration of the molecule. This occurs because as the molecule vibrates, fluctuations in its dipole moment induce an electric field that interacts with the IR radiation electric

field. If there is a match in frequency of the radiation and the natural vibration of the molecule, IR energy absorption occurs. Heteronuclear diatomic molecules are IR active because their dipole moment changes by lengthening and contracting of the bond. Examples of CO_2 vibrations due to the absorption IR radiation is shown in Figure 1.

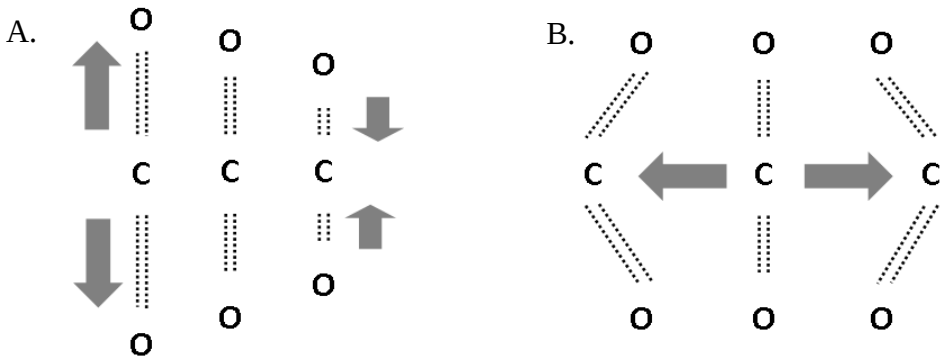

*Figure 1: Illustration of the symmetric stretching vibration (**A**.) and the symmetric bending vibrations (**B**.) of Carbon Dioxide.*

There are three main factors that affect the vibrations in a molecule: the mass of the atoms, the strength of molecular bonds and the type of vibration. The mass of the atoms, affects the bond vibration, as lighter atoms vibrate faster than heavier ones. Lighter atoms will vibrate at a higher frequency and will therefore absorb at a higher wavenumber. Stronger bonds also need more energy to make the bond vibrate and so these bonds will absorb IR radiation at higher wavenumbers. More energy is required to stretch a bond than it is to bend it, and so, absorptions due to stretching occur at higher wavenumbers than bending vibrations. Therefore, for the same bond, stretching vibrations are of higher energy than bending vibrations. Bonds can experience symmetric stretching, asymmetric stretching, rocking, wagging, twisting and scissoring depending on the energy of the IR radiation and its position in the molecule. IR radiation can also get absorbed by functional R groups, with the bonds collectively having a specific absorption of IR. These differences cause molecules to specifically absorb radiation of specific wavenumbers that can be measured and plotted. To collect these measurements, Fourier Transform Infrared Spectroscopy (FTIR) is used.

1.4.2 Fourier Transform

FTIR instruments consist of an IR radiation source and a beam splitter which splits the IR radiation, two mirrors, one is static and the other moves altering the pathlength between the beam splitter and the mirror and finally a sampling area and detector (*Figure 2*). When the polychromatic IR radiation is emitted it reaches the splitter, 50% passing through the splitter and 50% is reflected. These two beams are then reflected on the two mirrors back towards the splitter. At the splitter both beams are split again causing the reflected parts of the radiation from both the fixed and moving mirrors to recombine, passing through (Transmission) or reflecting off (Reflection) the sample and entering the detector. The path of the IR beam is illustrated in Figure 2. Depending on the position of the moving mirror with relation to the distance between the mirror and the beam splitter, the phase of the two reflected waves can either cause; constructive interference, when the wavelength (λ) distance is equal, or destructive interference when there is a difference of λ/2 (*Figure 2*). An interferogram is produced by measuring the intensity of the radiation that reaches the detector as the mirror is moved. An interferogram is produced which is the raw data that is produced by the instrument. The mathematical Fourier transform turns a distance (time) dependent signal into a frequency (wavelength / wavenumber) dependent signal i.e. the IR spectra.

In essence, the Fourier transform multiplies the signal produced in the interferogram by multiple test frequency. If the frequencies are identical between the interferogram and test frequency, then the integration of the result will be positive. A x A is the same as A^2, squaring the frequency will give positive values when summed over a given range. By doing this over all the frequencies, the presence (reflectance) or absence (absorbance) of a given frequency can be calculated in this way and plotted as an intensity of frequency against wavelength (wavenumber).

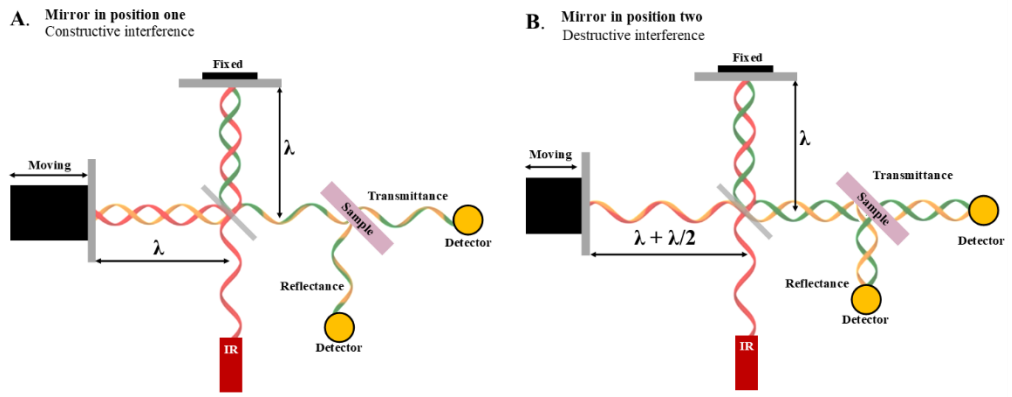

*Figure 2: The internal working of an FTIR spectrometer. The constructive and destructive phases are shown in **A**. and **B**., respectively. Red waveforms are emitted IR radiation. Yellow waveforms are those reflected of the moving mirror. Green waveforms are those that are reflected of the static mirror. In this illustration monochromatic light is presented for illustration purposes.*

The Fourier transform integration between zero and infinity, however the interferogram data has a beginning and end to the data. This is due to the limited movement of the mirror within the instrument. The data can therefore be considered as truncated, with a range -n to n. Because of this fact, the data in the interferogram can be viewed as encapsulated within a square wave form. The square wave data shape causes the Fourier transform to produce artifacts from the interferogram due to fractional sampling. This truncation of the data can be seen by fluctuations at the base of the peaks, so called 'pods' or feet. To reduce the effect of these fluctuations, an apodization function can be applied to the interferogram, which translates as 'feet removal'. This suppresses the signal to zero at the start and end and so the integration between zero and infinity required by the Fourier transform works better. This reduces the fluctuation around the peaks making the actual peaks more defined. There are several different types of apodization functions that can be applied to the data before transformed i.e. Triangular, Happ-Genzel and Gaussian. The final step to produce the final IR spectra is the ratio of a background data which takes into account the environmental parameter and setup of the device

before the sample is introduced. This becomes particularly important if environmental components interact with the path of the IR beam.

1.4.3 Fourier Transform Infrared

Using the materials ability to absorb IR radiation at specific wavelengths/wavenumbers and the use of the Fourier transform method, characterisation of materials is possible. As the bonds of the sample material absorb the emitted IR radiation from the instrument, peaks and troughs form in the spectra during the Fourier transform depending on the absorbance. Every bond that absorbs IR radiation in the Mid-infrared range has an associated spectral peak. These absorption wavelengths have been documented (Silverstein, Bassler & Morrill, 1992), and so using the known spectral absorption regions, the presence or absence of chemical bonds can be derived from the spectra. Not only have the specific bond absorptions been documented, but the entire spectrum has been recorded in spectral libraries using virgin, un-weathered materials. These libraries are now used as a reference when sampling a unknown material (Munno *et al.*, 2020).

In contrast to virgin plastics, the classification of weathered plastics becomes significantly less accurate when using spectral libraries due to degradation uncertainty (Kroon *et al.*, 2018; Tang *et al.*, 2019; Renner, Schmidt & Schram, 2017; Corcoran, Biesinger & Grifi, 2009). An understanding of the specific polymer degradation patterns underpin the use of such libraries (Shim, Hong & Eo, 2017; Boruta, 2012). Through the use of the corresponding degradation libraries it will allow for better identification of the plastics extracted from the environment (Kroon *et al.*, 2018). Work has been done with curve fitting of most relevant vibrational bands of the FTIR spectra for identification by (Renner, Schmidt & Schram, 2017), increasing the hit rate from 76% to 96%. Using this approach coupled with the appropriate weathered libraries can only increase the hit rate. In this work, the design of novel laboratory

apparatus to generate environmentally weathering plastic IR spectrum is explored, in an effort to improve the current standard of laboratory weathering practices.

1.4.3.1 Attenuated Total internal Reflection (ATR).

Solids are usually studied with FTIR using the reflection method as not all materials are transparent to IR radiation to utilise transmission setups. Both setups are highlighted in Figure 2, however most instruments are designed in one or the other configurations. The utilisation of the attenuated total internal reflection (ATiR, usually shortened to attenuated total reflectance, (ATR)) is the most widely used setup.

IR radiation passes through the ATR crystal so that it reflects off the internal surface of the crystal which is in contact with the sample. The internal reflection can occur once (single bounce) or multiple times (multi bounce). The interaction with the surface of the crystal causes an evanescent wave that interacts with the material being sampled. The penetration depth of the evanescent wave is determined by the wavelengths of the polychromatic IR light, the angle of incidence and the refraction index of the ATR crystal and the sample (Mirabella, 1993). Over the range of the polychromatic IR wavelengths, the depth of penetration therefore shifts which can cause the spectral data to skew as penetration depth increases causing a stronger signal. However, this can be corrected for in post processing using an ATR correction algorithm. Common crystal materials include diamond and germanium with the mechanical and chemical resistances properties of diamond making it perfect for measurements of harder samples.

1.4.3.2 External Reflectance

It is also possible for both diffuse and specular reflectance spectra to be measured by FTIR. Rather than the sample interaction with an evanescent wave, the IR radiation is reflected

off the surface of the material using optics such as mirrors. These techniques allow the IR to penetrate further into the sample material before being reflected. For diffuse FTIR it is assumed that the reflection is Lambertian, with the IR light reflecting off the surface in all directions equally. For specular reflectance, the reflectance is like that of a mirror and is intended for use with smooth samples. One drawback to both interfaces is that the internal mirror assemblies are housed within a chamber filled with atmospheric gases, which is exposed to the environment. The IR radiation beam must pass through these gases before and after interacting with the sample. Due to the high sensitivity of FTIR to chemicals in the atmosphere, such as water vapour and CO_2 there is a risk of signal contamination if the gas composition within the chamber changes during usage. This is not a consideration with ATR measurements as there is no atmospheric path length between the ATR crystal and the sample.

1.4.4 Use of FTIR in weathering studies (Carbonyl index)

During photooxidative weathering, the formation of carbonyl and hydroxyl groups is widely documented (Biber, Foggo & Thompson, 2019) and can be easily observed with FTIR (Lenz *et al.*, 2015). The main bond in the carbonyl group structure is the carbon-oxygen bond (C=O), has a known peak absorbance in the range 1600 cm^{-1} to 1800 cm^{-1} with the peak being recorded at 1705 cm^{-1} (Valadez-Gonzalez, Cervantes-Uc & Veleva, 1999), 1713 cm^{-1} (Biber, Foggo & Thompson, 2019) and 1720 cm^{-1} (Yang *et al.*, 2017). Standard wavenumbers have not been set which could be due to the fact that the peak shifts during oxidation as described by Rouillon *et al.* (2016), shifting from 1712 cm^{-1} to 1735 cm^{-1}. The carbonyl groups form during oxidation reactions, with increased production when exposed to UVR (Gardette *et al.*, 2013). During photooxidation, both cross-linking and random chain scission reactions occur between radicals (Gewert, Plassmann & MacLeod, 2015). Alongside these reactions, new functional groups, namely; carbonyl and hydroperoxides form (Valadez-Gonzalez, Cervantes-

Uc & Veleva, 1999). Impurities in the polymer allow radical formation, which react with oxygen in the environment (Gewert, Plassmann & MacLeod, 2015). These impurities can also form during the moulding of the plastic (Pelegrini *et al.*, 2019). FTIR can detect the carbonyl bonds (C=O bonds) that form during oxidation of the plastic and so offers a way to quantitatively define the extent of photodegradation.

The carbonyl index (CI) is used widely in the literature as the quantitative indicator of the chemical oxidation of polyolefins such PE and PP. This technique was first used in the 1970s by Mellor, Moir & Scott (1973). Benavides *et al.* (2001) calculated the CI as the ratio of the absorbance between 1720 cm^{-1} and 1425 cm^{-1}, whereas Arias Villamizar & Vázquez Morillas (2018) reported the values as 1715 cm^{-1} and 1465 cm^{-1}. CI has also been calculated using the area of the peaks rather than the intensity of the peaks by Pelegrini *et al.* (2019). It has been widely accepted that the CI reflects the mechanical degradation of the plastic as described by Allen, Mudher & Green (1984). With Song *et al.* (2017) reporting a linear relationship between the CI and time when subjected to UVR. However, Pelegrini *et al.* (2019) reported decreases in CIs for samples exposed to the marine environment, suggesting this phenomenon is due to the consumption of carbonyl groups by enzymes secreted by microorganisms. It has however been highlighted that the CI, which has been used for over 50 years, might not be an appropriate measure to quantitatively define the extent of photodegradation in PP (Rouillon *et al.*, 2016). It is suggested by Rouillon *et al.* (2016) that the methyl bands at 1456 cm^{-1} fit well with increased crystallinity, molecular weight and micro-hardness. CI has been reported to have a 40 days of latency compared to the 20 days seen by the methyl peak, and so fails to identify short term degradation (Rouillon *et al.*, 2016).

1.5 Summary

In the environment, neustonic plastics are subjected to photodegradation, temperature fluctuations, physical stresses, exposure to salts and organic pollutants, biofouling and microbial interactions. To design an experiment to look at every degradation pathway simultaneously would be challenging, and risks confounding results with ambiguous explanations without first understanding how each mechanism affects the plastics of interest. As UVR and temperature are the dominant forces driving degradation for most plastics, it is important to establish the rates and patterns of degradation before exploring confounding variables such as mechanical stress and bacterial degradation. The presence of saltwater and its effect on temperature are fundamental factors to incorporate when designing the experiment, to be as relevant to the marine environment as possible.

Building on the previous work of others, this thesis suggests a novel method to weather plastic in the laboratory under environmentally relevant conditions. This proposed method aims to standardise the way laboratory weathering experiments are conducted, by assessing the performance of this custom weather-o-meter design. A shift towards relating degradation to the energy received, rather than time may offer a novel way to standardise plastic weathering measurements for comparison between literature in future studies. For this study, stable, evenly distributed UVR conditions were implemented to produce weathering patterns that could be related to environmentally realistic irradiance over time. The integration of a low energy saltwater exposure system provided marine conditions without the effect of turbulence, wave action and biofilm formation in order to focus on the effect of UVR, temperature and salinity.

2 Methods

2.1 Sample Replication

Five commonly used plastics were chosen due to their heavy use in packaging and their known abundance as plastic in the environment (Hahladakis, J. N. 2020); HDPE, PP, PA, PS, and PET (Table 6). Each sample started as a 35 mm extruded rod supplied by Kingston plastics (Kingston Plastics, Hull, UK.) and was sectioned into pucks of 15 mm equal thickness. The puck size was dictated by the three interfaces of the Agilent Handheld 4300 FTIR (Agilent Technologies, Santa Clara, CA, United States) that would measure the plastic within a given area: Diffuse, Specular and Attenuated internal Total Reflectance (ATR).

The 8 mm threaded holes were bored into the centre of the reverse side of the puck, to permit the puck to be attached to a stage within the weather-o-meter, maintaining position within the illumination field (*Figure 3*). During testing both diffuse and specular measurement showed different FTIR spectra when measurements were taken over the drill hole. Therefore, during the experiment no scans were taken over this area. ATR measurements on the other hand were only taken around the edge of the puck, labelled in Figure 3 as ‘E’ shown in green. ATR measurements required force to be applied to the surface of the sample to gain sufficient contact with the diamond crystal. This caused minor mechanical stress to the surface of the sample. As stated, both the diffuse and specular measurements were susceptible to physical changes on the samples and so measurements were also taken away from the outer edge (*Figure 3*).

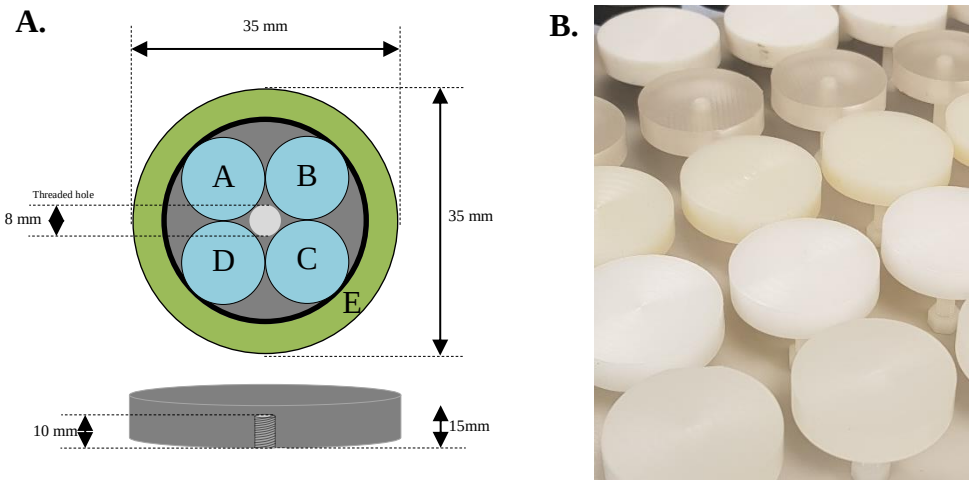

*Figure 3: (**A**.) Puck design showing the Scan areas for each FTIR measurement. Scanning area for Diffuse reflection and Specular reflection shown in Blue. Four scans per puck indicated by circles (A–D). Scanning area for Attenuated internal total reflection (E, Green). (**B**.)* Image of the 5 plastic species in their puck form.

Table 6: Polymer technical information.

Polymer type	***Abbreviation***	***Specific gravity***	***Water absorption***	***Isopropyl Alcohol Resistance***
Polypropylene Homopolymer Rod - Extruded	*PP*	*0.91 g/cm³*	*0.01%*	*yes*
Polyamide 6.6 Rod - Extruded	*PA (Nylon 66)*	*1.14 g/cm³*	*8%*	*yes*
Polyethylene terephthalate Rod - Extruded	*PET*	*1.39 g/cm³*	*0.50%*	*yes*
High Density Polyethylene 300 Rod - Extruded	*HDPE*	*0.96 g/cm³*	*0.01%*	*yes*
Styron™ 686E General purpose Polystyrene Resin	*PS*	*1.05 g/cm³*	*0.01%*	*yes*

Ten pucks were made of each of the five plastic types, providing five replicates for each treatment (Saltwater/Air). These 25 pucks were arranged in the same 'sudoku pattern' (i.e. one puck of each polymer in each row and each column) on each stage to evenly distribute the plastic under the illuminated area, minimising bias arising from sample position during the experiment (*Figure 4*) During analysis, four measurements were taken from each replicate,

totalling 20 scans for each polymer for each measurement step. The pucks were turned roughly 90° degrees to measure each quarter-segment of the puck. The position of the starting measurement was random, followed by three defined 90° turn measurements. Figure 3 shows 'A', a potential starting position followed by three subsequent positions, 'B', 'C', & 'D'. These positions were used to take Diffuse and Specular measurement only.

A.

1	2	3	4	5
4	1	5	3	2
5	3	4	2	1
2	4	1	5	3
3	5	2	1	4

B.

PP	PA	PET	HDPE	PS
HDPE	PP	PS	PET	PA
PS	PET	HDPE	PA	PP
PA	HDPE	PP	PS	PET
PET	PS	PA	PP	HDPE

*Figure 4: Weather-o-meter stage layout showing equal distribution of the samples in each row and column. (**A**.) Sudoku layout of the plastic pucks in number form. (**B**.) Layout of the plastic pucks in abbreviated names.*

2.2 Sample Preparation.

2.2.1 Dry treatment

Nitrile gloves were always worn to avoid contamination of the samples. Before the start of each weathering period the pucks were wiped with 75% isopropanol wipes to remove any surface contaminants. This was repeated upon removal of the samples from the weather-o-meter. Hydrocarbon oils had the potential to develop during some weathering periods and so the isopropanol removed these products before scanning. The properties of the material rather than the products produced were of interest in this study and so the removal of the 'oil substance' was required.

2.2.2 Saltwater treatment

Pucks that were subjected to the saltwater treatment were prepared in the same way as the air treatment, however, they underwent a washing step after being removed from the saltwater system. The entire stage with all 25 pucks was submerged in Reverse Osmosis Deionized water (RODI) bath with specific resistance between 8 to 15 MQ/cm^{-1}. This was gently agitated for a minute before each puck was unscrewed from the stage underwater, removed from the water and dried using paper towels. The pucks were then wiped with isopropanol wipes as described previously.

The saltwater reservoir and weathering chamber were sterilised with 96% ethanol before the addition of the saltwater at the beginning of the experiment. However, despite this step a biofilm started to develop during the experiment within the saltwater storage tank. This is likely analogous to the behaviour of plastic in the environment, but the film would inhibit the measurement of FTIR spectra from the pucks. These biofilms were effectively removed by the isopropanol wipe treatment made before measurement, and so no further sample preparation step was necessary.

2.3 Sample Exposure

The experiment was conducted in the Controlled Environment Laboratory (CEL) at the University of Hull, UK. The CEL was a climate-controlled cubicle fitted with an air conditioning unit which replenished air from the adjoining laboratory. There were no windows in the CEL and so the room was light-proof when the door was closed. This ensured that there were no external influences on the experiment from temperature changes or exposure to unwanted solar radiation. This also provided a safe area to run UV emitting lamps for long periods of time without compromising the health of other laboratory users.

2.3.1 Exposure time

Only exposure time spent under active UVR within the weather-o-meter was recorded in the data. The samples were removed from the weather-o-meter for exactly 4 hours between each exposure time in order to measure all the samples. When the samples were removed from the weather-o-meter they were shielded from any further UVR radiation by being removed from the CEL to an adjoining laboratory to be scanned, this laboratory lit by white LED batten lighting. The experimental rig was running for 21 days until experimentation was forced to stop at the University of Hull due to the COVID-19 global pandemic. During this time, the apparatus failed after the 19th day due to a suspected power-spike in the CEL while the experiment was running. This caused all 4 UVB fluorescent T8 lamp power units to stop working due to fuses blowing within the internal circuitry of each power unit. It is noted here that the original extension cables used during the first 19 days of the experiment did not have surge protection. There was a 26-day gap between the experimental rig breaking and restarting the experiment once the power units had been replaced. Power surge protection was also added to all the extension cables. During this down time, the samples were fully covered to prevent exposure to UVR and were stored at 12℃ within the CEL. Six days after restarting the

experiment the laboratory was closed due to COVID-19. Only one measurement time, that at 429 hours, was taken after the 26-day period of storage.

2.4 Sample regime

Measurement of the samples were planned to be collected with an exponentially increasing interval between each sampling date. Figure 5 shows the planned sampling regime. This regime was implemented to reduce the amount of data collected without losing any information. This method allowed the initial fast occurring changes to be captured in the data and then to capture the changes that occurred over a longer time frame without capturing excess data. The smallest increment was 24 hours (1 day) and was planned to progress to 834 hours (34.75 days).

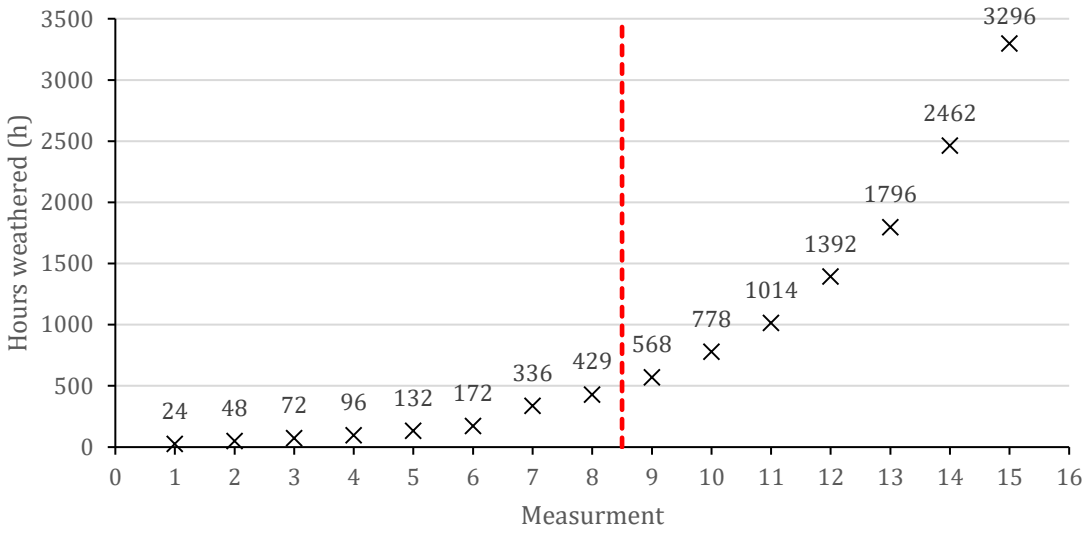

*Figure 5: The planned data sampling regime for the planned experiment. Black **X** markers indicate the hours of weathering that would have been received by the plastic samples. The **Red dashed line** highlights the closure of the experiment due to covid-19, within the planned sampling regime.*

2.5 Weather-o-meter design

No commercially available weather-o-meters are available with the low energy saltwater submersion system required for the experiment coupled with UV weathering. Some manufacturers offer corrosion cabinets that will periodically spray salt water on to the samples, but these units do not contain an ultraviolet weathering component. Furthermore, saltwater spray/fog does not adequately represent the environment in which neustonic plastic waste resides on the surface of the ocean. Enquiries to a leading manufacturer (Q-Lab, pers. comm.) indicated that they had experience of cutting a hole in the bottom of their commercial weather-o-meter equipment, and exposing materials placed in dishes provided by customers to the UV light from integral lamps. We therefore constructed a unique custom weather-o-meter with a similar principle, with the advantage that exposure to salt water was more reproducible and maintenance of constant salinity in that water was implemented within our design. Our unique instrument also permits the solar radiation to be tuned to the desired environmental conditions. This can be achieved by altering the lights fitted, mounting height of the lamps and depth of sample submersion under the saltwater within the chamber.

2.5.1 Stage design

Two identical stages were built, one for each of the salt and air treatments. The 25 polymer samples were attached to the weathering stage to ensure the sample remained stationary while maintaining a set height and position beneath the light rig. This ensured that irradiance levels at the puck surface could be measured at a set distance from the light rig. The stage was made from Trespa (Solid Phenolic Compact, www.phenolicresinlabs.com) which had a density of 1.416 g/cm^3, so that it would remain seated at the bottom of the saltwater tank when submerged. This high-density material would be able to compensate for the buoyancy of the plastic pucks that were attached to the upper surface *(Figure 6).* The pucks were raised above the stage to allow the saltwater to surround the puck (*Figure 6.d.*). This prevented

potential weathering differences occurring between the top and the bottom of the puck which could have caused both chemical and physical differences in the puck, namely swelling and cracking of the plastic.

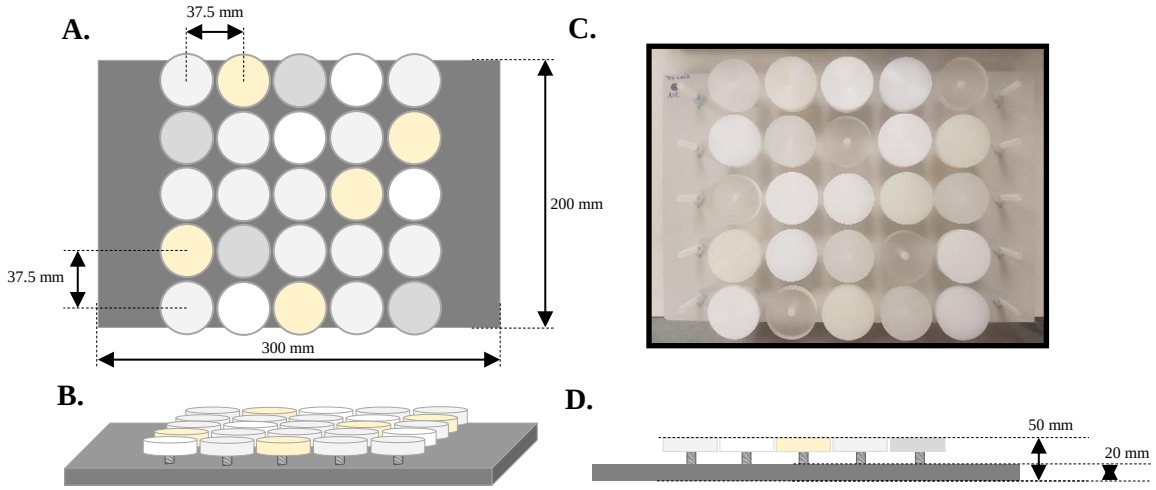

*Figure 6: Diagrams of the weathering stage with dimensions. (**A**.); Top down view. (**B**.); 3d view of the stage. (**C**.); Image of the Stage and the Pucks, top down view. (**D**.); Side on view of the stage and pucks highlighting the distance of the pucks from the stage.*

2.5.2 Lighting Rig

2.5.2.1 Radiation

The light rig consisted of 4 identical 18 Watt, T8, fluorescents tubes from Exo Terra (Reptile UVB 200 lamp) which supplied the UVB section of the spectrum between 280 - 320 nm (*Figure 7*). The four lamps were powered by two Exo Terra Light Unit Controllers 2x20W. These were wired so that one light controller powered the two outermost lamps and the other powered the two central bulbs. This was to ensure even power distribution. Four aluminium reflectors (Arcadia, 600 mm Lamp Reflectors) were placed over each tube to maximise the downward light reflection (*Figure. 6.b*). The UVA section of the spectrum (320 – 400 nm) was supplied by an array of 1500 LEDs. Four different wavelengths of light emitting diodes (LEDs) were used, namely, 395 nm, 390 nm, 378 nm, and 365 nm (*Table 7).*

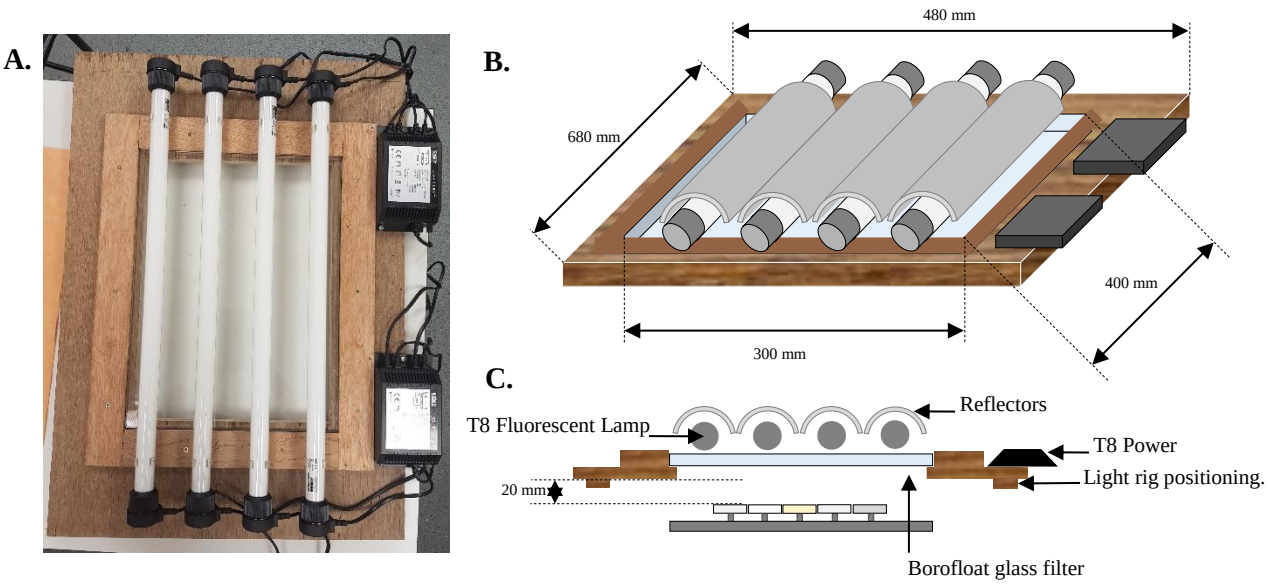

*Figure 7: Diagrams of the lighting Rig. (**A**.); Image of the lighting rig (top down) showing the placement of the T8 fluorescent tubes over the borofloat glass filtered window aperture. Reflectors removed for clarity. (**B**.); 3d diagram of the lighting rig with scale dimensions labelled of the total rig size and window aperture. (**C**.). Cross section of the light rig showing the placement of the sample stage beneath the light rig illustrating the height that the samples were placed under the rig.*

All the LED strips came as 5-meter lengths with 300 LEDs per strip, rated 12 volt, 24 Watts. Five strips were used on each light rig assembly. The LEDs were powered by a 12 V DC, 2A power supply. Both ends of the LED strip were connected to the live and ground of each power supply to eliminate the voltage drop over the 5-meter long strip caused by a changing resistance with length. This removed the energy output drop from the start of the LED strip to the end. The LEDs were fastened to the underside of the aluminium reflectors surrounding the fluorescent lamps which provided a solid flat mounting surface which angled the lights towards the samples. The reflector also acted as a heat sink that dissipated the heat generated during operation. A schematic diagram and image of one of the light rigs is shown in Figure 7. Due to the number of LEDs that had to be mounted on the reflective surface, the reflective surface was almost completely covered by the LED strip lights. However, the LEDs were white, so still reflected much of the UVB light from the T8 fluorescent lamps down towards the samples.

Table 7: A table showing the breakdown of LEDs used to provide the UVA spectrum in the weather-o-meter.

Wavelength Range (Stated on Box)	*Peak Wavelength (Measured)*	*Number of LEDs Per strip*	*Number of LEDs Per light rig.*
385 – 400 nm	*395 nm*	*300*	*300*
385 -395 nm	*390 nm*	*300*	*300*
375 – 385 nm	*378 nm*	*300*	*600*
365 – 375 nm	*365 nm*	*300*	*300*

2.5.2.2 UVR Filter

To ensure that the light produced by the lighting rig was close to the environmental solar spectrum, a cut off filter was added between the lamps and the samples to ensure any ionising UVC radiation was removed. Borofloat glass, also known by the trademarked name Pyrex™, was used in the design as it is known to restrict the transmission of wavelengths below 290 nm (Lepre *et al.*, 1998). A 300 x 200 x 6 mm sheet of Borofloat glass was mounted in a frame under the lamps (*Figure 7.c*). This also protected the lamps from any saltwater splashing that might occur during the weathering period by acting as a physical barrier.

2.5.2.3 Instrumentation.

An Ocean Insight, Flame-S-UV-VIS (Flame-S) spectrometer assembly with a wavelength range of 200 – 850 nm was used for measuring the irradiance of the light rig. The spectrometer was outfitted with a 2-meter, 400 nm premium fibre optic cable (QP400-2-UV-BX, Ocean Insights) and a cosine corrector with spectrolon diffusion material (CC-3-UV-S, Ocean Insights). The device had been calibrated by Ocean Insight using a NIST-traceable light source at the start of the experiment. All the data shown in this work was collected within a year after calibration with no alteration to the factory assembly.

2.5.3 Energy distribution

To quantify the energy that the surface of the plastic sample would receive, a 'calibration table' was designed to map the irradiance energy over the area of the weathering chamber. Figure 8 illustrates the design which consisted of a sheet of 9mm plywood with 165 holes drilled into the surface at a fixed distance of 25 mm apart to form a matrix. There was 25 mm between each hole which ensured that each puck location would be covered by at least one measurement, given that the size of the plastic samples was 35 mm in diameter. This also produced a high enough resolution of energy differences between different locations without

excess data, as each spectrum was collected manually. The ‘measurement holes’ allowed the fibre-optic cosine corrector from the Flame-S to be inserted into the calibration table at precise locations beneath the light rig. This allowed for reproducible quantification of the energy field produced by the lighting rig at a given time. Before the energy field was measured using the table, the lights had a 30-minute warm up period. This has been shown to be adequate time for thermal stability of the system. (See section 2.5.4). Each of the 165 locations were measured manually over a period of 15 minutes and so thermal stability of the lights was essential. The cable was held in each location for 3 seconds before measuring the spectra, this was to ensure that the software averaging of the last 3 scans, was of the target spectra (*section 2.7*). The cosine corrector could also be correctly seated against the glass before measurement within this time, ensuring that the angle each measurement was taken at was the same. This was directly perpendicular to the face of the borofloat glass filter (*Figure 8.D*). As depicted in Figure 8, during the calibration measurements, two sheets of borofloat glass were used. The first formed part of the light rig to ensure that any diffraction that occurred was captured by the calibration table measurements and the second piece, shown in Figure 8.b and 9 was placed over the measurement hole locations to ensure a perfectly flat surface area to take the measurements from. This was important in ensuring the height that the measurements were taken from was the same across the entire matrix of locations. The height of the light rig was adjusted using the three Hex-nuts mounted on the calibration table and could be adjusted independently. The light rig had corresponding holes drilled into the bottom that line up with the three hex-nuts on the calibration stand. This design ensures the correct orientation of the light rig in the exact same location every time. This allowed the height from the light to the top of the cosine corrector to be equal to the distance between the light and the surface of the plastic puck during weathering. This ensured that the exact pathlength could be known between the light rig and

the plastic samples, ensuring the irradiance the plastics received was calibrated and quantified, a method unique to the design of this weather-o-meter.

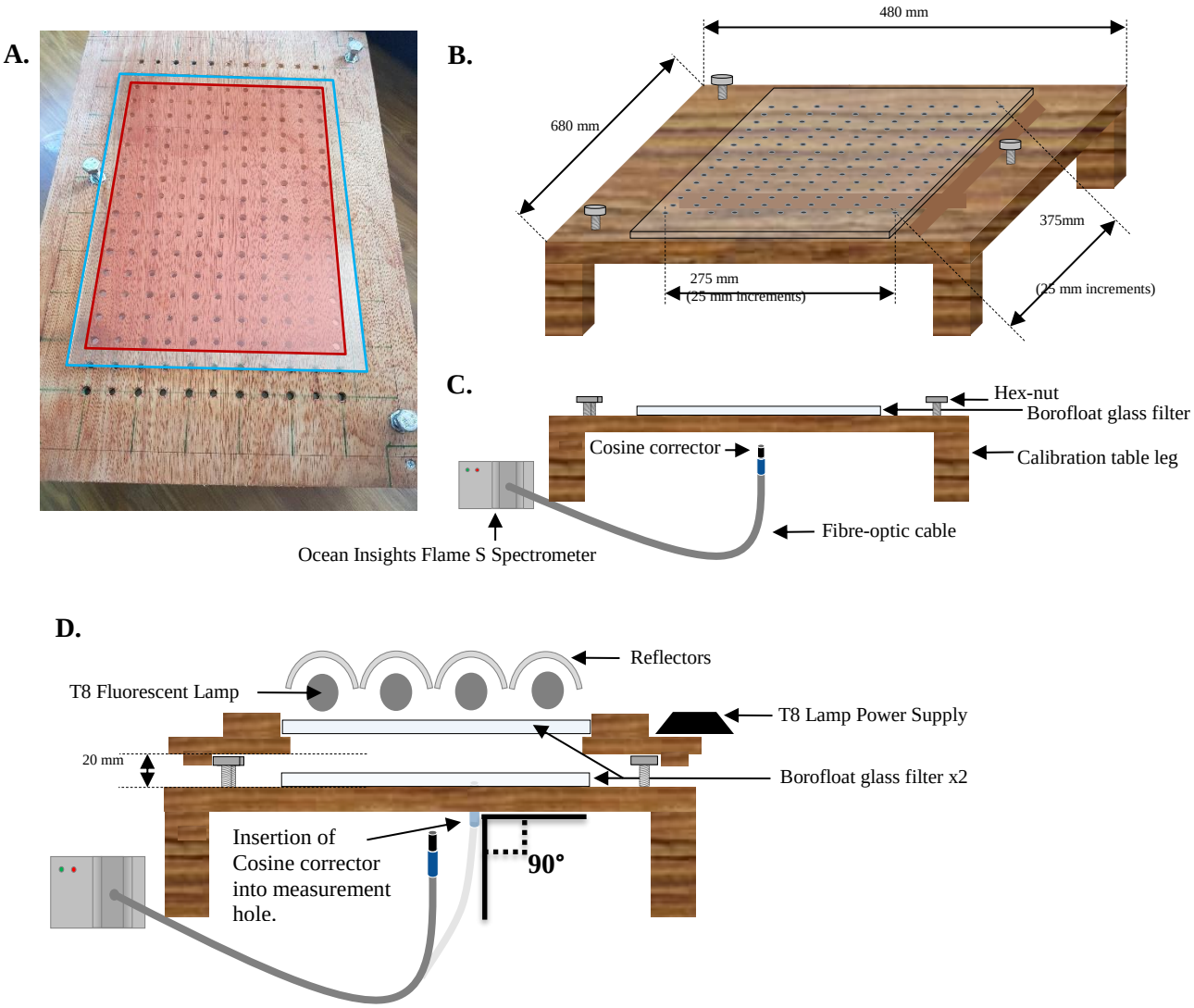

*Figure 8: Diagrams of the Calibration table used to measure the energy of the light rig over the weathering chamber area. (**A**.); Images of the calibration table showing the measurement holes and the hex-nuts for height adjustment of the light rig. 165 (11 x 15) measurement hole locations are highlighted in red. This corresponds to the size of the borofloat glass filter size, outlined in light blue. (**B**.); Diagram of the calibration table showing the dimensions of both the table and the positioning of the measurement holes (25 mm increment spacing). (**C**.); Diagram of how the fibre-optic cable was used to collect the irradiance from each measurement hole to build the energy map over the area of the weathering chamber. (**D**.); Diagram of the lighting rig mounted on to the calibration table at a height of 20 mm, the same as the surface of the plastic samples. An example of how the fibre-optic cable was used to collect the irradiance measurements by insertion in to one of the 165 measurement holes.*

Energy underwater

To test if the 1cm depth of saltwater submersion had an effect on the energy and spectra the samples received. Four walls of waterproof plumber's putty were added to the edges of a borofloat glass sheet placed on the calibration table. The walls were high enough so they could hold approximately 1 litre of saltwater. This produced a surface height of the water of 1cm. This is the same pathlength of water that the samples would have been subjected to during the flood part of the flood/drain cycle. The light rig was lowered onto the calibration table, now filled with saltwater. Six measurement locations in the middle of the weathering area were averaged. The same locations were used for both the dry and 1 cm saltwater depth measurements for direct comparison between the two.

Average spectra energy

To get the average energy from each rig, an energy map of 165 spectra was collected using the cosine-corrected fibre-optic of a spectroradiometer from the calibration table matrix. This covered the entire area under the lighting rig. To remove the low irradiance values around the edges, 81 central spectra were averaged that correspond to the locations of the plastic samples. A 9 by 9 central matrix was selected as the area where the plastic samples would sit within the weathering chamber (*Figure 9*). The average spectrum of the light rig was calculated using these 81 measurements.

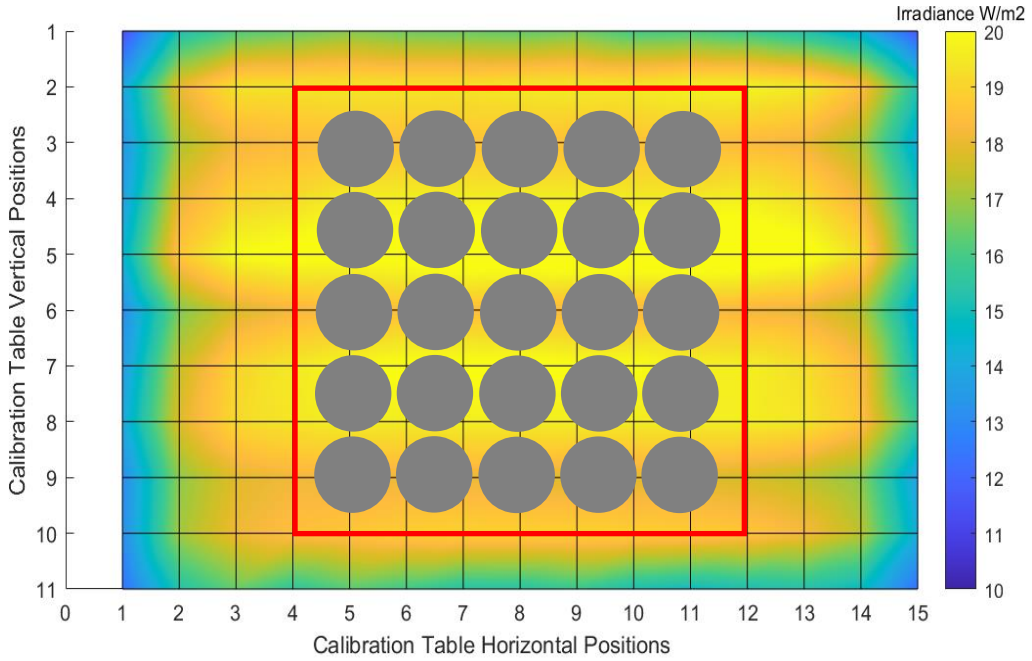

*Figure 9: Energy map created using the calibration table with all 165 measurment locations. Spacial area of 9 by 9 measurement locations used to calculate the average rig spectra (**Red square**). Gray circles reprisent the pastic sample pucks in their location within the weather-o-meter as justification for the selected measurment locations to average.*

2.5.4 Thermal properties and cooling

Both the fluorescence lamps and the LEDs produced a significant amount of heat. The temperature rise and fall of the system was recorded using a FLIR T460 thermal camera (FLIR, 2019) using the FOL18 lens. Table 8 shows the setting used to capture the footage.

Table 8: Setting used to measure the temperature of the light rig during warm up and cooling using the FLIR T460 thermal camera.

Settings	Value
Emissivity	0.94
Distance	2 m
Reflected temperature	0 °C
Atmospheric temperature	20 °C
Relative humidity	14 %
External optics temp	20 °C
External optics transmission	0.99

A thermal video of the light rig was taken from beneath, without the borofloat glass filter in place. This was to ensure the temperature of the lamps was measured rather than the glass. The glass reflected the infrared radiation (IR) radiation away from the camera which was mounted on a tripod at a 45^{o} angle. Regions of interest (ROI) were placed over an LED and the fluorescent lamp using the FLIR ResearchIR Software (FLIR® Systems, Inc, USA). A rectangular ROI was placed over an area of the rig containing both LEDs and a large section of the fluorescent lamp as shown in Figure 10.

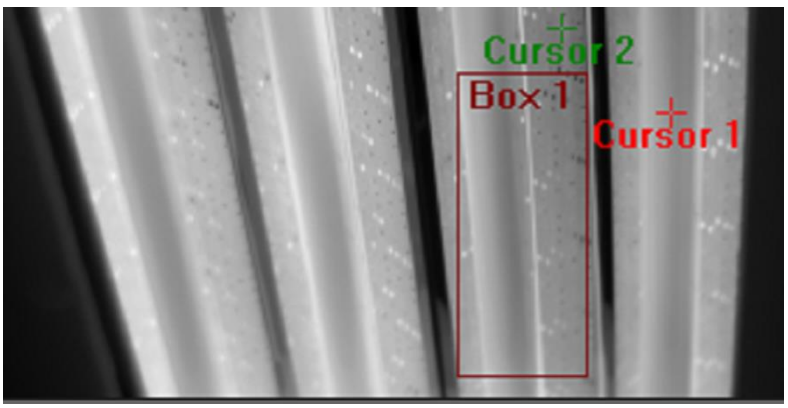

Figure 10: Screen capture of the FLIR thermal Video of the light rig from beneath without the borofloat glass filter. ***Curser 1*** *was placed over the fluorescent lamp.* ***Curser 2*** *was placed over a single LED.* ***Box 1*** *was to collect an average temperature over a representative area of the rig.*

To get a better idea of the temperature changes, the light rig was turned on after being at room temperature overnight (17.5 ℃). The rig was run without cooling until the temperature stabilised. Two fans, providing air cooling, placed on the top of the rig were then turned on. Both fans were set to high, causing the air to move at a max speed of 4 m/s, measured with a handheld anemometer (XPLORER 1 Rotary Vane Air Velocity Anemometer) directly in front of the fan. The heat produced by the light rig was then dissipated by air conditioning within the CEL. This maintained a temperature of 12 ±1 °C within the experiment cubicle to match the annual average Hull, UK air temperature of 11.54 °C. This average temperature was calculated from data collected using a Davis Vantage Pro 2 Weather Station mounted on the roof of the Cohen building at the University of Hull, Hull, UK, between 4th June 2018 and 18th September 2019 (*Figure 11*).

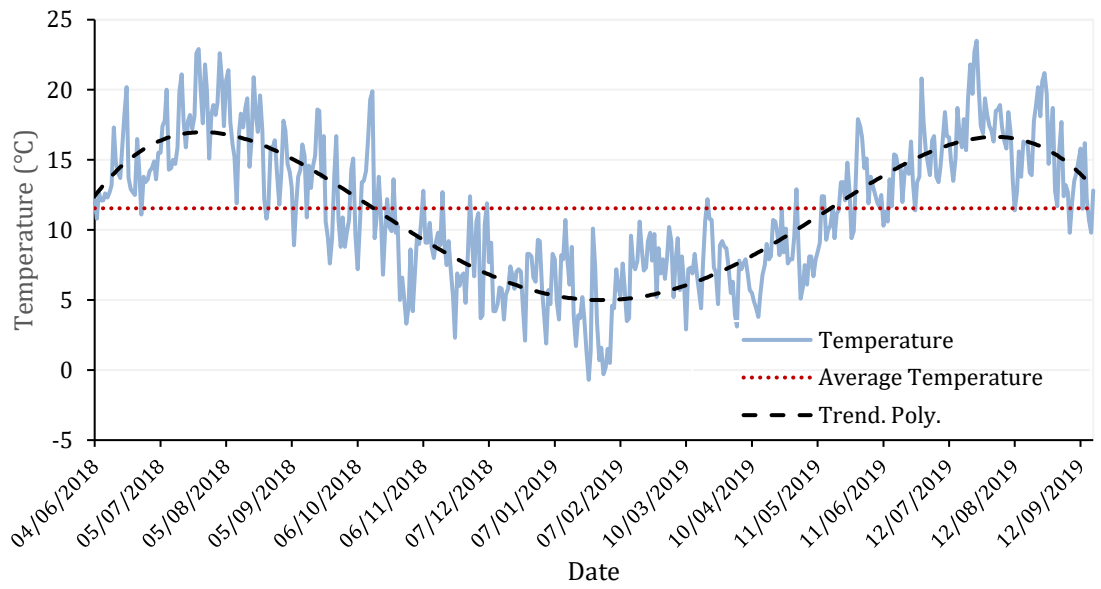

Figure 11: Daily temperature in Hull, UK, from 4th June 2018 and 18th September 2019, measured with a Davis Vantage Pro 2 Weather Station mounted on the roof of the Cohen building at the University of Hull.

2.5.5 Saltwater system

The function of the saltwater system is to maintain a constant salinity throughout the weathering experiment. The experiment needed to last a minimum of six months and so the saltwater reservoir was fitted with an auto-top-off (ATO) system. This was filled with reverse osmosis deionized (RODI) water in a separate reservoir (*Figure 13*). The system was controlled by a microcontroller from Arduino (Arduino LLC, Massachusetts, USA). A float switches within the weathering chamber activates a delay protocol that switches the pump off for a predefined period. The pump is controlled by a mains relay switch, controlled by the Arduino mounted microcontroller. This allows the water to drain back into the saltwater reservoir, uncovering the samples (*Figure 13*). The saltwater pump fills the tank very slowly and so the water enters the weathering chamber with low energy. This causes the surface of the water to remain still with little to no ripples as the water covers the samples. Ripples in the water could cause lensing of the lights into hot spots on the surface of the samples which needed to be reduced to a minimum. The low energy water movement also prevents splashing of saltwater onto the borofloat glass filter. This would cause salt crystals to form on the glass filter surface, interfering with the irradiance levels that the sample would receive.

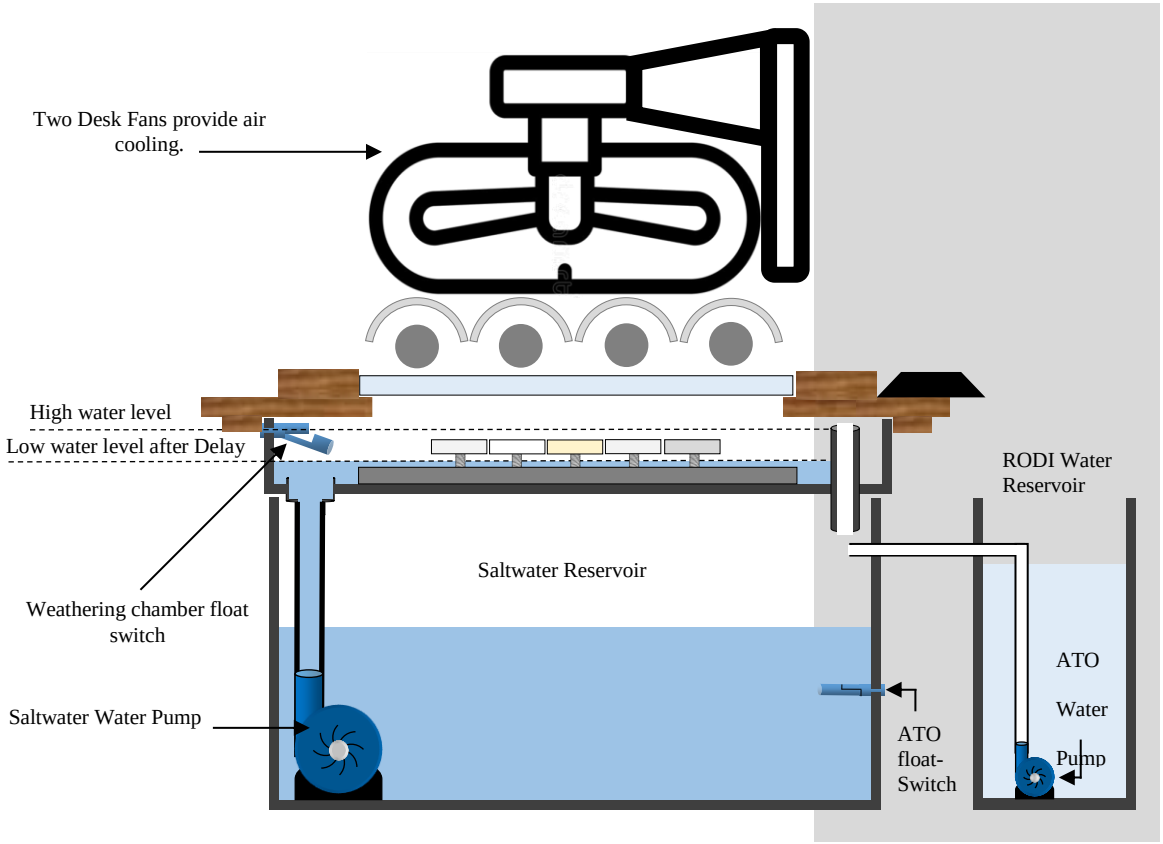

Figure 12: Illustration of the lighting rig in position over the saltwater cycle system and Reverse Osmosis De-Ionised (RODI) auto top off system. The white and grey background correspond to the background colours of Figure 13 for easy comparison.

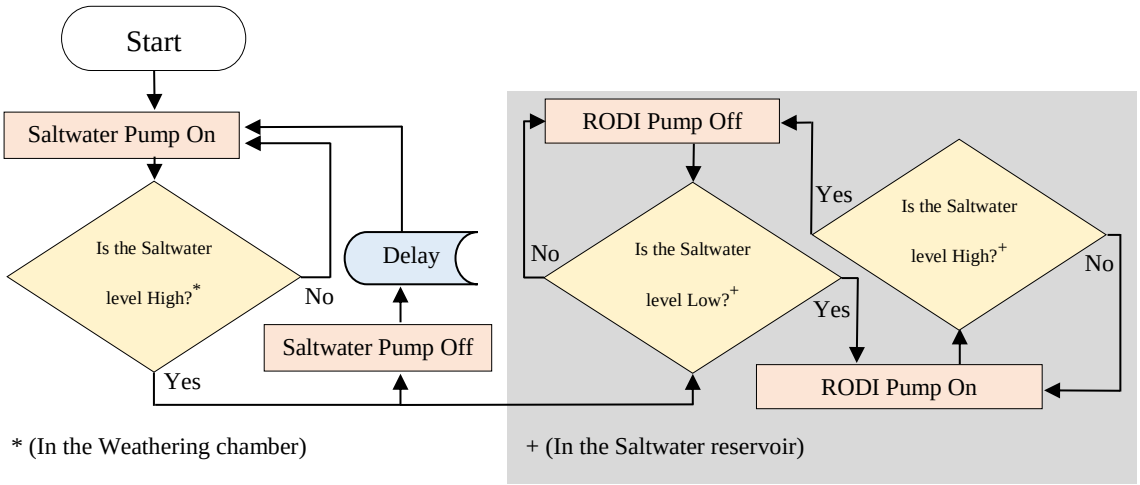

*Figure 13: Flow chart showing the feedback loop system for controlling both the saltwater and Reverse Osmosis De-Ionised (RODI) pumps. The White section **(left)** refers to the weathering chamber float switch decisions and the Grey area **(Right)** refers to the saltwater reservoir float switch decisions. **Squares** represent Actions. **Diamonds** represent logical Decisions. **Open cylinders** represent stored data.*

2.6 Environmental Radiation

UVR data collected using a Davis Vantage Pro 2 Weather Station mounted on the roof of the Cohen building at the University of Hull, Hull, UK, between 4th June 2018 and 18th September 2019 was used as an environmental estimation of UVR. 5.92 % of the radiation was assumed to equal the UVR proportion of the data collected as calculated from the percentage of the UVR in the standard solar spectrum over the range 280 - 800 (UV-VIS). UVR data was also used from Germany, collected using the European Light Dosimeter Network (ELDONET) project in 1997.

2.7 Software and Data Analysis

All spectral data collected with the Flame-S-UV-VIS miniature spectrometer was processed using Ocean View Spectroscopy Software 1.6.7 (Ocean (Optics) Insight, Oxford, UK). The spectra were averages of 3 absolute irradiance measurements taken at an integration time of 100 ms and boxcar width of zero. Irradiance calibration file was created on the 10th September 2019. All light source spectra were collected by manual trigger and exported to Microsoft Excel (Microsoft 365) for graphical representation of the data.

Irradiance spectra, collected as part of the 'calibration table' for the energy distribution mapping of the weather-o-meter for the creation of the surface plots, were processed with MATLAB (MATLAB, R2019b, version 9.7, The MathWorks, Inc. Natick, Massachusetts).

FTIR spectra were collected using MicroLab PC (Agilent Technologies, Santa Clara, CA, United States) in the pass-through mode on the Agilent 4300 handheld FTIR spectrometer so that all data was stored on the PC directly. MicroLab Expert (Agilent Technologies, Santa Clara, CA, United States) was used to average the 20 individual replicates into a single spectrum for each plastic at each time point. Standard Normal variate (SNV) and baseline

correction (BC) using the horizontal algorithm with an absolute height of zero was used on all the averaged spectra within MicroLab Expert. All data was saved as .CSV text files for import into MATLAB to be plotted.

Thermal data collected with the FLIR T460 thermal camera was processed with FLIR ResearchIR software (FLIR, Inc, USA) by adding regions of interest and export of the .csv temperature data for graphing in Microsoft Excel.

The saltwater flood and drain control system, was controlled by an Arduino microcontroller and the code written within the Arduino IDE (Arduino IDE, Arduino Software). The code is available in Appendix 1.

2.8 Presence of CO_2

To test the effect that the exhaled CO_2 would have on the interfaces was tested. The FTIR specular interface was used for this experiment as it contained the fewest parts in its design, allowing the interface chamber to be purged of CO_2 easily. The FTIR first measured a background spectrum of the ambient air. This was achieved by removing the interface from the FTIR body just before scanning and moving it left and right, within the orientation of the opening in the direction of travel, to purge the gas that was in the chamber. The researcher ensured that exhalation in the direction of the interface was avoided while it was purged, the use of a face covering aided this. The interface was then attached to the FTIR and the gold reference cap was attached. This sealed the air within the chamber from any external gas mixing. 128 background measurements were taken and averaged by the FTIR. The researcher then removed the gold reference cap and exhaled in the direction of the interface at a distance of 30 cm from the mouth. It should be noted that the interface opening was facing upwards, the same orientation that it was used in to collect the weathering data. The gold reference cap was then reattached. The sample measurements used the exact same plastic puck samples that were

used in the weathering experiment. The samples were lifted 10 cm off the interface and then returned after three seconds to simulate changing a sample. After 15 samples the reference cap was attached to the interface and a second background was taken. There remained a three second interval between the 15^{th} measurement and the second background measurement. Throughout this experiment care was taken not to breathe on the interface by the researcher. Only breathing when a seal was made between the sample and the interface. After the second background scan, five more measurements of the samples were taken. This same procedure was conducted with no airflow and with the addition of a fan pointing at the interface towards the researcher.

3 Results

The aim of this thesis is to provide a critical assessment of the current weathering research methodologies in an effort to highlight issues and propose solutions to overcome them. Firstly, the performance of the custom weather-o-meter designed as part of this thesis is reported here. Secondly, plastic degradation, observed over the 429 hours of weathering using this design are reported.

3.1 Weather-o-meter design

3.1.1 Lighting rig irradiance

The light rigs were composed of two independent light systems, the four T8 fluorescent tubes and the five LED light strips containing 1500 individual LEDs. The combined lamp setup produced UVR in the wavelength range from 290 nm to 390 nm. The target was to produce a realistic level of irradiance in both the UVA and UVB position of the spectrum. As a comparison, a solar spectrum from the Cohen roof and the solar standard (ASTM-G173-03, D20 Committee, 2013) were used as target irradiance levels. The uncooled rig had unrealistically high UVB below 325 nm (*Figure 14*). This was reduced on the final design by cooling the UVB lamps.

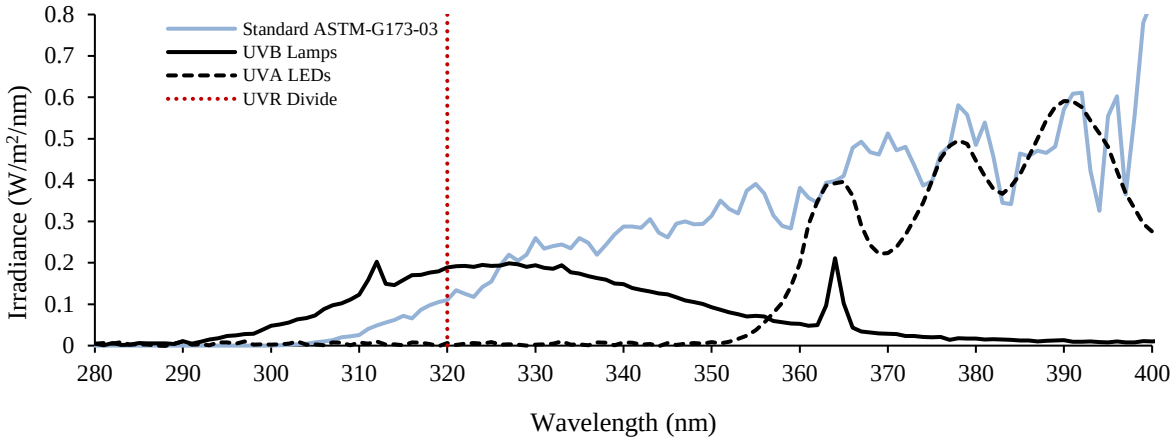

*Figure 14: Irradiance output without cooling from the saltwater rig in W/m2. Four Exoterra Reptile UVB 200 18W T8 Fluorescent lamps uncooled (**Solid black line**). All LEDs uncooled (**Dashed black line**) and the ASTM-G173-03 Solar Standard **(Light-blue solid line**). The dividing line showing the change from UVB and UVA is also highlighted (**Red dotted line**). All spectra taken with the UVC borofloat cut off filter.*

3.1.2 Rig cooling

The cooling of the rig reduced the amount of UVB that the samples received, as the cooling of the fluorescent lamp caused a decrease in peak output at 320 nm from 0.19 $W/m^2/nm^{-1}$ to 0.04 $W/m^2/nm^{-1}$ (*Figure 15*). Over the UVB range (280 - 320 nm) the levels were then much closer to the target solar levels falling from 2.64 W/m^2 to 0.36 W/m^2 (*Figure 15*).

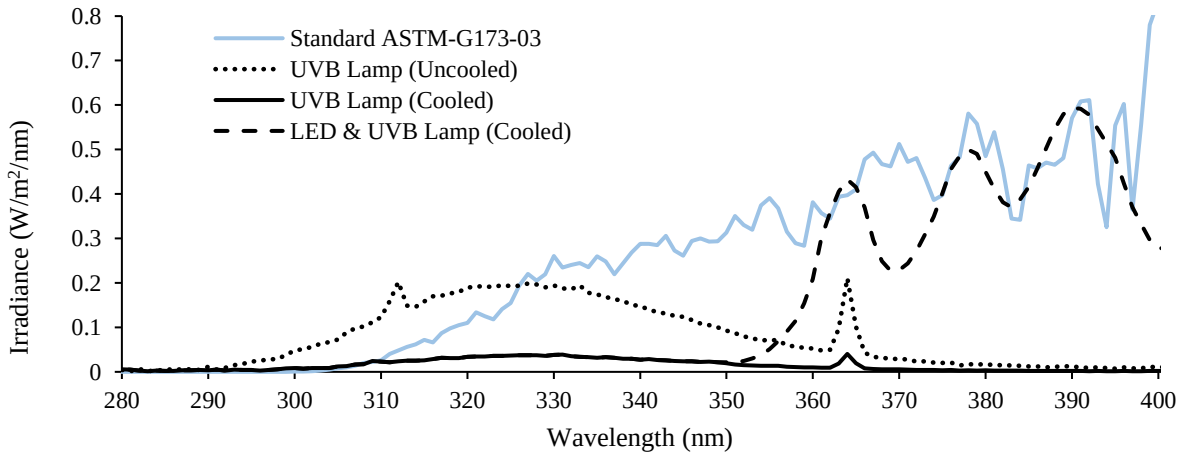

*Figure 15: Graph showing the cooled **(Solid black line**) and uncooled (**Dotted black line**) UVB Fluorescent Lamp. Combined LED and UVB Lamp used on the light rig (**Dashed black line**) and the ASTM-G173-03 Solar Standard (**Light-blue solid line**)*

3.1.3 Irradiance comparison

The rigs had an average irradiance of UVB (295 - 320) between 0.36 W/m^2 and 0.33 W/m^2 at the start of the experiment for the Salt and Air treatment respectively. Compared to the 0.74 W/m^2 from the Cohen solar spectrum (July at 12:00 noon) which became the target value (*Figure 16*). These values were reduced considerably from a value of 2.64 W/m^2 as seen from the uncooled salt treatment spectrum data (*Figure 16*). This shows that cooling the rig was effective at reducing the UVB output down to more environmentally relevant levels, however, the cooling resulted in UVB levels more than half that of the solar equivalent. On the other hand, the wavelength specific nature of degradation, with lower wavelength having a larger effect on the plastic degradation, means that this may not be important. The key wavelength to match closely in terms of dose is at the lower UVB wavelengths e.g. 295 to 310 nm, whereas the primary range of irradiance loss from cooling was between 310 and 320 nm (*Figure 15*). Consequently, the active irradiance received by samples was of the same magnitude as the target solar spectrum.

Cooling the light rig also ensured that the LEDs were cooled, prolonging their operational life. LEDs have been known to burn out if insufficient cooling is provided and so, with the experiment planning to last several months using 1500 LEDs, adequate cooling was a necessity. The aluminium reflectors mounted to the T8 fluorescent lamps were cooled directly by the two desk fans and acted as the heat sink for the LEDs. The performance of the LEDs increased when cooled in comparison to the uncooled LEDs, with increased UVA output (*Figure 16*). This shows an increase in irradiance output from 17.49 W/m^2 to 17.73 W/m^2 in the salt treatment rig when cooled.

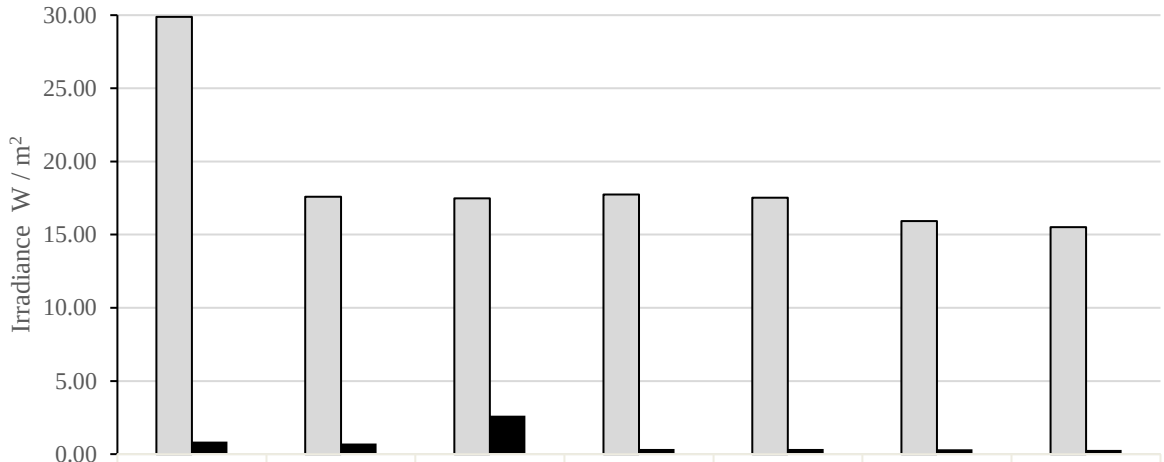

	Standard	Cohen	Uncooled (Salt Start)	Salt Start	Salt End	Air Start	Air End
UVA	29.87	17.60	17.49	17.73	17.52	15.92	15.50
UVB	0.86	0.74	2.6384	0.36	0.34	0.33	0.28

*Figure 16: Avergae irradiance (W/m^2) over the 165 data points from the calibration table, split between UVA (**Grey, black border**) and UVB (**Solid black**). Numeric data table (below) showing absolute (W/m^2) values for clarity in highlighting subtle difference.*

The UVA produced by the LEDs had a similar peak irradiance output to the standard solar spectrum, however, there was a significant lack of UVA between 320 nm and 360 nm (*Figure 17*). This was due to the lack of availability of LEDs that covered this UVA range. The energy from the Cohen roof solar spectrum has much less UVA than the standard solar spectrum meaning that the UVA energy from the rigs, summed over the UVA range 320 to 400 nm, was similar to the Cohen total UVA energy. Although the rig irradiance was over a shorter wavelength range (360 to 390 nm) with higher peak energy corresponding to the LED output wavelengths at 365 nm, 378 nm, 390 nm and 395 nm (*Figure 17*).

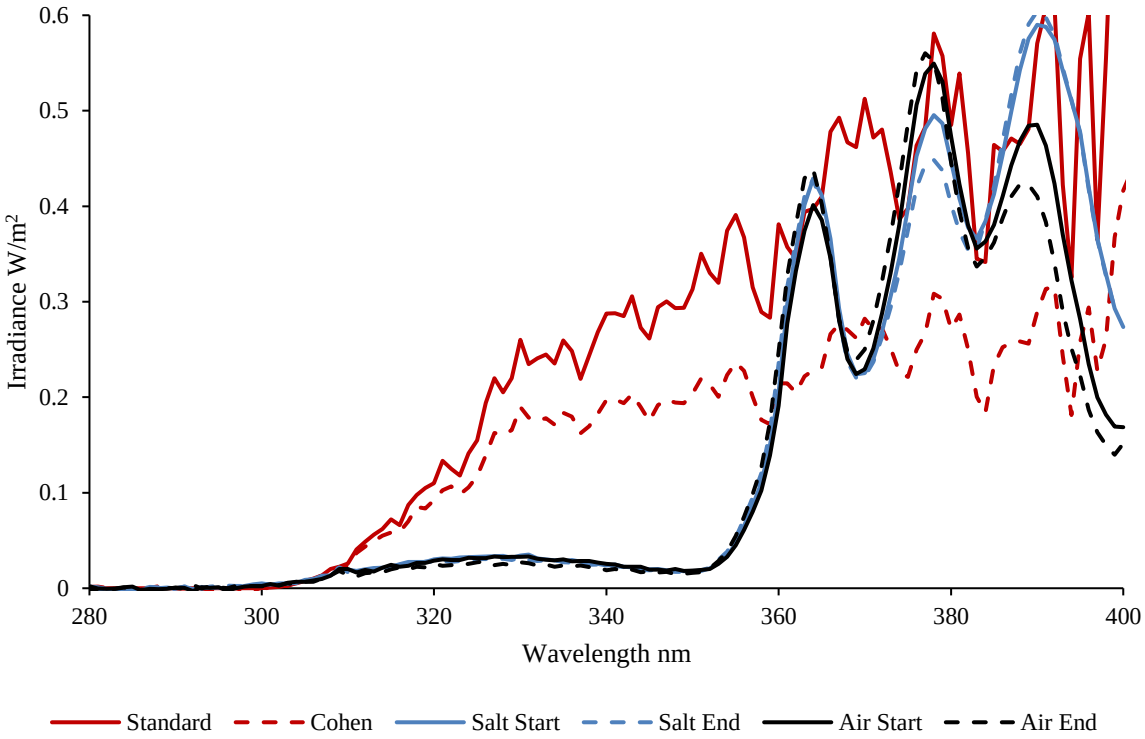

Figure 17: ***Solid red line*** *showes the Standard solar spectrum.* ***Dashed red line*** *shows the Cohen solar spectrum. (****Blue****) and Air (****Black****) treatment light rigs.* ***Solid blue line*** *showed the average starting spectra of the saltwater rig.* ***Dashed blue line*** *showed the average end spectra after 429 hours of the saltwater rig.* ***Solid black line*** *showed the average starting spectra of the Air rig.* ***Dashed black line*** *showed the average end spectra after 429 hours of the Air rig.*

3.1.4 Irradiance over time

It was initially assumed that the output from the light would remain constant throughout the experiment, however during the 25 days of experimentation the UVB lamps showed a decrease in output over time (*Figure 18*). The irradiance of the peak UVB in the salt treatment decreased by an average of 0.0058 W/m^2 and 0.0050 W/m^2 in the Air treatment which equates to a fall of 1.3% and 2.9% respectively (*Figure 18*). There is also a change in the LED output shown in Figure 18. However, it is clear to see that each specific LED wavelength changes independently from start to finish. LEDs outputting 390 - 395 nm UVR on the saltwater rig showed little change. However, on the Air rig, the same LEDs showed a considerable decrease at 390 - 395 nm. LEDs outputting 365 nm UVR show an increase in irradiance from the Air rig compared to no change in the saltwater rig.

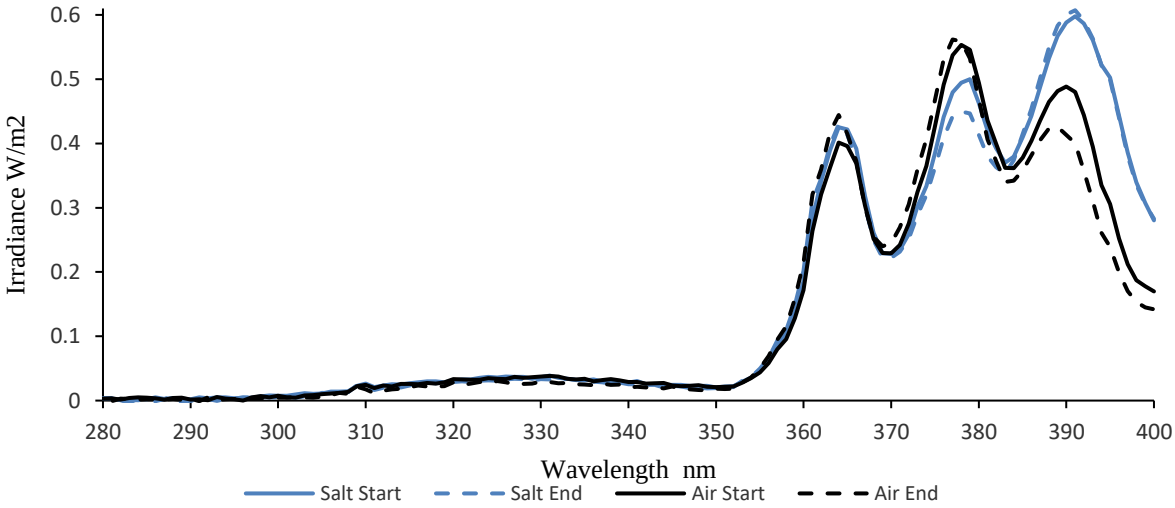

*Figure 18: Graphs showing the spectra averaged over the 165 data points from both saltwater (**Blue**) and Air (**Black**) treatment light rigs. **Solid blue line** showed the average starting spectra of the saltwater rig. **Dashed blue line** showed the average end spectra after 429 hours of the saltwater rig. **Solid black line** showed the average starting spectra of the Air rig. **Dashed black line** showed the average end spectra after 429 hours of the Air rig.*

The energy maps produced using the calibration table for each rig, both at the start and end of the experiment, clearly show a fall in irradiance of UVB and to a lesser extent the same is true for the UVA (*Figure 19*).

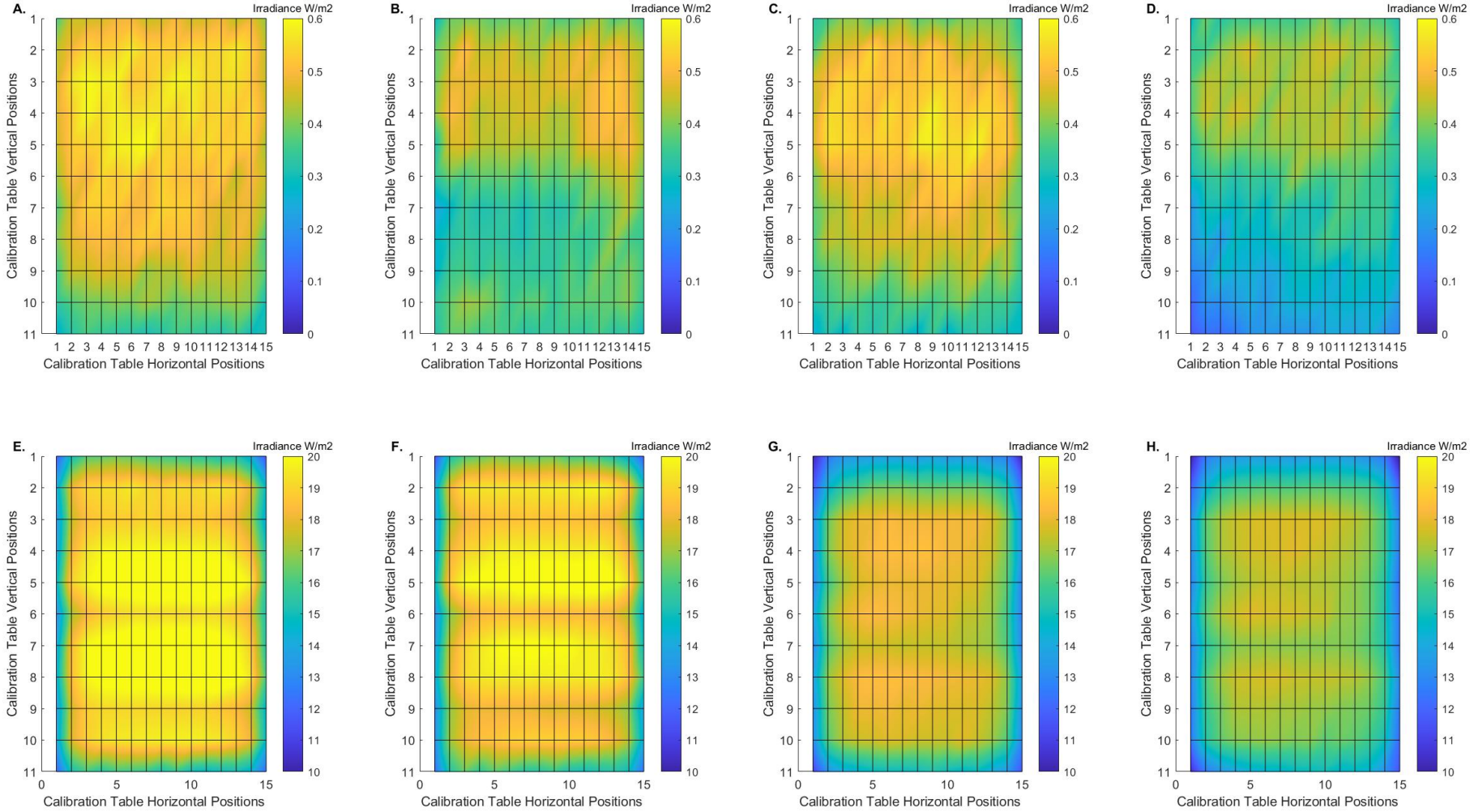

*Figure 19: Energy maps of the energy received by the surface of the plastic samples measured in W/m2. 165 data points mapped in a 15 by 11 matrix (in increments of 2.5 cm) covering the area of the weather-o-meter. The surface plots have been stretched in the vertical direction to show the difference between the lighting 4 sections on each rig. Top row. Fluorescent lamp UVB energy maps (**A.-D.**). Bottom Row. LED UVA energy maps (**E.-H.**). Column 1. Salt rig starting energy maps; UVB (**A.**) & UVA (**E.**). Column 2. Salt rig ending energy maps; UVB (**B.**) & UVA (**F.**). Column 3. Air starting energy maps; UVB (**C.**) & UVA (**G.**). Column 4. Air ending energy maps; UVB (**D.**) & UVA (**H.**).*

3.1.5 Equivalent Weathering

The weathering performance of the system shows similarities with outdoor environmental weathering which was an aim of this work. It was measured in Hull, UK, during Summer (June, 2018) at 12 noon, that the irradiance of UVR (over the range 280 - 400 nm) was 18.34 W/m^2, with a theoretical maximum of 30.73 W/m^2, as calculated from the (ASTM-G173-03, D20 Committee, 2013). The irradiance supplied by other authors was; 143 W/m^2 (295 - 400 nm), 90 W/m^2 (300 - 400 nm) and 105-140 W/m^2 (300 - 400 nm) by (Chang *et al.*, 2018; Rouillon *et al.*, 2016; Fashandi, Zadhoush & Haghighat, 2008), respectively. This highlights that many weather-o-meters used for photodegradation experiments supply more UVR to accelerate the weathering. The rig proposed in this thesis supplied an irradiance of 18.09 W/m^2 and 16.25 W/m^2 for the salt and air rigs respectively (*Figure 16*). It should be noted that despite identical setups between the salt and air rigs, the irradiance output was less in the air rig. This was likely due to differences in the lamps and LEDs between the two rigs.

The energy received by the surface of the plastic during 24 hours (one day) of weathering within the weather-o-meter design was 1563 KJ/m^2/day and 1404 KJ/m^2/day for the saltwater and air treatment respectively (*Table 9*). These values have been calculated from the average irradiance for each rig measured using the calibration table (*Figure 8*), averaging the central 81 spectra corresponding to the location of the 25 plastic samples (*Figure 9*). It has been calculated that UVR at the same latitude as UK / Northern Germany is 1040 KJ/m^2/day, averaged over the summer month of June. The data is shown in Table 9 can be compared to the graphical representation of environmental irradiance shown in Figure 20. Therefore, during the 25 days of weathering during the experiment will equate to 37.6 and 33.8 days from the salt and air rig, respectively.

Table 9: The graph shows the calculated energy received by the surface of the plastic during 24 hours of weathering for both the salt and air treatments.

KJ/m^2/day	Starting irradiance	Ending irradiance
Salt	1563	1543
Air	1404	1363

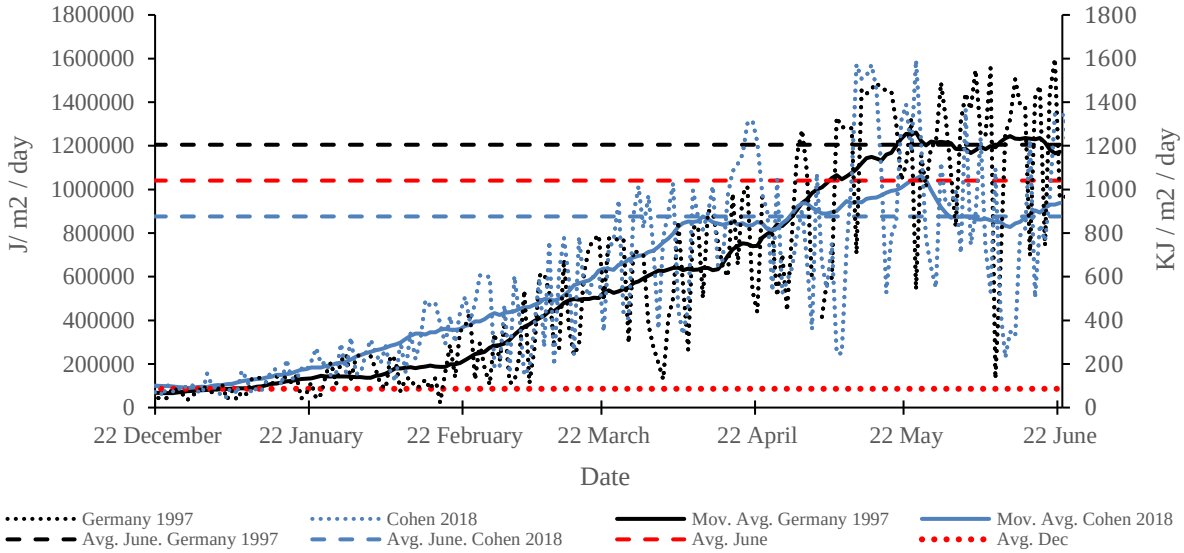

Figure 20: Energy in joules and kilo-joules for both a weather station in Zingst, Germany and a weather station mounted on the roof of the Cohen building at the University of Hull, Hull, UK, between 22nd December and 22nd June in 1997 and 2018 respectively. ***Black dotted line*** *shows the raw data for Germany.* ***Blue dotted line*** *shows the raw data from the Cohen roof weather station data.* ***Black solid line*** *shows the average data from a 30-day moving average around a centre value form the raw Germany data.* ***Blue solid line*** *shows the average data from a 30-day moving average around a centre value form the raw Cohen data.* ***Black dashed lines*** *show the average value for the month of June in Germany 1997.* ***Blue dashed lines*** *show the average energy value from the Cohen roof weather station during June 2018.* ***Red dashed line*** *shows an average of the 1997 June average from Germany and the June 2018 average from Cohen.* ***Red dotted line*** *shows an average of the 1997 December average from Germany and the December 2018 average from Cohen.*

These values fell from the start of the experiment to the end of the experiment due to the irradiance decay over time (*Table 9*). After the 25 days the energy output from the lamps had fallen by 1.3% and 2.9% in the saltwater and air treatments, respectively. Therefore, in the saltwater treatment, after 25 days, the equivalent weathering would have shortened by 12 hours from the start to end of the experiment based on the summer equivalent.

3.1.6 Saltwater Pathlength

The spectrum of light under a 1cm pathlength of light through saltwater, showed that there was a small uniform decrease in irradiance over the entire spectral range (*Figure 21*). The irradiance had a maximum decrease of 0.01 W/m^2 at 400 cm^{-1}. This fall of 0.01 W/m^2 is considered a negligible decrease in the UVR irradiance received by the plastic samples as noise in the spectra accounts for similar energy fluctuations.

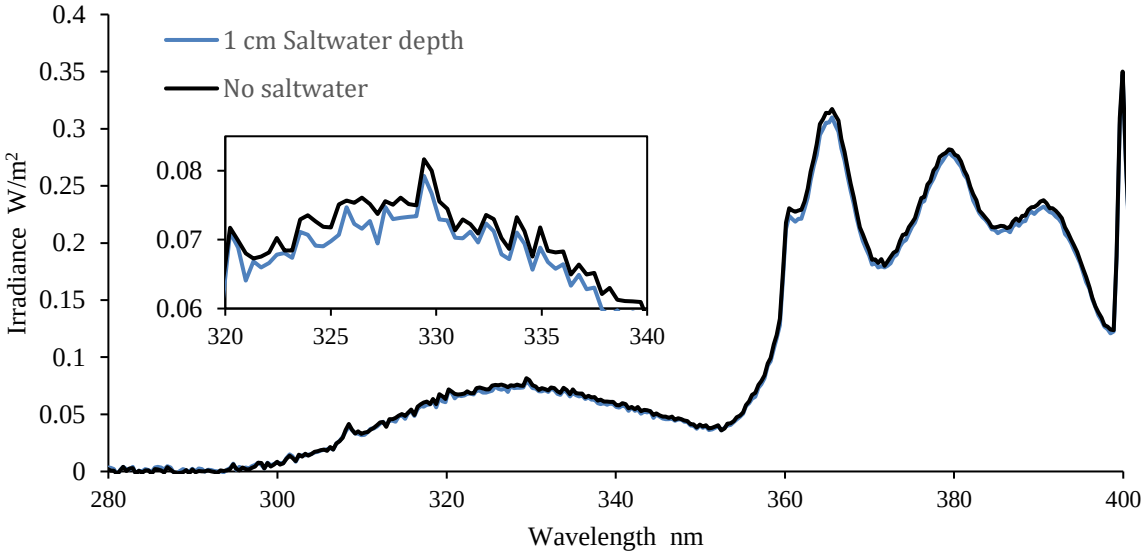

Figure 21: Uncooled light rig spectra average over 6 central measurement locations of the calibration table. ***Solid blue line*** *shows the spectra through 1cm path length of water in comparison to the* ***Solid black line*** *showing the spectra without the presence of saltwater.*

3.1.7 Introduction of Saltwater

The flooding and draining of the weathering chamber, controlled by the microcontroller throughout the 429-hour experiment, maintained the salinity at 1.025 g/cm^3. The borofloat glass filter remained clean throughout, without any watermark or salt crystal formation. The system didn't experience any 'salt creep' around the edges of the chamber. The RODI chamber, initially filled with 25 litres, lasted the length of the experiment. After the 25 days, approximately 5 litres of RODI water remained, and could have been easily topped up to continue the experiment. The saltwater reservoir developed a bacterial layer on the inside which caused bacteria to collect and settle on the filter floss placed over the return pipe used for flooding and draining the water from the chamber (*Figure 12*). This was likely a bacterial contaminant introduced from the retrieval of the samples after the initial sterilisation.

3.2 Plastic Degradation

Here, the results of both the dry and saltwater exposure treatment are reported. The dry data provides a baseline for changes, without the influence of saltwater. Then the findings from the saltwater experiment are compared to this baseline. Each treatment was measured using three FTIR interfaces to compare different regions/depths of the plastic, from surface changes using ATR (~2µm), to near surface specular reflection (100 - 200 µm) and those found deeper within the plastic, using diffuse reflection (>200 - 500 µm).

HDPE.

The FTIR spectra produced by the different interfaces shows peek shape difference. In figure 22 below, a virgin high density polyethylene (HDPE) sample was measured with specular, diffuse and ATR interfaces on the Agilent 4300 handheld FTIR. All spectra were taken of the same HDPE sample which had a smooth uniform surface with reflective properties.

It is therefore clear to see in figure 22, that both the specular and ATR samples have the least amount of noise in the FTIR spectra. This is because the uniform surface allowed a large contact of the plastic with the diamond crystal of the ATR interface and the smooth reflective surface was much more suited to the specular interface. The diffuse interface on the other hand, which assumes lambertian distribution of the reflected infrared, developed noise in the spectrum. The noise could easily be mistaken for peak formation to the untrained eye or even a computer matching to a spectra library.

The main shape difference between the contact (ATR) and reflectance (Specular and Diffuse) interfaces is that the spectrum produced by Fourier-transform gives single positive peeks by ATR and a negative peak in the specular and diffuse measurements. This can be seen by the yellow arrows in figure 22. This occurs due to the restrahlen effect, where the IR radiation cannot penetrate a material due to the change is refractive index. As the refractive index will change between different materials, not all materials will exhibit the restrahlen effect and those

that do may not exhibit the derivative style negative peaks for the entirety of the spectrums as the wavenumber changes along the spectrum. This effect usually results from strong to total reflection of the sample as highlighted from the smooth HDPE measured in figure 22.

Both output spectra can distinguish absorbance feature of a given material but the ability to resolve close together peaks, such as the two C-H bending absorption features of HDPE at 1472 and 1461 cm^{-1}, are more easily observed in the ATR spectrum compared to diffuse or specular reflectance FTIR spectra. The ATR spectra in figure 22 can just about resolved the two peaks at 1472 and 1461 cm^{-1} with a resolution of 8 cm^{-1} whereas this absorption feature is lost in the diffuse and specular.

The presents of Co2 in the spectra is discussed in section 3.2.

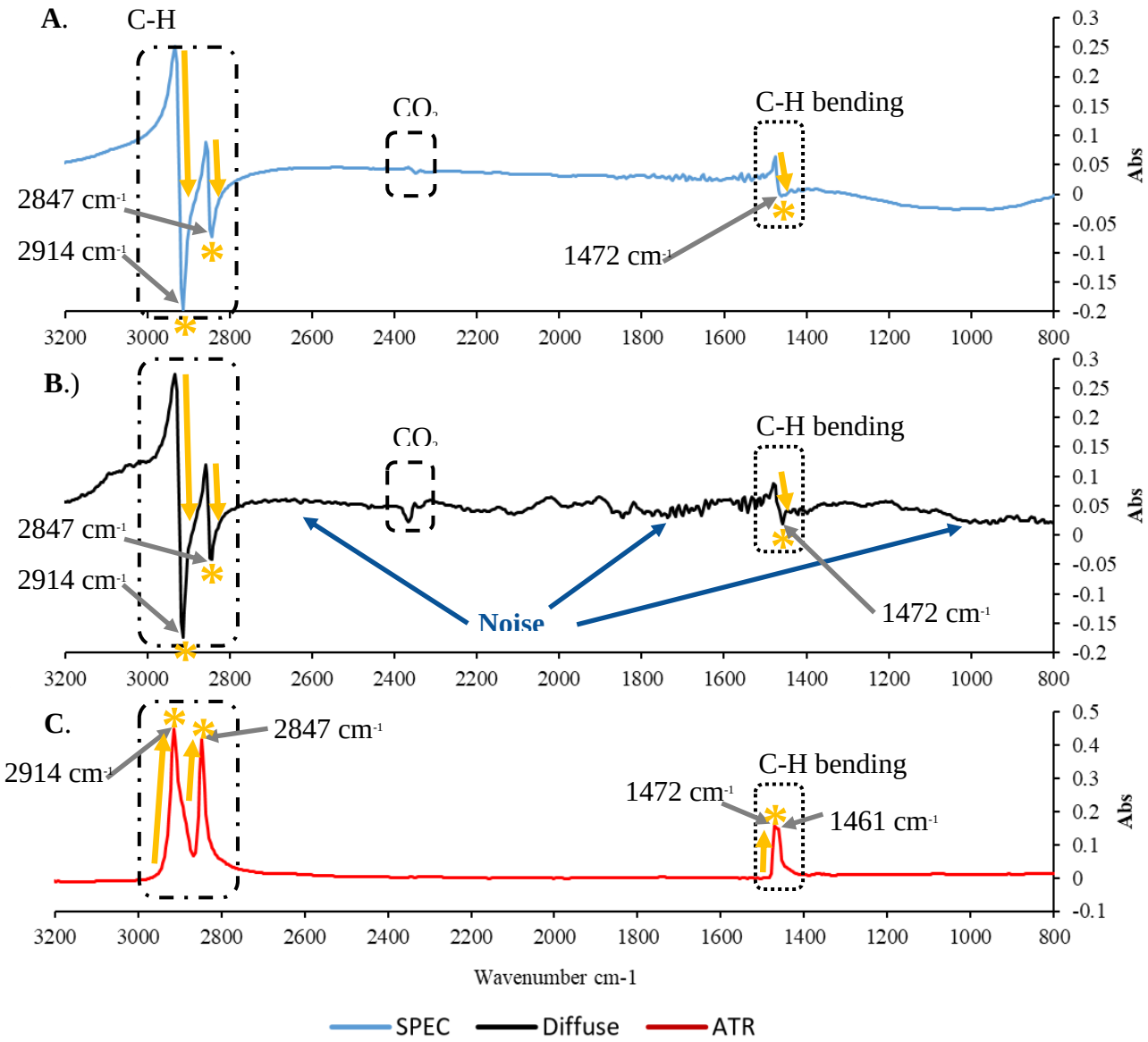

Figure 22: Three FTIR spectra of HDPE taken using ***A****.) Specular interface FTIR (blue),* ***B****.) Diffuse interface FTIR (black), and* ***C****.) ATR interface FTIR (red). HDPE peaks at 2914, 2847, 1472 and 1462 cm^{-1} have been highlighted. The Yellow Arrows highlight the direction of the peak. The Yellow Asterisks highlight the peak location for comparison between interface measurements.*

During the experiment, the HDPE pucks showed no significant physical changes and remained the same colour throughout. There are also no changes in chemical bond structure across both salt and air treatments in HDPE over the 429 hours (*Figure 23.A*). ATR measurements show a single change at 429 hours in the Air treatment. A peak at 1748 cm^{-1} can be observed and an increased absorbance over a broad area from 900 cm^{-1} and 1500 cm^{-1}. In comparison, the saltwater ATR treatment of HDPE shows no change from 0 to 429 hours (*Figure 23.B*). HDPE measured with the diffuse interface in the dry treatment (*Figure 23.C*) shows a development of negative peaks over the range from 900 cm^{-1} and 1500 cm^{-1}, much like the ATR spectra. A peak between 2300 cm^{-1} and 2400 cm^{-1} indicates the presence of CO_2 but remains unchanged from 0 - 429 hours. This CO_2 peak cannot be seen in the ATR measurements. A negative absorbance change can be seen at 2982 cm^{-1}. In comparison, the saltwater treatment does not show the peak change at 2982 cm^{-1}. There is however a peak increase at 172 hours indicating an increased CO_2 presence in the salt treatment (*Figure 23.D*). HDPE measured with the specular interface in the dry treatment shows no change in the samples between 0 - 429 hours, with the exception of a pronounced CO_2 double peak at 336 hours, which then disappears in the following measurement at 429 hours (*Figure 23.E*). The saltwater treatment shows no changes (*Figure 23.F*).

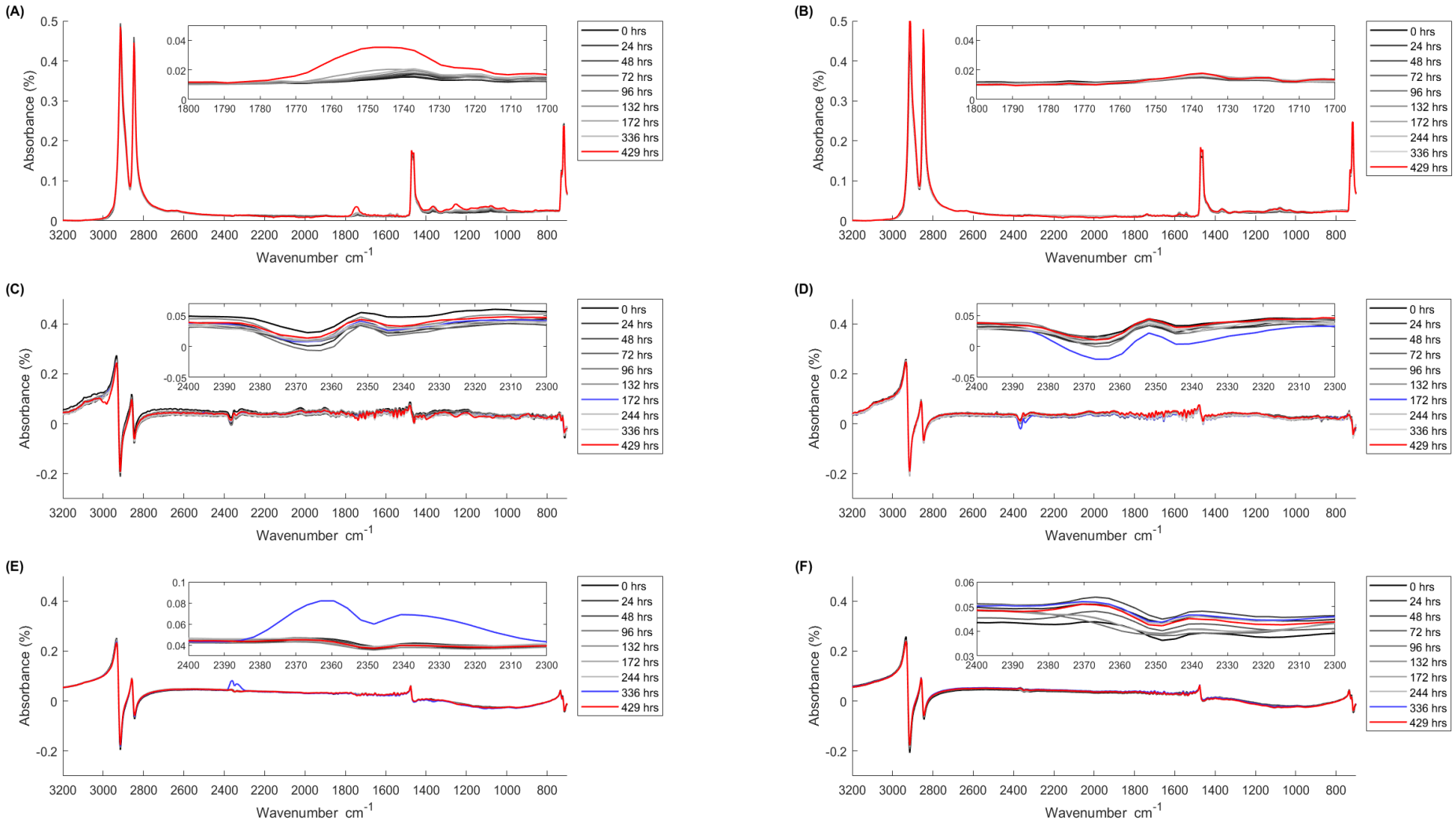

Figure 23: High Density Polyethylene (HDPE) FTIR absorption spectrum with respect to Wavenumber (cm^{-1}) showing the temporal degradation of the IR spectrum from 0 – 429 hours. Zero hours (Solid Black Line), 429 hours (Solid Red Line) and 24 – 366 hours (Solid Gradient Grey Lines, which transition from dark to light as a function of time). Each FTIR spectrum has been normalised using standard normal variate (SNV) and horizontally baseline correction. ***A.*** *Air treatment using an ATR interface.* ***B****. Salt treatment using an ATR interface.* ***C.*** *Air treatment using a Diffuse interface, 172 hours highlighted (Solid Blue Line).* ***D.*** *Salt treatment using a Diffuse interface, 172 hours highlighted (Solid blue line).* ***E.*** *Air treatment using a Specular interface, 336 hours highlighted (Solid Blue Line).* ***F****. Salt treatment using a Specular interface, 336 hours highlighted (Solid Blue Line). Regions of Interest in the spectra have be enlarged in each (sub)figure with the corresponding colours.*

PA (Nylon-66).

The PA pucks showed no physical changes, however, the samples appeared to yellow over time with the colour change more prevalent around the edges. The outer edges also become a lighter shade while still yellowing. The ATR results from PA show no peak differences in absorbance between the un-weathered and weathered PA. There is however, a clear decrease in absorption over the entire spectra. (*Figure 24.A*). The ATR saltwater treatment of PA also shows a decreased absorption but there is an initial jump of 0.1 absorbance from 0.5 to 0.6 between 0 hours and 24 hours. The gradual fall in absorbance starts from 24 hours to 429 hours where it returns to the initial level over the 429 hours (*Figure 24.B*). PA measured with the Diffuse interface in the dry treatment shows an overall lack of change up until 429 hours where changes can be seen (*Figure 24.C*). At 2978 cm^{-1}, negative peaks form. A negative peak between 2300 cm^{-1} and 2400 cm^{-1} remains present from 0 - 429 hours showing CO_2 fluctuations throughout the time series. There are also noticeable differences between the range 900 cm^{-1} and 1500 cm^{-1} at 429 hours, with large changes at 1383 cm^{-1}, 1150 cm^{-1}, and 950 cm^{-1} with negative peak formation. In comparison, the saltwater treatment does not show the peak formation at 2978 cm^{-1} or within the range 900 cm^{-1} to 1500 cm^{-1} (*Figure 24.D*). There is however a peak increase at 172 hours indicating fluctuations of CO_2 between 2300 cm^{-1} and 2400 cm^{-1}, much like the one seen in the HDPE data at this time (*Figure 24.D*). PA measured with the specular interface in the dry treatment shows no change in the samples between 0 - 429 hours (*Figure 24.E*). The saltwater treatment also shows no change over the time series (*Figure 24.F*), except for fluctuations in the CO_2 wavenumber bands changes between measurement intervals.

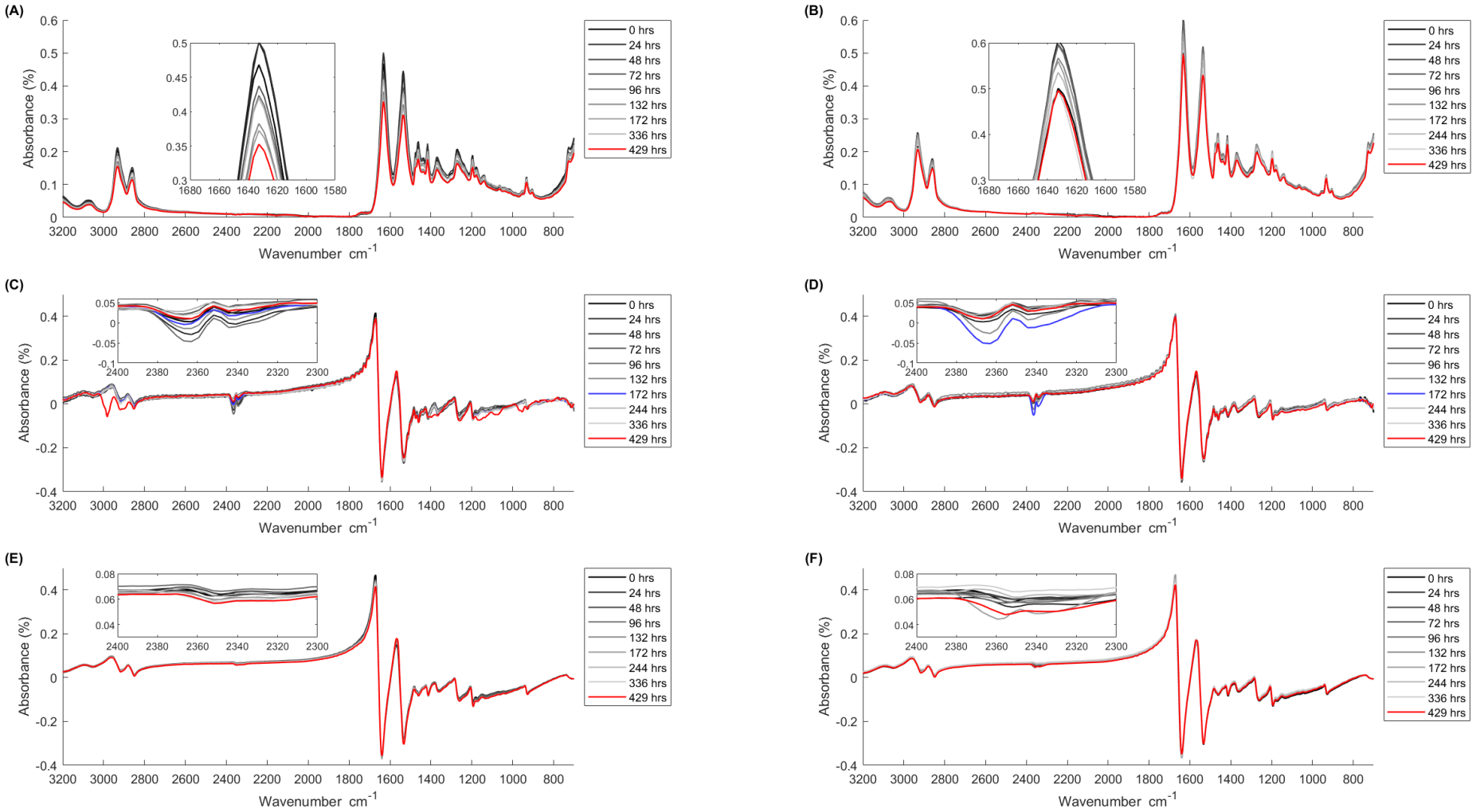

Figure 24: Polyamide (PA, Nylon 66) FTIR absorption spectrum with respect to Wavenumber (cm^{-1}) showing the temporal degradation of the IR spectrum from 0 – 429 hours. Zero hours (Solid Black Line), 429 hours (Solid Red Line) and 24 – 366 hours (Solid Gradient Grey Lines, which transition from dark to light as a function of time). Each FTIR spectrum has been normalised using standard normal variate (SNV) and horizontally baseline correction. ***A.*** *Air treatment using an ATR interface.* ***B****. Salt treatment using an ATR interface.* ***C.*** *Air treatment using a Diffuse interface, 172 hours highlighted (Solid Blue Line).* ***D.*** *Salt treatment using a Diffuse interface, 172 hours highlighted (Solid blue line).* ***E.*** *Air treatment using a Specular interface.* ***F****. Salt treatment using a Specular interface. Regions of Interest in the spectra have be enlarged in each (sub)figure with the corresponding colours.*

PET.

During the experiment, the PET pucks showed no significant physical changes and remained the same colour throughout. The ATR results from PET show no differences in absorbance in the dry treatments between 24 - 429 hours (*Figure 25.A*). The ATR saltwater treatment also shows no difference (*Figure 25.B*) except for a peak formation in absorbance at 132 hours. It can be observed that there is a gradual peak increase in the range 2800 - 3000 cm^{-1}, however the outlier at 132 hours does not fit this gradual increase. PA measured with the diffuse interface in the dry treatment (*Figure 25.C*) shows an overall lack of change until 429 hours where a single negative peak can be seen over the range 2800 - 3000 cm^{-1}. A peak between 2300 cm^{-1} and 2400 cm^{-1} indicates the presence of CO_2 but remains unchanged from 0 - 429 hours with fluctuations through the time series. In comparison, the saltwater treatment does not show the peak change seen over the range 2800 - 3000 cm^{-1} (*Figure 25.D*). Fluctuations in the CO_2 wavenumber bands can still be seen. PA measured with the specular interface in the dry treatment shows no change in the samples between 0 - 429 hours (*Figure 25.E*). There is a subtle decrease in absorption over the entire spectra, falling by 0.02 absorbance over the 429 hours. The saltwater treatment also shows a subtle decrease in absorption over the entire spectra, however only falling by 0.01 absorbance over the 429 hours (*Figure 25.F*).

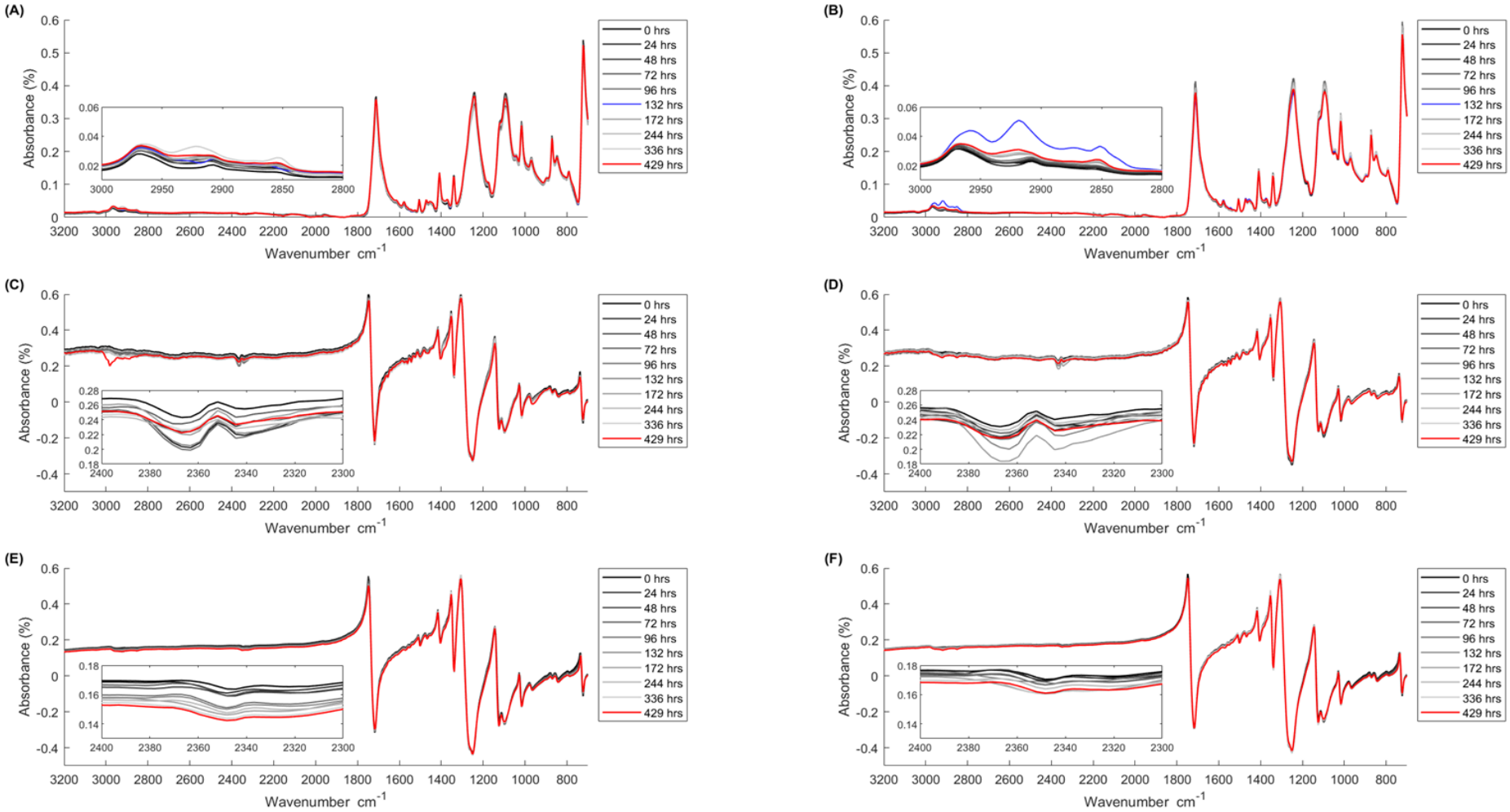

Figure 25: Polyethylene terephthanlate (PET) FTIR absorption spectrum with respect to Wavenumber (cm^{-1}) showing the temporal degradation of the IR spectrum from 0 – 429 hours. Zero hours (Solid Black Line), 429 hours (Solid Red Line) and 24 – 366 hours (Solid Gradient Grey Lines, which transition from dark to light as a function of time). Each FTIR spectrum has been normalised using standard normal variate (SNV) and horizontally baseline correction. ***A.*** *Air treatment using an ATR interface, 132 hours highlighted (Solid Blue Line).* ***B****. Salt treatment using an ATR interface, 132 hours highlighted (Solid Blue Line).* ***C.*** *Air treatment using a Diffuse interface.* ***D.*** *Salt treatment using a Diffuse interface.* ***E.*** *Air treatment using a Specular interface.* ***F****. Salt treatment using a Specular interface. Regions of Interest in the spectra have be enlarged in each (sub)figure with the corresponding colours.*

PP.

The ATR results from PP show no differences in absorbance between treatments over the whole experiment (*Figure 26.A*). At 24 hours, the baseline of the spectra seems to pull away from the other spectra with wavenumber less than 2600 cm^{-1}. ATR is known to have a wavenumber specific depth of penetration that could have caused the effect. The spectrum shape doesn't appear to change only the baseline pointing towards this being an outlier as all software processing steps remain the same. The ATR saltwater treatment of PP shows no difference (*Figure 26.B*). PP measured with the diffuse interface in the dry treatment shows no change until 429 hours where a peak can be seen over the range 2800 - 3000 cm^{-1} (*Figure 26.C*). A negative double peak between 2300 cm^{-1} and 2400 cm^{-1}, again indicating CO_2 fluctuations, reaching a minimum absorption at 96 hours but fluctuates through the time series. In comparison, the saltwater treatment does not show the peak change at 2989 cm^{-1} (*Figure 26.D*). Fluctuations between the CO_2 wavenumber bands can still be seen; however, the minimum absorbance is at 172 hours. PP measured with the specular interface in the dry treatment shows almost no change in the samples between 0 - 429 hours (*Figure 26.E*). Fluctuations between 2300 cm^{-1} and 2400 cm^{-1} are again present, however the minimum absorbance occurs at 336 hours, only to rise again at 429 hours. The saltwater treatment shows a similar CO_2 fluctuation, however with a minimum absorbance at 132 hours (*Figure 26.F*).

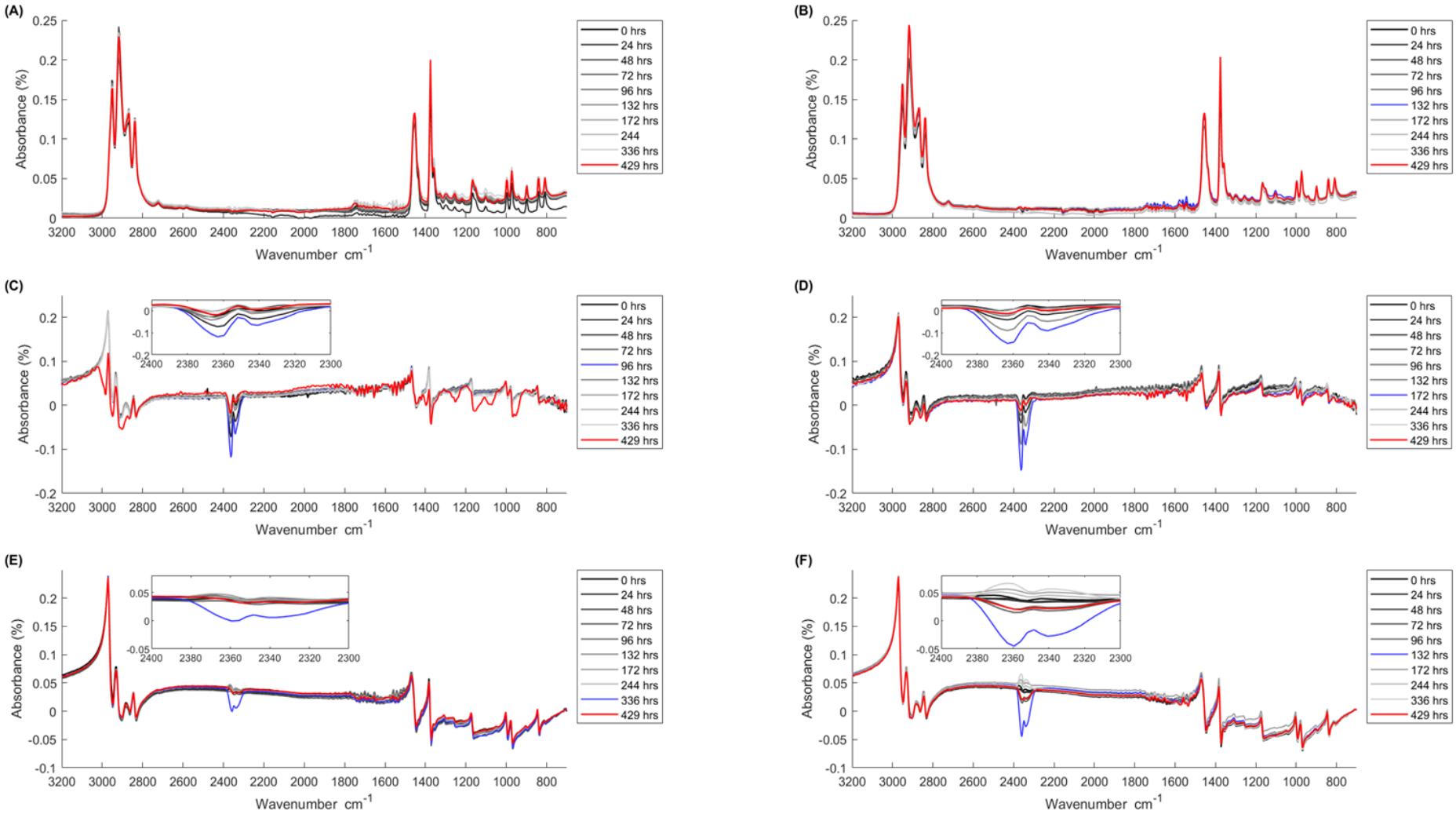

Figure 26: Polypropylene (PP) FTIR absorption spectrum with respect to Wavenumber (cm^{-1}) showing the temporal degradation of the IR spectrum from 0 – 429 hours. Zero hours (Solid Black Line), 429 hours (Solid Red Line) and 24 – 366 hours (Solid Gradient Grey Lines, which transition from dark to light as a function of time). Each FTIR spectrum has been normalised using standard normal variate (SNV) and horizontally baseline correction. ***A.*** *Air treatment using an ATR interface.* ***B****. Salt treatment using an ATR interface.* ***C.*** *Air treatment using a Diffuse interface, 96 hours highlights (Solid Blue Line).* ***D.*** *Salt treatment using a Diffuse interface, 172 hours highlights (Solid Blue Line).* ***E.*** *Air treatment using a Specular interface, 366 hours highlights (Solid Blue Line).* ***F****. Salt treatment using a Specular interface, 132 hours highlights (Solid Blue Line). Regions of Interest in the spectra have be enlarged in each (sub)figure with the corresponding colours.*

PS.

During the experiment, the PS pucks showed no significant physical changes and remained the same colour throughout. The ATR results from PS show no differences in absorbance between 24 - 336 hours (*Figure 27.A*). At 429 hours, peaks at 2919 cm^{-1}, 1756 cm^{-1} and 1249 cm^{-1} diminish in size. The saltwater treatment shows no difference from 0 - 429 hours (*Figure 27.B*). PS measured with the diffuse interface in the dry treatment shows no change, but the spectra appear to have more noise (*Figure 27.C*). This also seems to be a reduction in absorbance over the entire spectra >800 cm^{-1} over the time series. This could be the first signs of weathering of any of the plastics tested. PS is known to degrade at a much faster rate than other plastics. The diffuse interface is ideal to pick up on the physical changes of the plastic surface. In comparison, the saltwater treatment also shows a downwards shift over the entire spectra but to a lesser extent (*Figure 27.D*). Fluctuations at the CO_2 wavenumber bands can also be seen in both air and salt treatments. PS measured with the specular interface in the dry treatment shows almost no change in the samples between 0 - 429 hours (*Figure 27.E*). A CO_2 double peak between 2300 cm^{-1} and 2400 cm^{-1} can be seen at 132 hours, no other fluctuations can be seen in either air or salt treatments. Both treatments also show a decrease in peak height at 1590 cm^{-1} which is not present in the ATR or Diffuse measurements (*Figure 27.F*).

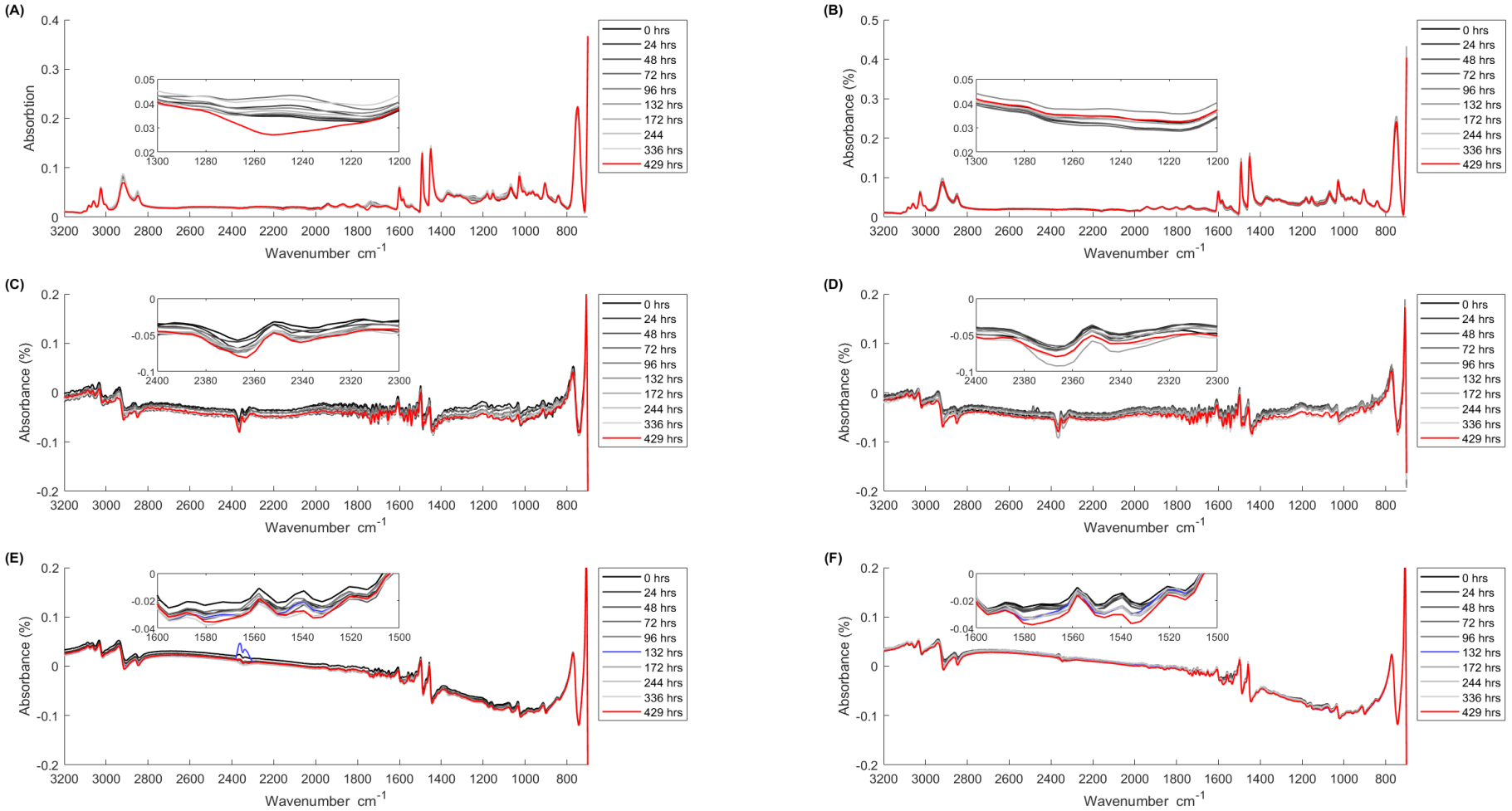

Figure 27: Polystyrene (PS) FTIR absorption spectrum with respect to Wavenumber (cm^{-1}) showing the temporal degradation of the IR spectrum from 0 – 429 hours. Zero hours (Solid Black Line), 429 hours (Solid Red Line) and 24 – 366 hours (Solid Gradient Grey Lines, which transition from dark to light as a function of time). Each FTIR spectrum has been normalised using standard normal variate (SNV) and horizontally baseline correction. ***A.*** *Air treatment using an ATR interface.* ***B****. Salt treatment using an ATR interface.* ***C.*** *Air treatment using a Diffuse interface.* ***D.*** *Salt treatment using a Diffuse interface.* ***E.*** *Air treatment using a Specular interface, 132 hours highlights (Solid Blue Line).* ***F****. Salt treatment using a Specular interface, 132 hours highlights (Solid Blue Line). Regions of Interest in the spectra have be enlarged in each (sub)figure with the corresponding colours.*

3.3 Presence of CO_2

The CO_2 fluctuations seen in the FTIR data were explored to explain the occurrences. The CO_2 FTIR peak area absorption results from a single breath aimed towards the specular FTIR interface on the Agilent 4300 handheld FTIR are shown in Figure 28. A time series of repeated measurements from R1 (Initial breath) to R15 (Recalibration) and beyond to R20 were collected (*Figure 28*). The initial breath (R1) was larger in the air movement treatment than in the no air movement treatment (*Figure 28*). The fan was only turned on after the initial breath to get similar CO_2 starting concentrations. It can be seen with both the air movement and no air movement treatments that moving the sample and replacing it caused mixing of the air in the interface chamber with the external laboratory atmospheric air. With no air movement, the CO_2 leaves the chamber in a linear fashion. Whereas exponential decay of the CO_2 in the interface chamber is seen with the air movement. By R15 there is still CO_2 remaining in the interface chamber from the initial breath with no air movement, whereas there is no CO_2 left with the air movement, having plateaued and reached equilibrium with the laboratory atmosphere by R10 (*Figure 28*). At R12 in the air movement treatment a small amount of CO_2 is present but disappears again in the next measurement. After the second background measurement has been taken the CO_2 that was remaining in the chamber has been set as the baseline CO_2 by the instrument. The CO_2 continues to leave the interface chamber in a linear fashion as before, however a negative average peak area is then measured. The air peak area in the air movement treatment remains at a low level even after the second background scan (*Figure 28*).

These results show that CO_2 remains in the chamber after a single breath. The data collected during the weathering experiment had no air movement and so the effect of a single breath would have a big impact on the data, persisting throughout the measurements.

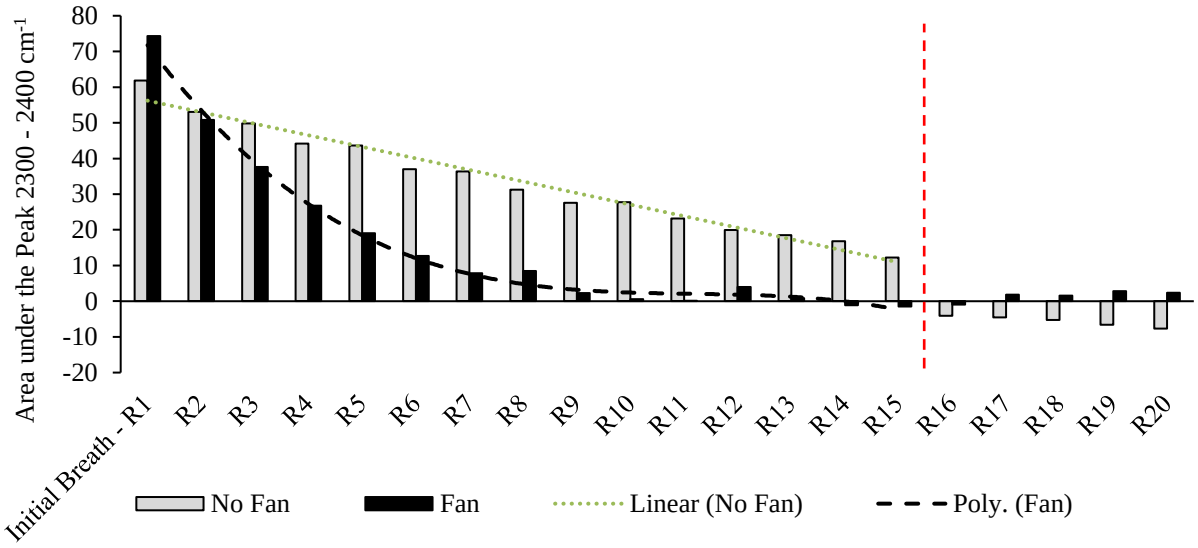

Figure 28: The peak area between 2300 cm^{-1} and 2400 cm^{-1} showing the CO_2 FTIR absorbtion from a single breath aimed at the specular FTIR interface on the Agilent 4300 handheld FTIR. Time series of repeat measurments from R1 (Initial breath) to R15 (New background collection, ***Red dashed line****) and after to R20.*

4. Discussion

4.1 Irradiance of UVR

4.1.1 Irradiance equivalence

It is common for authors to report the energy output of the light source as a single metric, with no regards to the wavelength range covered or wavelength specific intensities (Chen *et al.*, 2019; Gewert *et al.*, 2018). Some authors do not even report the irradiance levels (Cai *et al.*, 2018; Leonas, 1993). For the comparisons of studies looking at photooxidative degradation using laboratory setups however, it is difficult to scale the energy if the wavelength intensities are not known. Even more so if the wavelength ranges are not specified at all. In this thesis, the spectral irradiance was integrated over the wavelength range 280-320 nm and 320 - 400 nm, which aligns with the agreed UVB and UVA ranges respectively and was measured in W/m^2.

The approach of comparing weathering results based on the time (Weathering per Day) makes many assumptions about the experimental parameters. Firstly: this approach assumes that the daily irradiance of a given location (latitude) is the same. This is used to calculate the number of days that a given irradiance equates to in the environment. Secondly: the amount of energy that is received by the samples is integrated over the same wavelength range, i.e. 280 - 400 nm. Finally, the distribution of the energy within the wavelength range must be the same.

4.1.2 Irradiance design

In the design presented here, two independent light sources were implemented: An Exo Terra Reptile UVB 200 lamp with a peak output at 325 nm and an array of 1500 LEDs consisting of four different wavelengths of light, namely; 395 nm, 390 nm, 378 nm, and 365 nm. This design was an evolution of previous work using independent UVA and UVB lamps (Tang *et al.*, 2019). To condense the system and to provide a more even energy field over the samples, the UVA fluorescent tubes were replaced by LEDs. This was only the second design to the author's knowledge that has used LEDs as part of the irradiance source in a weathering study, the first being Chen *et al.* (2019), using a single 400 nm LED lamp coupled with a fluorescent UV lamp (365 nm; UVP, UVL-21, Analytik Jena, Upland, CA). This design had a much smaller area to irradiate, whereas the design presented here irradiated a 300 mm x 400 mm area.

This light rig required active cooling. The cooling reduced the UVB output down to environmentally relevant levels. In doing so the life expectancy of the fluorescent lamp was reduced causing irradiance decay over time. However, the cooling increased the life expectancy of the 1500 LEDs ensuring that they would last over long experiments without burning out. These competing and independent systems made alterations to the spectra hard to achieve. The use of both LEDs and fluorescent tubes to create a single spectrum was not the best implementation, and future work should stick with either all LEDs or all fluorescent lamps. This will make adjusting the spectra much easier. LEDs are hard to source that produce UVB wavelengths and so could not be implemented in this design. This led to the wavelength range from 310 - 365 to be missing from the produced spectrum using this system (*Figure 17*). This caused the irradiance from the rig to be much less than the standard solar irradiance integrated over the range 280 - 400 nm (UVA and UVB). However, the irradiance energy output from the rig, over the full UVR range, was similar to that of the solar spectrum in Hull, UK and Northern

Germany. By the standard of reporting a single irradiance value, the energy reported here fits with the irradiance values of other works. However, the known lack of wavelengths between 310 and 365 mean that direct environmental comparison should be done carefully, and future works should seek to close the knowledge gap.

The spectrum used for each experiment should be reported to provide a better understanding of the irradiance energy reported in weathering studies. Ratios between sections of the spectrum would also aid in standardising the reported irradiance values. As UVA and UVB are already defined regions of UVR, providing a ratio between the irradiance in these wavelength ranges would allow for much better comparison between studies. There is also a need to produce action spectra from the plastics under study to quantify the effect each wavelength has on the plastic. Only a few papers have detailed action spectra for plastics, and the literature is still in its infancy (Vaskuri *et al.*, 2017; Ktimpf, Sommer & Zirngiebl, 1991). These action spectra would then allow for the effect of the wavelength specific irradiance to be known.

4.1.2.1 Future work - Action Spectra

UVB is known to cause more photo-oxidative degradation than UVA (Andrady, 2011; Ktimpf, Sommer & Zirngiebl, 1990), and therefore must be taken into account. An action spectrum defines the effect each wavelength will have on a material during weathering providing a way to account for the effect of UVB over UVA. This can be measured by determining the yellowing of the plastic over exposure time to specific wavelengths of light (Vaskuri *et al.*, 2017), radical formation (Ktimpf, Sommer & Zirngiebl, 1991) or any quantifiable measure of degradation over time. Figure 29 illustrates the effect of a hypothetical action spectrum which increases the effect of UVB energy. This action spectrum is applied as a multiplication factor to each wavelength for simplicity. From this simple calculation, the 'effective energy' that a sample would receive can be calculated, taking into account potential

of each wavelength to degrade the sample. This 'effective energy' can be compared to the total irradiance energy that has been measured, to highlight the influence that each wavelength has on the degradation (*Figure 29*). Three spectra, with a total energy of 39.0 W/m^2 are compared. When applying the weighted function of the action spectra to the irradiance energy at each wavelength, the 'effective energy' of each spectrum changes. The spectrum with more UVB, has an 'effective energy' of 53.0 w/m^2 compared with the 43.2 W/m^2 of the spectrum with higher UVA (*Figure 29*). All three spectra have the same irradiance of 39 W/m^2, however the effect that each spectrum has on the sample is different, with spectrum containing more UVB having a greater effect.

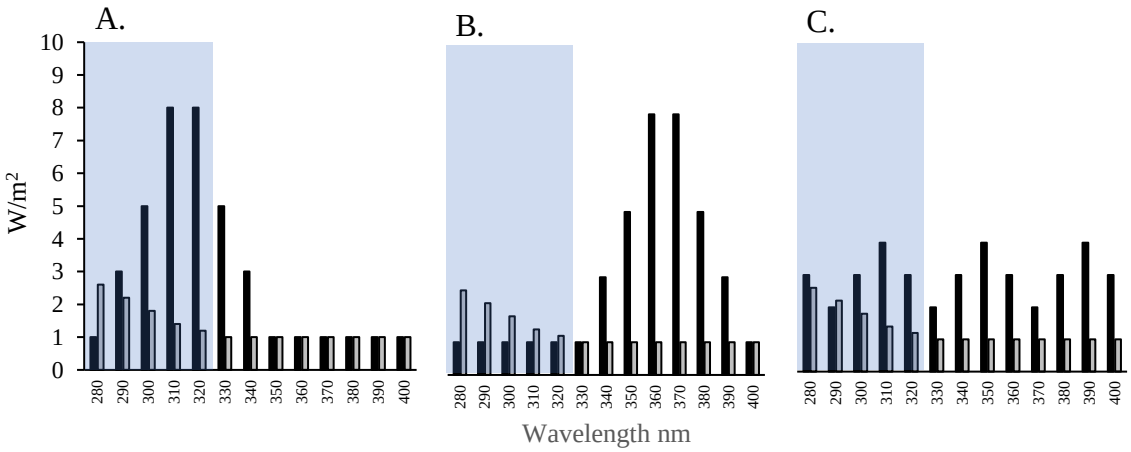

	A	*B*	*C*
Total Energy	*39*	*39*	*39*
Effective Energy	*53*	*43.2*	*50.8*

Figure 29: An ilistration of an action spectra is applied as a multiplication factor to each wavelength to calculate the 'effective energy' that a sample would receive given the potential of each wavelength to degrade the sample. ***Black bars*** *show the spectrum in each graph. The* ***Blue area*** *highlights the UVB portion of the spectrum affected by the action spectra. The* ***Grey bars*** *show the applied action spectrum which is identical in each graph.* ***A.*** *UVB weighted spectrum.* ***B.*** *UVA weighted spectrum.* ***C.*** *Even spectrum.*

It is therefore an oversight to relate two studies without knowing: the energy at each wavelength, or at the very least the ratio between UVA to UVB; The wavelength range which the energy was measured over; and the specific energies of each wavelength (Spectrum). These values should be reported for a comparison to be made. Further work should be undertaken to create comprehensive action spectra for plastics, which at the time of writing, have not been developed for community wide usage.

4.1.3 Spread of light

A uniform spread of the light over the samples under test ensures that each of the samples received the same amount of UVR, ensuring the sample can be reliably compared once weathered. Andrade *et al.* (2019) measured the irradiance of the UVR at the bottom of their custom designed weather-o-meter (*Pyrex measuring tubes*), however the plastic samples were free to move within the experimental tubes. This meant that the pathlength from source to sample was constantly changing, and the illumination was therefore variable and incompletely constrained, and as the spectrum was not taken under water the spectrum acting on the plastics may not be the same as produced by the light. In this thesis, the implementation of a borofloat glass sheet allowed the spectra to be taken under a pathlength of 1cm of saltwater. This was possible due to the design of the rig and its adaptability. Andrade *et al.* (2019) also reorder the positions of the sample tubes throughout the experiment to ensure the samples got similar irradiance. This complicates analysis of the measured weathering in relation to the light emitted from the source, as some form of averaging and estimation of the received illumination must have been done. Ultimately, an even energy illumination field will yield more reproducible results. In the design presented here, a uniform energy field was produced using fluorescent lamps and LED strips stretching the entire length of the weathering area. To ensure equal energy output from the LED these were wired in parallel between a live and neutral track which

ran the length of the LED strip. This was connected at both ends to avoid voltage drop over the five meter length of the LED strip cable. Using a novel calibration table design (*Figure 8*), the energy field was measured at an exact distance from the light source. This distance can be set depending on the application, ensuring that the measured irradiance is the same as the energy that will be received by the sample surface. This measured energy is also taken over a wide area to ensure that all the samples within a given area are receiving the same energy. This design and implementation offer a more accurate and quantifiable way to measure the irradiance in a more reproducible way than previously published systems. The calibration table also allows the irradiance of the light rig assembly to be measured over time to account for any energy difference over the length of the experiment, which is not considered in previous experiments (Andrade *et al.*, 2019; (Rummel *et al.*, 2019; Chen *et al.*, 2019; Gewert *et al.*, 2018; Cai *et al.*, 2018)

4.1.4 Irradiance decay

It is generally assumed that the law of reciprocity applies during photooxidative weathering. It states that 'for the same cumulative UV energy under two types of ageing, the degradation degrees are similar even if light intensities differ' (Badji *et al.*, 2018). It is also assumed that the output from the lamps is the same at the end of the experiment as the beginning. As a consequence, authors do not provide spectrum or note whether it has changed throughout their experiment. However, the assumption that there is no change in the lamps output throughout time is known to be incorrect. As reported by Kalogerakis *et al.* (2017) the energy received is not always linear with time, especially when using natural solar radiation. The Q-LAB QUV chamber can be fitted with a Solar Eye® (Q-Lab, Bolton, UK) to adjust the irradiance throughout the weathering experiment due to the known fluctuations of the lamps over time (Philip & Al-Azzawi, 2018). Future work must engage with this question of irradiance stability of the systems used rather than ignore it. In custom rigs, periodic measuring

of the irradiance decay allows for any differences to be accounted for and corrected for during the experimentation or in post calculations. Wavelength specific irradiance changes are not reported in other work and are assumed fixed output over time. Here, using the system developed in this thesis, the aim was to calibrate the light rig every month by collecting an energy map of the rig. However, only two were collected due to the shutdown of the experiment due to the COVID-19 pandemic and so patterns over time cannot be assessed.

The irradiance of the light rig used in this work, shows an overall decrease of 1.3% and 2.9% in irradiance over the 25-day experiment in the saltwater and air treatments respectively (*Figure 16*). The larger irradiance decay in the air treatment is largely due to the movement of the LEDs rather than a decay in irradiance output by the rig (*Figure 18*). The irradiance of the UVB from the fluorescent tubes remained relatively constant in comparison to the UVA LEDs which changed significantly. This can be explained by movement of the LEDs through changing the mounting angles of the LEDs during use. As the plastic samples are removed to be measured, the light rig is lifted and moved. This seems to have changed the position of the reflectors causing the spectra that the plastic receives between measurement times to change. Reducing the irradiance of 1 LED strip (Wavelength of LED), increases another based on the angle and height from the plastic samples surface (*Figure 18*). The outermost LED strip mounted on the reflectors was emitting 395 nm wavelength of light, and so any movement of the reflectors would cause the greatest movement of these LEDs. Therefore, the peak at 395 nm shows the most fluctuation in the air treatment light rig. The ability of the reflectors with the LEDs attached to move around the fluorescent lamps was a flaw in the design. Future designs must consider the stability of the light rigs and their ability to withstand being moved. Any movement introduces error into the calculations of irradiance over time and recalibration of the setup throughout the weathering becomes crucial.

The use of the calibration table to quantify the irradiance change and decay throughout a weathering experiment using a custom designed weather-o-meter has been proposed. Regular measurements of the irradiance output are suggested here. To build on this idea of monitoring irradiance changes, it might be possible to build in a logging function and capability of the spectrum throughout the weathering process, similar to that of the Q-LAB Solar Eye® but built with a logging function. However, the use of the calibration table used here allows not only for changes in the spectrum to be tracked but also any changes over the energy field.

4.2 Lamp cooling

Cooling xenon arc lamps has been implemented by Rummel *et al.* (2019) and Gewert *et al.* (2018). This is necessary because the heat from the lamps raises the temperature of the samples, even while supplying strong air flow for cooling. Gewert *et al.* (2018) maintained the temperature of the samples at 35℃ using cool air supplies via a pipe directive at the xenon arc lamp. Q-Lab QUV chambers on the other hand are not actively cooled. The average temperature of the chamber being 40 - 60℃ as set by industrial standards (Hirsch, Barel & Segal, 2019; Lizárraga-Laborín *et al.*, 2018; Philip & Al-Azzawi, 2018). Temperature measurements of the fluorescent tubes used here were measured at 44℃, taking 25 minutes to reach thermal equilibrium in the laboratory with an ambient temperature of 17.5℃ (*Figure 30*). The QUV chambers also use fluorescent lamps which will have a similar operational temperature. This could explain why the Q-Labs weather-o-meters operate at these elevated temperatures, in comparison to the environment, other than for accelerating the weathering process (Table 1). In the design presented here, the fluorescent lamps operated at 22℃ when under cooling, whereas the normal (optimal) operating temperature is 44℃ (*Figure 30*). The cooling of the rig in this work served the purpose of reducing the irradiance from the fluorescent lamps, however in doing so, the filament within the fluorescent lamp (Cathode) remained cold

and was prevented from getting up to optimal working temperature. When cold, the ions have a higher velocity when impacting due to the higher work function. This knocks metal atoms off the cathode in the process. This greatly reduced the life of filament, causing the ends of the lamp to darken as metal from the cathode is knocked off causing metal dust to coat the inner surface (Cosine Developments, 2016). Over a longer experiment the output from the lamp could be expected to fall. A better implementation of the fluorescent tubes would be to raise the lamps higher away from the samples to reduce the irradiance, rather than cooling the lamp to suppress the irradiance output. This could be easily implemented using the proposed system by simply raising the light rig higher above the weathering chamber. This is planned for future

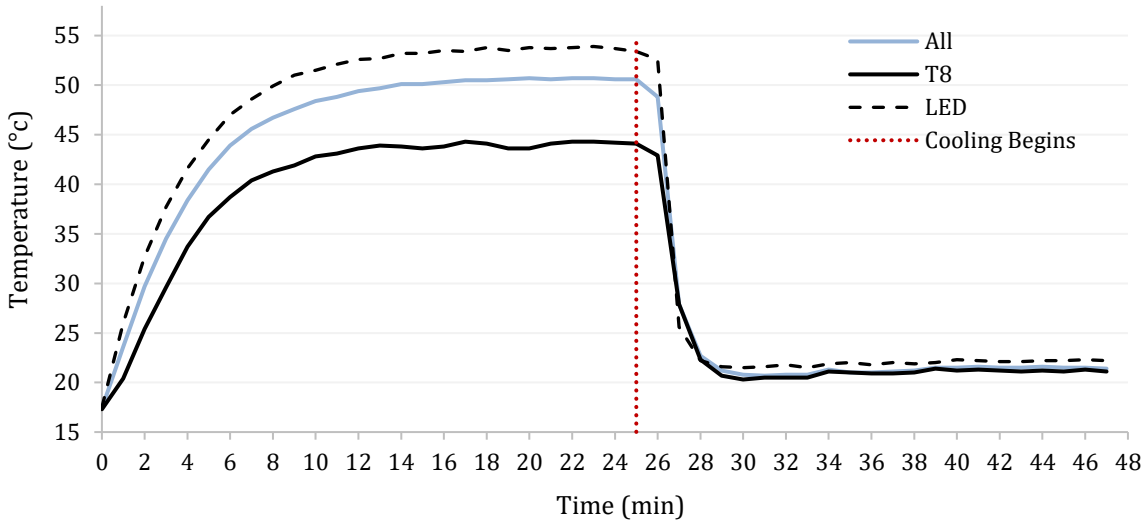

work, extending the life of the lamps and reducing the irradiance decay due to cooling the lamps.

*Figure 30: Graph showing the heating and cooling profiles of the light rig. The temperature of the fluorescent lamp (**Solid black line**), the temperature of a LED mounted to the reflector (**Dashed black line**) and All, the Average over a section of the rig containing both fluorescent lamp and LEDs (**Solid light blue line**).*

4.3 Oxygen availability

The photo-oxidative degradation of plastics required oxygen. The production of carbonyl groups (C=O bonded) in plastic samples increases with increased oxygen pressure (Richaud *et al.*, 2006). It is known that in the marine environment the concentration of oxygen is reduced, containing only 3.8% of that present in air (Fondriest Environmental, Inc., 2013). This reduced oxygen retards the effect of photo-oxidative degradation (Andrady, 2011). The lack of surface mixing of oxygen below the water's surface further limits the photo-oxidative degradation pathway (Gewert, Plassmann & MacLeod, 2015). The design proposed by Gewert *et al.* (2018) consists of 6 sealed 350 ml glass bottles filled with 250 ml of Milli-Q water (RODI). This same design has also been implemented by Rummel *et al.* (2019), adopting saltwater instead of Milli-Q water, with both designs based on the design used by Gardette *et al.* (2013). The use of sealed bottles was implemented to ensure both the positively and negatively buoyant plastic samples were irradiated equally while rotating around the light source. Due to the light source used, 5 days in this design was calculated to be the equivalent of 513 days of simulated radiation. This design was not designed for long experiments due to the accelerated nature of weathering. Over the 5 days, oxygen depletion within the sealed bottles was not addressed by these authors. However, this design has the potential to deplete oxygen within the small volume of water and air within the bottles, especially during longer experiments. More environmentally relevant weathering experiments would require much longer exposure times, and so the depletion of oxygen could become a limiting factor. The design presented by this thesis can subject all of the samples to the same irradiance, irrespective of buoyancy, while not limiting oxygen. By fixing the location of the samples to a weathering stage, the buoyancy of the samples was removed as a complicating factor. This allowed the design presented here, to remove the need for the rotation around the light, requiring the bottles to be sealed. Furthermore, as the water used in our system is in a closed circuit, the formation

of leachates could be researched using this weather-o-meter without the concern regarding oxygen availability as the samples and water would be in contact with the air. This implementation of the rig would however miss the leachates which can dissolve or outgas from the sample during weathering. The movement of the water's surface within the weathering chamber, rising and falling during the flood and drain cycle also acts like a baffle. This pushes and pulls air in and out of the weathering chamber as it cycles, thus replenishing the air within the chamber. The CEL also had fresh air supply from the air conditioning unit, bringing fresh air in the lab. The only concern regarding the oxygen content of the water is that due to the low energy movement of the water, there was little to no surface agitation, so oxygen replenishment to the water and spread within the water as entirely by diffusion. To solve this in future designs, the addition of an air pump within the reservoir could oxygenate the water without affecting the weathering chamber (i.e. Low splash and no ripples).

4.4 Introduction of Saltwater

Many weather-o-meters on the market today have a wetting and drying function built into the weathering chamber. This is usually achieved by spraying the materials under test with freshwater and then allowing the samples to dry. In the marine environment however, samples will not have the opportunity to dry as they are constantly moved and flipped by the water movement on the surface boundary layer. It is estimated that marine debris is submerged 60% of the time, caused by waves and wind mixing (Kukulka *et al.*, 2012). The approach of spraying water may simulate rain for terrestrial environments, however, does not represent the exposure of saltwater in the marine environment. Spray will also rapidly lead to mineral build-up, where there is a dissolved content within the water (Salts), on the spray nozzle, the UVR filter, the inside of the experimental chamber and the material being tested. This mineral accumulation can cause localised increase in salinity, an overall decrease in the salinity of the circulated saltwater and create spots where the plastic surface is no longer receiving illumination. The mineral can also block pipes, coat and corrode surfaces and lead to severely impaired performance of equipment and shortened lifetime for the rig. Industrial salt spray corrosion cabinets are available but without UVR exposure to the samples, and no commercial device has yet been brought to market resolving these difficulties (Q-Lab pers. Comm., 2019).

Our unique instrument implements a novel, low energy introduction of saltwater. This method utilises a large and externally-accessible reservoir of the water, which can be monitored for changes in composition to maintain salinity and replaced with fresh solution as needed. It also introduces seawater to the surface of the plastic samples without generating spray aerosols which contaminate the instrument, by implementing a flooding and draining cycle. This is a significant advance for experimental studies of marine plastic weathering.

4.4.1 Salinity maintenance

Evaporation is expected in all setups however, especially when the water is exposed to the high temperature of the weathering lamps. Cai *et al.* (2018) weathered plastic pellets within a custom weather-o-meter, placing the pellets inside glass petri dishes in air, fresh and saltwater treatments for 3 months. The method of salinity maintenance is not reported but it can be assumed that the salinity would have fluctuated significantly within the petri dish within the 3 months. Kalogerakis *et al.* (2017) also omitted the reporting of salinity, focusing on logging light and temperature over the 6 month experiment. Some weathering experiments are so short (24 hours) that the effect of evaporation is negligible (Chen *et al.*, 2019) or are sealed to prevent loss of water all together (Rummel *et al.*, 2019; Gewert *et al.*, 2018; Gardette *et al.*, 2013). Andrade *et al.* (2019) had the opinion that the involvement of 'pumps and tubes' may be inconvenient to maintain salinity, and so opted for small containers of liquid. Andrade *et al.* (2019) also stated that each container was topped up with plain water to account for evaporation, However the scale of evaporation was not reported. Here we show that the implementation of 'pumps and tubes' provided accurate and stable conditions throughout the experiment, while also straightforwardly automated.

To maintain salinity in the novel design presented here, an Auto Top-Off (ATO) system which adds pure Reverse Osmosis Di-Ionised (RODI) water back into the system is an essential automation process to ensure stability. A simple float switch was adequate to control the ATO systems. The simplicity of the design ensured that the water level, and therefore salinity was maintained throughout the experiment. The specific gravity of the saltwater (salinity) was maintained at 1.025 g/cm^3 (35 ‰ ppt) throughout the entire experiment. The only intervention on the part of the researcher was to maintain a supply of RODI in the ATO reservoir. However, during the 25 days of the experiment only 20 litres of the 25-litre reserve was used.

4.4.2 Flood-Drain cycle

A key goal for this experiment was to develop a novel way of introducing saltwater into the experiment. The majority of the commercially available units on the market today spray freshwater onto the surface of the samples in an attempt to simulate rain. This is an unsuitable method of dispersal for saltwater. Halite crystal build-up and salt spray residue was addressed in the custom weather-o-meter design by implementing a low energy saltwater flood and drain cycle. This was achieved by slowly filling and draining the weathering chamber with saltwater. This approach prevented splashing and water agitation, thus reducing evaporation and the formation of salt crystals. This also ensured the boro-float glass filter remained clean and residue free. The water surface also remained almost ripple free ensuring the UVR would pass through the filter and surface boundary layer with minimal lensing effects due to water droplets and ripples. This design can also be programmed, to subject the samples to varying degrees of water exposure with periodic fluctuation, both in the height of the water within the chamber and the duration. If so desired, the samples could remain completely submerged while supplying circulating saltwater, with only minor alterations needed to the setup. This could be useful to look at the weathering of non-neustonic plastics in the sublittoral zones influenced by tidal depth changes. This setup does have far more moving parts and control systems compared to other custom weathering experiments. However, the versatility of the design and ease of setup clearly shows that the design presented here is an effective way of adding saltwater to a weathering system without the aforementioned issues. This design also prevents the effect of mechanical breakdown of the weathered plastics. Mechanical degradation is known to lead to the formation of both microplastics (Hebner & Maurer-Jones, 2020; Chen *et al.*, 2019; Biber, Foggo & Thompson, 2019; Julienne, Delorme & Lagarde, 2019) and nanoplastics (Tian *et al.*, 2019; Shen *et al.*, 2019). This process is usually amplified by the reduction in tensile strength and brittleness caused by photodegradation (Biber, Foggo & Thompson, 2019; Arias

Villamizar & Vázquez Morillas, 2018; Biesinger, Corcoran & Walzak, 2011). The novel flood / drain design prevents the plastics from moving and colliding and erosion of the surface layer. This ensures that long experiments can be carried out preventing the weathering data being 'reset' as un-weathered plastic is exposed. No other plastic weathering papers have been found utilising this method of saltwater weathering.

4.5 Recurring results

From all the FTIR weathering data, three recurring trends emerged. The first being that over the 429 hours, little weathering was seen in the FTIR data. The second being that CO_2 fluctuations were present in both the diffuse and specular FTIR measurements. And finally, for all plastic types, it was clear to see that at 429 hours, when measuring with the diffuse interface, there was a negative peak formation (Peak absorbance decrease) that was often coupled with similar absorption decrease in the range 900 - 1500 cm^{-1}. Each of these data trends are reported here.

4.5.1 CO_2(g) Fluctuations

CO_2(g) is known to absorb IR radiation (Vincent, Urasinska-Wojcik & Gardner, 2015), and can be resolved by FTIR (Yang et al., 2020). Fluctuations in the FTIR spectra occurred between 2300 - 2400 cm^{-1}. The Asymmetric stretch of the CO_2 occurs in this range, with a prominent double peak (Yang *et al.*, 2020). This peak was visible on measurements taken with both the diffuse and specular interface on the Agilent 4300 handheld FTIR. However, these peaks were not seen in the ATR measurements. The CO_2 peaks in the data occur at random throughout the time series, showing no progressive increase or decrease between each measurement interval as can be clearly seen in Figure P.25.F.

If the carbon dioxide level changes between the source and the sample (IR path) in the time between the background measurement and the sample measurement, a change in

absorbance of the CO_2 will appear in the FTIR spectrum. This is because if there is a CO_2 peak in the background, but not in the sample, a CO_2 peak will be ratio-ed 'out', causing a negative peak formation. The opposite is true for positive peaks, but CO_2 will not be present in the background measurement but is present in the sample measurement. This effect can be minimised by shortening the time between the background measurement and the sample measurement. During this experiment, a 10-minute background validity time was set. This was due to the time it took to complete all the measurements for a single plastic type. The most effective mitigation is by purging the interface chamber with dry air or high-purity nitrogen to remove any CO_2 before each background and sample measurement. Nitrogen gas does not absorb Mid-infrared used by the FTIR (Joslin, Gray & Gburski, 1984). However, the IR wavenumbers between 2300 - 2400 cm^{-1} are not used to categorise the plastics before or after weathering.

A likely cause for these CO_2 features presented in the data here, is the introduction of CO_2 into the interface chamber from the breath of the researcher. The laboratory in which the measurements were carried out had an air circulation system that was always on. A fume cupboard was also located in the room extracting continuously and in addition, a window was also usually open for more fresh air. All these factors kept the air in the room well circulated and replaced during the experiment at all measurement time intervals. This would have prevented any accumulation of CO_2 in the laboratory during measurements. However, individual exhalations from the researcher into the FTIR interface would cause detectable CO_2 to show up in the FTIR measurements as seen by the results in Figure 28.

All 20 data points from the data presented in this thesis were collected within a single background scan. However, the interfaces were not removed and purged after each set of measurements. These CO_2 spectral peaks do not interfere with the categorisation of the plastics from the data during weathering experiments as the CO_2 absorbance bands are narrow and

specific to CO_2. In order to remove the effect of these peaks, for use of the spectra in a weathering library, these CO_2 peaks can be removed or suppressed to zero, or removed all together without losing any plastic characterisation data. However, it would save operator effort if they were prevented from occurring. In this study they are also reported to highlight considerations when selecting the interfaces for plastic weathering studies. Most studies use ATR as the standard practice for FTIR measurements, however ATR measurements potentially miss some of the physical changes that the plastic experiences in early stages of weathering. With the data collected in this study it is clear that some subtle physical changes can be seen within the 25 days of weathering and so the diffuse and specular interface FTIR data could prove to yield information that ATR alone cannot. Data collected over a longer experiment will be conducted in future work to assess the value of using the trio of FTIR interfaces.

4.5.2 Contamination

The only noticeable change that can be seen in the FTIR data, apart from the CO_2 fluctuations, are the peak changes at 429 hours, peaks at 2919 cm^{-1}, 1756 cm^{-1} and 1249 cm^{-1} which diminish in size. As these peaks only occur in the final data set in the time series, at 429 hours, it was unknown if the peaks would continue to develop given more time within the weather-o-meter. The negative appearance of the peaks however pointed towards a contamination of the samples at that given time, rather than the formation of new bonds. Furthermore, these negative peaks were also only visible in the data collected with the diffuse interface and wasn't seen in any of the other data. To determine if the chemical signal was a contaminant, a spectral subtracting between the spectra at 336 hours from the 429 hours data was performed. This revealed similar contaminant spectra for PE, PP, PA, PET and PS which are shown in Figure 31, however the spectral subtraction revealed that the PS contained small amounts of the contaminant. The surface of the PS was much smoother than that of the other four plastic types, which could explain the difference if the suspected contaminant was being absorbed by the surface of the other plastics, which were observed to be becoming rougher, permitting penetration of the contaminant into the surface of the plastic. Surface roughening has been shown by Cai *et al.*, (2018) after a similar 1 month of weathering to the experiment reported here. Gulmine *et al.*, (2003) subjected low density PE samples to 0.35 ± 0.03 W/m^2 with a peak of 340 nm (similar to the conditions used in this thesis) and also found roughening and minor cracks formed in the surface of the plastic.

The contaminant was identified as isopropyl alcohol by the characterization of its peaks matching with the contaminant spectra. Figure 31 compares the isopropyl alcohol spectra to the subtraction spectra from all 5 plastics. As the peaks in the FTIR data are negative, this implies that there was a presence of isopropyl alcohol present during the background measurement then as the isopropyl alcohol evaporates. The related peak intensities fell, leaving

the negative peaks seen in the data. It is therefore important to note that there must be a period between cleaning the samples with the isopropyl alcohol wipes and the first measurements to avoid contamination of the isopropyl alcohol within the interface chamber.

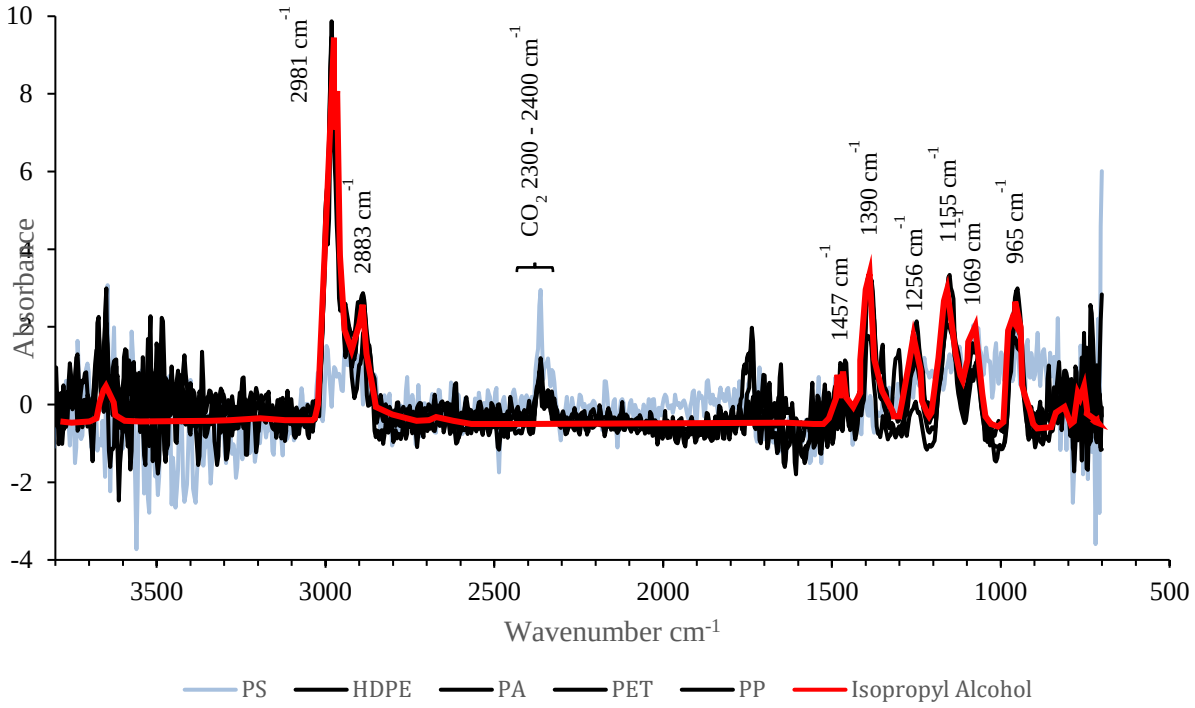

*Figure 31: Spectra of the contaminant compared to the spectra of isopropyl alcohol (**Solid red line).** HDPE, PA, PET and PP all contained the contaminant (**Solid black lines**). PS only had very trace amounts that were almost undetectable (**Solid light-blue line**). Sample contamination spectra were produced by subtracting the spectra at 336 hours from the suspected contaminated spectra at 429 hours. CO_2 fluctuations in the spectra are highlighted between 2300 – 2400 cm^{-1}.*

4.5.3 Lack of weathering

It is generally agreed that the weathering of plastic for less than 40 days in dry outdoor summer conditions has little to no effect on plastic samples. Rajakumar *et al.* (2009) showed that only after 40 days of weathering, did the lactone, ketone, ester and carboxylic acid indices show significant increase due to outdoor weathering. This 40-day limit was seen in both summer and winter weathering conditions. At 25 days, very little changes had occurred (Rajakumar *et al.*, 2009). It has also been shown by Hirsch *et al.* (2017) that after a month (30 days) of outdoor weathering very few changes can be seen in the FTIR spectra, only after two months (60 days) were significant spectral changes seen. Biber, Foggo & Thompson (2019) however, found that PS showed considerable weathering using ATR-FTIR after only 28 days of outdoor weathering. The results reported in this thesis do not show significant weathering, despite the irradiance energy being slightly increased compared to the summer irradiance levels (*Table 9*). Over the 25 days of this experiment, both rigs delivered less than the equivalent of 40 days of summer outdoor weathering to the samples (*Table 10*). Therefore, the matching findings between the outdoor weathering studies and this work suggests that the design presented replicates the effects of natural outdoor solar irradiance on the plastics under study.

Table 10: The calculated equivalent environmental weathering of the 25 days of weathering in the design presented in this thesis. Calculated for the Average; Annual, Summer and Winter irradiance.

25 Days of Equivalent Weathering (Days)		
Annual Irradiance (581009 KJ/m^2/day)		
Salt	67.25	66.39
Air	60.41	58.64
Summer Irradiance (1040477 KJ/m2/day)		
Salt	37.57	37.09
Air	33.75	32.76
Winter Irradiance (86160 KJ/m2/day)		
Salt	454.36	448.55
Air	408.14	396.22

When using the carbonyl index as a measure of weathering, it has been shown that the effects of early stages of degradation are underrepresented due to the insensitivity of the index to the steps prior to "carboxylation" (Rouillon *et al.*, 2016), therefore would not detect any weathering using this method for the data presented in this thesis. In the data presented here, no carbonyl formation was seen within the equivalent 37.09 to 37.57 hours. From the diffuse and specular interfaces, it can be seen that there is a shift in the spectra, which hints at a physical change of the surface of the plastic, especially in the PS samples. This physical change however falls short of the significant weathering of PS reported by Biber, Foggo & Thompson (2019).

The aim of this work was to develop a weathering rig that could provide irradiance similar to that of the environment. Here we measured the environmental irradiance as 18.34 W/m^2 and produced 18.09 W/m^2 and 16.25 W/m^2 in our laboratory setup. These energy levels are much more relevant to the environmental conditions than those reported used by accelerated weathering experiments (Chang *et al.*, 2018; Gewert *et al.*, 2018; Rouillon *et al.*, 2016; Fashandi, Zadhoush & Haghighat, 2008). The ability of the system to maintain summer levels of irradiance, month after month, provides a way to accelerate the weathering process without providing unreal levels of irradiance.

4.6 Sample regime

Due to the shutdown of the experiment due to the COVID-19 pandemic it is hard to accurately report the effectiveness of the sampling regime. As stated, the experiment yielded weathering results equivalent to less than 40 days of environmental weathering, a known limit of FTIR data to distinguish weathering. This regime did however highlight that very little changes occur during the first 40 days of equivalent weathering, as reported by other authors (Biber, Foggo & Thompson, 2019; Hirsch *et al.*, 2017; Rouillon *et al.*, 2016; Rajakumar *et al.*,

2009). The exception to this, is when using the diffuse interface. Physical changes of the surface of the plastic sample could be seen by the shifting of the spectra, although no chemical changes could be seen. In future work, rapid successions of measurements, within this equivalent 40-day time frame, would be expected to yield few results and so measurements should be spaced out more in the early stages.

4.7 FTIR Interfaces

Three FTIR interfaces were used to measure FTIR spectra in this thesis. There were clear differences between the three interfaces used to collect the FTIR data. The diffuse data had more noise than the other interfaces which was likely due to the specular nature of the plastic surface. In the diffuse and specular interfaces, both of which have an internal atmospheric space between the sample and the instrument within the interface optics, show CO_2 peaks in almost all measurements. The diffuse interface had an array of mirrors within the interface chamber with no direct path through, unlike the specular interface. This could have caused atmospheric CO_2 to get trapped more easily within the interface, in comparison to the specular interface chamber which was void of internal components. This interface chamber contamination is likely to be caused by the CO_2 in an exhalation by the researcher. However, the presence of CO_2 might be due to the increased IR penetration depth of the diffuse and specular interfaces, as CO_2 has been observed to be a product of photooxidative degradation in polystyrene (Ward *et al.*, 2019). The data reported is insufficient to provide a definitive answer to this question as it was collected without CO_2 contamination mitigation protocols in place. The random pattern of fluctuations also points towards contamination rather than a product of degradation. The specular interface had low noise like that of the ATR interface, especially on the smooth PS samples which had an almost glass finish compared to the rough surface of the other 4 plastics. As the plastic starts to weather, the performance of the specular interface might

start to fall. No decrease in performance is shown here over the 25 days as there was a lack of significant weathering effects.

The ATR measurements require force to be applied to get any good contact with the diamond crystal and leaves small indentations in the surface of the pucks after each measurement. The diffuse and specular however did not. Due to this fact, out of the diffuse and specular interfaces which left no trace of the prior measurement and can be considered completely non-destructive. The trio of FTIR interfaces used in this thesis hints at the ability to measure both physical and chemical changes during photooxidative degradation. However due to the lack of weathering, the performance of each interface remained constant throughout this work. A longer experiment implementing all three interfaces would provide a better set of data to assess the performance of each interface for use in weathering studies.

4.8 Standardising methodologies

It can be seen in industrial weathering literature (Tab Lam/art) that the standard practices are followed due to the use of commercial weathering chamber systems which have been designed to meet industrial standards. Liu, Mandelis & Huan (2018), highlights deficiencies in the metrics and the experimental conditions used in plastics degradation research, calling for a more standardised approach to plastics degradation and weathering research. This thesis also calls for similar standardisation. Kalogerakis *et al.* (2017) related the degradation of plastic to the Lux per day (Lux*d). Lux is a unit of measurement related to the perception of light by the human eye, rather than a quantified irradiance energy of light. There is no exact conversion between Lux and W/m^2 without first knowing the exact wavelength intensities of light used. In the case of Kalogerakis *et al.* (2017), natural solar radiation was used. A conversion factor for solar radiation is known to be 0.0079 W/m2 per Lux, and so the conversion can be made. However, a standard unit, preferably the S.I. W/m^2 should be used for

ease of comparison between studies. In this study a spectrometer calibrated using a NIST traceable light source was used to ensure accurate irradiance measurements, with precision using known path length between the light source and sample. This was achieved by using the custom calibration table. This value however remains a single value and can still hide spectral discrepancies so reporting the spectrum used remains important. Water parameters such as salinity and temperature should also be reported, with a surprising amount of authors not include these basic measurements (Cai *et al.*, 2019; Pelegrini *et al.*, 2019; Biesinger, Corcoran & Walzak, 2011; Ioakeimidis *et al.*, 2016; Brandon, Goldstein & Ohman, 2016; Satoto *et al.*, 1997).

Rummel et al. (2019) and Gewert et al. (2018) used a wavelength range of 241 - 400 nm comparing the 5 days of irradiance to the equivalent of 513 days of environmental weathering. This was based on European mean irradiance of approximately 1200 kWh/(m² · year). This, in addition, raises the issue regarding the calculated environmental irradiance used to convert the laboratory irradiance to an environmental equivalent. Other authors fail to report any environmental equivalence despite the claim (Chen *et al.*, 2019) or weathering using a partial spectrum (UVA only) and still relate the effects of weathering to an environmental equivalent (Kalogerakis *et al.*, 2017). There is a clear need to standardise reporting of the irradiance used for weathering studies.

5 Conclusion

In response to the call for more environmentally relevant experiments, here we develop a novel method for replicating marine weathering in the laboratory. Ultraviolet Radiation is known to be the main cause of photooxidative degradation which is heavily influenced by the temperature of the reaction. A 10℃ rise in temperature can cause approximately 25% more photooxidative degradation in PS which is known to degrade easily in the marine environment. The presence of saltwater cools the plastic due to its high thermal diffusivity, limits the availability of oxygen and attenuates the irradiance of UVR through scattering and absorption. For this reason, the irradiance, temperature and presence of saltwater were key parameters to simulate when designing the custom system presented here.

Outdoor environmental weathering offers the most realistic conditions in real time. These experiments cannot however study the individual factors that influence the weathering process. Weathering experiments conducted using commercial units focus on weathering for industrial purposes, however some researchers have attempted to utilise the commercial units relating the results to the environment. Here we discuss the problems with applying such methodologies and aim to provide a more environmentally relevant method for weathering in the laboratory.

The design presented in this thesis attempts to replicate the solar irradiation at the surface boundary layer of the ocean, at UK / Northern German latitudes (North Sea). The influence of saltwater on both, light penetration and temperature in clean surface seawater and air were replicated. The design removes the effects of wave agitation, abrasion (mechanical stress) and biofilm formation in order to remove confounding variables known to influence the weathering of plastic, in an effort to focus on the effect of photooxidative degradation of plastic in the marine environment. This novel system uses an auto top off system to maintain the salinity during the weathering experiment and the low energy introduction of the saltwater has

been used for the first time in this work during a weathering experiment. The low energy saltwater addition prevented the surface layer of the plastic being exposed due to wave action effects. Wave action and mechanical aberration by collision of particles has been shown to produce microplastics, revealing un-weathered surfaces. By fixing the samples in the system these effects were prevented to collect long term data without microplastic production. This also allows the irradiance to be explicitly quantified due to the fixed path length coupled with the known energy field to match environmental levels. These measures should become standard practice when designing laboratory experiments that simulate environmental marine weathering.

Another key design innovation for the system presented here is that it automatically stabilised the saltwater parameter by maintaining salinity, the availability of oxygen and temperature of the plastics throughout the experiment, as would be experienced in the environment. This system works well to maintain the salinity levels of the water throughout the experiment showing robustness of the simple design. This novel design can also be altered and changed to suit a range of research interests. By changing the distances, light source used, temperature and water parameters the system could be used to weather plastic at different depths, different latitudes and from different environments, respectively. The production of leachates could also be assessed due to the closed loop design.

Custom laboratory experiment designs allow for the control of all experimental parameters. However, this has the potential to cause research to diverge from standard practices. Without a set of standard practices, comparison of results from different authors may not be possible due to vast methodological differences. This work falls into this category, attempting to produce a methodology that has not been used before. However, this approach aims to become the standard practice. Reporting the spectrum alongside irradiance levels while using defined pathlengths to produce an even energy field. The Thesis also reports data using

uncommon measurements, such as diffuse and specular FTIR data, in an effort to push the use of a commonly used FTIR instrument, to produce physical change data alongside chemical change data. This work also attempted to replicate solar radiation in a nonstandard way by utilising LEDs coupled with fluorescent lamps. Although the irradiance energy produced by this rig is analogous with UVR irradiance over the range 280 - 400 nm, that is received at UK / North German latitudes, the wavelength specific intensities might cause different weathering compared to a full solar spectrum. Future designs should implement light sources that more accurately represent the solar spectrum. To achieve this and create an even energy field, it is suggested that QUV-340 lamps from Q-Labs would offer an alternative fluorescent tube than the lamps used here, bringing the methodology in line with other works while also filling the gap in the spectrum presented by this work. Despite the spectrum gap, the data collected using this design has shown that the weathering patterns measured in the plastic samples coincide with other reports obtained in outdoor weathering conditions. The equivalent of 37 days of summer irradiance produced little, to no weathering.

FTIR-ATR data showed no changes over the 429 hours of weathering. Both the diffuse and specular FTIR interfaces showed signs of CO_2 fluctuations throughout the experiments which were concluded to be caused by exhalation by the researcher during measurements. Mitigation measures should be put in place during the measurements with the diffuse and specular FTIR interfaces. Air flow around the interface helps to remove CO_2 that has accumulated in the interface, bringing the levels back to the atmospheric baseline. However, it is advised that breathing around and in the direction of the diffuse and specular interface should be avoided. The presence of CO_2 however in the data does not compromise the characterisation of the plastic degradation.

The data presented in this thesis has limitations due to the longevity of the study being cut short due to the COVID-19 pandemic. Of the planned six months study, only 25 days were achieved, and a failure of the system occurs at day 19, due to an electrical failure which paused the experiment. Despite these setbacks, outdoor environmental weathering results from other studies agree with the weathering seen in this study. Future work should aim to build upon the methodology set out in this thesis, correct the mistakes made and conduct a longer scale weathering study and then relate the data back to outdoor natural environmental weathering. The fate of plastic waste in the marine environment required laboratory experiments like the method detailed here, to quantify the effect that each variable has on the varied and complex process of marine plastic degradation. Such results could provide a way to quantify the time a plastic sample has been in the environment which should be the direction of future work.

Bibliography

Ahmed, K. (2016) Performance evaluation of chlorinated polyethylene compatibilized-industrial waste-filled acrylonitrile butadiene rubber/low-density polyethylene blends. *Journal of Vinyl and Additive Technology*. [Online] 22 (4), 460–469. Available from: doi:10.1002/vnl.21459.

Albertsson, A. & Karlsson, S. (1990) The influence of biotic and abiotic environments on the degradation of polyethylene. *Progress in Polymer Science*. [Online] 15 (2), 177–192. Available from: doi:10.1016/0079-6700(90)90027-X.

Allen, N.S., Mudher, M. & Green, P. (1984) Photo-stabilising action of ortho-hydroxy aromatic compounds in polypropylene film: UV absorption versus radical scavenging. *Polymer Degradation and Stability*. [Online] 7 (2), 83–94. Available from: doi:10.1016/0141-3910(84)90116-2.

Al-Salem, S.M., Behbehani, M.H., Al-Hazza'a, A., Arnold, J.C., et al. (2019) Study of the degradation profile for virgin linear low-density polyethylene (LLDPE) and polyolefin (PO) plastic waste blends. *Journal of Material Cycles and Waste Management*. [Online] 21 (5), 1106–1122. Available from: doi:10.1007/s10163-019-00868-8.

Andrade, J., Fernández-González, V., López-Mahía, P. & Muniategui, S. (2019) A low-cost system to simulate environmental microplastic weathering. *Marine Pollution Bulletin*. [Online] 149, 110663. Available from: doi:10.1016/j.marpolbul.2019.110663.

Andrady, A.L. (2011) Microplastics in the marine environment. *Marine Pollution Bulletin*. [Online] 62 (8), 1596–1605. Available from: doi:10.1016/j.marpolbul.2011.05.030.

Arias Villamizar, C.A. & Vázquez Morillas, A. (2018) Degradation of conventional and oxodegradable high density polyethylene in tropical aqueous and outdoor environments. *Revista Internacional de Contaminación Ambiental*. [Online] 34 (1), 137–147. Available from: doi:10.20937/RICA.2018.34.01.12.

Arrieta, C., Dong, Y., Lan, A. & Vu-Khanh, T. (2013) Outdoor weathering of polyamide and polyester ropes used in fall arrest equipment. *Journal of Applied Polymer Science*. [Online] 130 (5), 3058–3065. Available from: doi:10.1002/app.39524.

Atlas-mts (2020) *Xenon Weathering - Suntest family*. [Online]. 2020. Available from: https://www.atlas-mts.com/products/standard-instruments/xenon-weathering/suntest [Accessed: 11 September 2020].

Badji, C., Beigbeder, J., Garay, H., Bergeret, A., et al. (2018) Correlation between artificial and natural weathering of hemp fibers reinforced polypropylene biocomposites. *Polymer Degradation and Stability*. [Online] 148, 117–131. Available from: doi:10.1016/j.polymdegradstab.2018.01.002.

Benavides, R., Castillo, B.M., Castañeda, A.O., López, G.M., et al. (2001) Different thermo-oxidative degradation routes in poly(vinyl chloride). *Polymer Degradation and Stability*. [Online] 73 (3), 417–423. Available from: doi:10.1016/S0141-3910(01)00122-7.

Biber, N.F.A., Foggo, A. & Thompson, R.C. (2019) Characterising the deterioration of different plastics in air and seawater. *Marine Pollution Bulletin*. [Online] 141, 595–602. Available from: doi:10.1016/j.marpolbul.2019.02.068.

Biesinger, M.C., Corcoran, P.L. & Walzak, M.J. (2011) Developing ToF-SIMS methods for investigating the degradation of plastic debris on beaches. *Surface and Interface Analysis*. [Online] 43 (1–2), 443–445. Available from: doi:10.1002/sia.3397.

Boruta, M. (2012) FT-IR search algorithm-assessing the quality of a match. *Spectrosc. Mag.* [Online]. (47). Available from: https://scholar.google.com/scholar_lookup?title=FT-IR%20search%20algorithm%20-%20assessing%20the%20quality%20of%20a%20match&author=M.%20Boruta&publication_year=2012 [Accessed: 13 September 2020].

Brandon, J., Goldstein, M. & Ohman, M.D. (2016) Long-term aging and degradation of microplastic particles: Comparing in situ oceanic and experimental weathering patterns. *Marine Pollution Bulletin*. [Online] 110 (1), 299–308. Available from: doi:10.1016/j.marpolbul.2016.06.048.

Brennecke, D., Duarte, B., Paiva, F., Caçador, I., et al. (2016) Microplastics as vector for heavy metal contamination from the marine environment. *Estuarine, Coastal and Shelf Science*. [Online] 178, 189–195. Available from: doi:10.1016/j.ecss.2015.12.003.

Cai, H., Du, F., Li, L., Li, B., et al. (2019) A practical approach based on FT-IR spectroscopy for identification of semi-synthetic and natural celluloses in microplastic investigation. *Science of The Total Environment*. [Online] 669, 692–701. Available from: doi:10.1016/j.scitotenv.2019.03.124.

Cai, L., Wang, J., Peng, J., Wu, Z., et al. (2018) Observation of the degradation of three types of plastic pellets exposed to UV irradiation in three different environments. *Science of The Total Environment*. [Online] 628–629, 740–747. Available from: doi:10.1016/j.scitotenv.2018.02.079.

Capanescu, C. & Cincu, C. (2003) Evaluation of UV inhibitors in polyester gelcoats. *ADVANCES IN POLYMER TECHNOLOGY*. [Online] 22 (4), 8. Available from: doi:10.1002/adv.10063.

Caron, A.G.M., Thomas, C.R., Berry, K.L.E., Motti, C.A., et al. (2018) Ingestion of microplastic debris by green sea turtles (Chelonia mydas) in the Great Barrier Reef: Validation of a sequential extraction protocol. *Marine Pollution Bulletin*. [Online] 127, 743–751. Available from: doi:10.1016/j.marpolbul.2017.12.062.

Carpenter, E.J., Anderson, S.J., Harvery, G.R., Miklas, H.P., et al. (1972) Polystyrene Spherules in Coastal Waters. *Science*. [Online] 178 (4062), 749–750. Available from: doi:10.1126/science.178.4062.749.

Carpenter, E.J. & Smith, K.L. (1972) Plastics on the Sargasso Sea Surface. *Science*. [Online] 175 (4027), 1240–1241. Available from: doi:10.1126/science.175.4027.1240.

Chamas, A., Moon, H., Zheng, J., Qiu, Y., et al. (2020) Degradation Rates of Plastics in the Environment. *ACS Sustainable Chemistry & Engineering*. [Online] 8 (9), 3494–3511. Available from: doi:10.1021/acssuschemeng.9b06635.

Chang, C.-H., Tien, C.-C., Hsueh, H.-C. & Sung, L. (2018) A macroscopically nondestructive method for characterizing surface mechanical properties of polymeric coatings under accelerated weathering. *Journal of Coatings Technology and Research*. [Online] 15 (5), 913–922. Available from: doi:10.1007/s11998-017-0042-3.

Chen, B., Luo, Z., Chen, H., Chen, C., et al. (2020) Wood Plastic Composites from the Waste Lignocellulosic Biomass Fibers of Bio-Fuels Processes: A Comparative Study on Mechanical Properties and Weathering Effects. *Waste and Biomass Valorization*. [Online] 11 (5), 1701–1710. Available from: doi:10.1007/s12649-018-0413-8.

Chen, C., Chen, L., Yoa, Y., Artigas, F., et al. (2019) Organotin Release from Polyvinyl Chloride Microplastics and 4 Concurrent Photodegradation in Water: Impacts from Salinity, 5 Dissolved Organic Matter, and Light Exposure. *Environmental Science & Technology*. [Online] 53 (18), 10741–10752. Available from: doi:10.1021/acs.est.9b03428.

Corcoran, P.L., Biesinger, M.C. & Grifi, M. (2009) Plastics and beaches: A degrading relationship. *Marine Pollution Bulletin*. [Online] 58 (1), 80–84. Available from: doi:10.1016/j.marpolbul.2008.08.022.

Cosine Developments (2016) Analysing the causes of blackening of ends of fluorescent lamps. *EE Publishers*. [Online]. Available from: https://www.ee.co.za/article/analysing-causes-blackening-ends-fluorescent-lamps.html [Accessed: 15 September 2020].

Courtene-Jones, W., Quinn, B., Murphy, F., Gary, S.F., et al. (2017) Optimisation of enzymatic digestion and validation of specimen preservation methods for the analysis of ingested microplastics. *Analytical Methods*. [Online] 9 (9), 1437–1445. Available from: doi:10.1039/C6AY02343F.

D20 Committee (2013) *Practice for Fluorescent Ultraviolet (UV) Lamp Apparatus Exposure of Plastics*. [Online]. Available from: doi:10.1520/D4329-13 [Accessed: 12 September 2020].

Déniel, M., Lagarde, F., Caruso, A. & Errien, N. (2020) Infrared spectroscopy as a tool to monitor interactions between nanoplastics and microalgae. *Analytical and Bioanalytical Chemistry*. [Online] Available from: doi:10.1007/s00216-020-02683-9 [Accessed: 24 June 2020].

Enders, K., Lenz, R., Stedmon, C.A. & Nielsen, T.G. (2015) Abundance, size and polymer composition of marine microplastics ≥ 10 μm in the Atlantic Ocean and their modelled vertical distribution. *Marine Pollution Bulletin*. [Online] 100 (1), 70–81. Available from: doi:10.1016/j.marpolbul.2015.09.027.

Erni-Cassola, G., Wright, R.J., Gibson, M.I. & Christie-Oleza, J.A. (2020) Early Colonization of Weathered Polyethylene by Distinct Bacteria in Marine Coastal Seawater. *Microbial Ecology*. [Online] 79 (3), 517–526. Available from: doi:10.1007/s00248-019-01424-5.

Fashandi, H., Zadhoush, A. & Haghighat, M. (2008) Effect of orientation and crystallinity on the photodegradation of poly(ethylene terephthalate) fibers. *Polymer Engineering & Science*. [Online] 48 (5), 949–956. Available from: doi:10.1002/pen.21043.

Fiorio, R., Villanueva Díez, S., Sánchez, A., D'hooge, D.R., et al. (2020) Influence of Different Stabilization Systems and Multiple Ultraviolet A (UVA) Aging/Recycling Steps on Physicochemical, Mechanical, Colorimetric, and Thermal-Oxidative Properties of ABS. *Materials*. [Online] 13 (1), 212. Available from: doi:10.3390/ma13010212.

Fleischmann, E.M. (1989) The measurement and penetration of ultraviolet radiation into tropical marine water: UV radiation in tropical water. *Limnology and Oceanography*. [Online] 34 (8), 1623–1629. Available from: doi:10.4319/lo.1989.34.8.1623.

Fondriest Environmental, Inc. (2013) *"Dissolved Oxygen."* [Online]. 9 November 2013. Fundamentals of Environmental Measurements. Available from: https://www.fondriest.com/environmental-measurements/parameters/water-quality/dissolved-oxygen/ [Accessed: 31 August 2020].

Franco, J., Fort, J., García-Barón, I., Loubat, P., et al. (2019) Incidence of plastic ingestion in seabirds from the Bay of Biscay (southwestern Europe). *Marine Pollution Bulletin*. [Online] 146, 387–392. Available from: doi:10.1016/j.marpolbul.2019.06.077.

Franklin, L. & Forster, R. (1997) *The changing irradiance environment: consequences for marine macrophyte physiology, productivity and*. [Online] (32), 207–232. Available from: doi:10.1080/09670269710001737149.

Gardette, M., Perthue, A., Gardette, J.-L., Janecska, T., et al. (2013) Photo- and thermal-oxidation of polyethylene: Comparison of mechanisms and influence of unsaturation content. *Polymer Degradation and Stability*. [Online] 98 (11), 2383–2390. Available from: doi:10.1016/j.polymdegradstab.2013.07.017.

Gewert, B., Plassmann, M., Sandblom, O. & MacLeod, M. (2018) Identification of Chain Scission Products Released to Water by Plastic Exposed to Ultraviolet Light. *Environmental Science & Technology Letters*. [Online] 5 (5), 272–276. Available from: doi:10.1021/acs.estlett.8b00119.

Gewert, B., Plassmann, M.M. & MacLeod, M. (2015) Pathways for degradation of plastic polymers floating in the marine environment. *Environmental Science: Processes & Impacts*. [Online] 17 (9), 1513–1521. Available from: doi:10.1039/C5EM00207A.

Gijsman, P., Meijers, G. & Vitarelli, G. (1999) Comparison of the UV-degradation chemistry of polypropylene, polyethylene, polyamide 6 and polybutylene terephthalate. *Polymer Degradation and Stability*. [Online] 65 (3), 433–441. Available from: doi:10.1016/S0141-3910(99)00033-6.

Gu, J.-D. (2003) Microbiological deterioration and degradation of synthetic polymeric materials: recent research advances. *International Biodeterioration & Biodegradation*. [Online] 52 (2), 69–91. Available from: doi:10.1016/S0964-8305(02)00177-4.

Gulmine, J.V., Janissek, P.R., Heise, H.M. & Akcelrud, L. (2003) Degradation profile of polyethylene after artificial accelerated weathering. *Polymer Degradation and Stability*. [Online] 79 (3), 385–397. Available from: doi:10.1016/S0141-3910(02)00338-5.

Hahladakis, J.N. (2020) Delineating the global plastic marine litter challenge: clarifying the misconceptions. *Environmental Monitoring and Assessment*. [Online] 192 (5), 267. Available from: doi:10.1007/s10661-020-8202-9.

ter Halle, A., Ladirat, L., Martignac, M., Mingotaud, A.F., et al. (2017) To what extent are microplastics from the open ocean weathered? *Environmental Pollution*. [Online] 227, 167–174. Available from: doi:10.1016/j.envpol.2017.04.051.

Hebner, T.S. & Maurer-Jones, M.A. (2020) Characterizing microplastic size and morphology of photodegraded polymers placed in simulated moving water conditions. *Environmental Science: Processes & Impacts*. [Online] 22 (2), 398–407. Available from: doi:10.1039/C9EM00475K.

Hirsch, S.G., Barel, B. & Segal, E. (2019) Characterization of surface phenomena: probing early stage degradation of low-density polyethylene films. *Polymer Engineering & Science*. [Online] 59 (S1), E129–E137. Available from: doi:10.1002/pen.24886.

Hirsch, S.G., Barel, B., Shpasser, D., Segal, E., et al. (2017) Correlating chemical and physical changes of photo-oxidized low-density polyethylene to the activation energy of water release. *Polymer Testing*. [Online] 64, 194–199. Available from: doi:10.1016/j.polymertesting.2017.10.005.

Ho, K.-L.G. & Pometto III, A.L. (1999) Effects of electron-beam irradiation and ultraviolet light (365 nm) on polylactic acid plastic films. *Journal of Polymers and the Environment*. [Online] 7 (2), 93–100. Available from: doi:10.1023/A:1021860301487.

Ioakeimidis, C., Fotopoulou, K.N., Karapanagioti, H.K., Geraga, M., et al. (2016) The degradation potential of PET bottles in the marine environment: An ATR-FTIR based approach. *Scientific Reports*. [Online] 6 (1), 23501. Available from: doi:10.1038/srep23501.

Jahnke, A., Arp, H.P.H., Escher, B.I., Gewert, B., et al. (2017) Reducing Uncertainty and Confronting Ignorance about the Possible Impacts of Weathering Plastic in the Marine Environment. *Environmental Science & Technology Letters*. [Online] 4 (3), 85–90. Available from: doi:10.1021/acs.estlett.7b00008.

Joslin, C.G., Gray, C.G. & Gburski, Z. (1984) Far-infrared absorption in nitrogen gas. *Molecular Physics*. [Online] 53 (1), 203–223. Available from: doi:10.1080/00268978400102221.

Julienne, F., Delorme, N. & Lagarde, F. (2019) From macroplastics to microplastics: Role of water in the fragmentation of polyethylene. *Chemosphere*. [Online] 236, 124409. Available from: doi:10.1016/j.chemosphere.2019.124409.

Kalogerakis, N., Karkanorachaki, K., Kalogerakis, G.C., Triantafyllidi, E.I., et al. (2017) Microplastics Generation: Onset of Fragmentation of Polyethylene Films in Marine Environment Mesocosms. *Frontiers in Marine Science*. [Online] 4. Available from: doi:10.3389/fmars.2017.00084.

Käppler, A., Fischer, D., Oberbeckmann, S., Schernewski, G., et al. (2016) Analysis of environmental microplastics by vibrational microspectroscopy: FTIR, Raman or both? *Analytical and Bioanalytical Chemistry*. [Online] 408 (29), 8377–8391. Available from: doi:10.1007/s00216-016-9956-3.

Kim, J.W., Park, S.-B., Tran, Q.-G., Cho, D.-H., et al. (2020) Functional expression of polyethylene terephthalate-degrading enzyme (PETase) in green microalgae. *Microbial Cell Factories*. [Online] 19 (1), 97. Available from: doi:10.1186/s12934-020-01355-8.

Kroon, F., Motti, C., Talbot, S., Sobral, P., et al. (2018) A workflow for improving estimates of microplastic contamination in marine waters: A case study from North-Western Australia. *Environmental Pollution*. [Online] 238, 26–38. Available from: doi:10.1016/j.envpol.2018.03.010.

Ktimpf, G., Sommer, K. & Zirngiebl, E. (1991) *Studies in accelerated weathering. Part I. Determination of the activation spectrum of photodegradation in polymers*. 19, 69–77.

Kukulka, T., Proskurowski, G., Morét-Ferguson, S., Meyer, D.W., et al. (2012) The effect of wind mixing on the vertical distribution of buoyant plastic debris. *Geophysical Research Letters*. [Online] 39 (7). Available from: doi:10.1029/2012GL051116.

Lankone, R.S., Ruggiero, E., Goodwin, D.G., Vilsmeier, K., et al. (2020) Evaluating performance, degradation, and release behavior of a nanoform pigmented coating after natural and accelerated weathering. *NanoImpact*. [Online] 17, 100199. Available from: doi:10.1016/j.impact.2019.100199.

Lebreton, L., Slat, B., Ferrari, F., Sainte-Rose, B., et al. (2018) Evidence that the Great Pacific Garbage Patch is rapidly accumulating plastic. *Scientific Reports*. [Online] 8 (1), 4666. Available from: doi:10.1038/s41598-018-22939-w.

Lenz, R., Enders, K., Stedmon, C.A., Mackenzie, D.M.A., et al. (2015) A critical assessment of visual identification of marine microplastic using Raman spectroscopy for analysis improvement. *Marine Pollution Bulletin*. [Online] 100 (1), 82–91. Available from: doi:10.1016/j.marpolbul.2015.09.026.

Leonas, K.K. (1993) The disintegration rate of traditional and chemically modified plastic films in simulated fresh- and sea-water environments. *Journal of Applied Polymer Science*. [Online] 47 (12), 2103–2110. Available from: doi:10.1002/app.1993.070471203.

Lepre, A.M., Sutherland, J.C., Trunk, J.G. & Sutherland, B.M. (1998) A robust, inexpensive filter for blocking UVC radiation in broad-spectrum 'UVB' lamps. *Journal of Photochemistry and Photobiology B: Biology*. [Online] 43 (1), 34–40. Available from: doi:10.1016/S1011-1344(98)00079-7.

Liu, G., Liao, S., Zhu, D., Hua, Y., et al. (2012) Innovative photocatalytic degradation of polyethylene film with boron-doped cryptomelane under UV and visible light irradiation. *Chemical Engineering Journal*. [Online] 213, 286–294. Available from: doi:10.1016/j.cej.2012.09.105.

Liu, L., Mandelis, A. & Huan, H. (2018) Fourier-Transform Infrared Differential Photoacoustic Spectroscopy (FTIR-DPAS) for Simultaneous Monitoring of Multiple Air Contaminants/Trace Gases. *International Journal of Thermophysics*. [Online] 39 (8), 94. Available from: doi:10.1007/s10765-018-2411-2.

Liu, P., Zhan, X., Wu, X., Li, J., et al. (2020) Effect of weathering on environmental behavior of microplastics: Properties, sorption and potential risks. *Chemosphere*. [Online] 242, 125193. Available from: doi:10.1016/j.chemosphere.2019.125193.

Lizárraga-Laborín, L.L., Quiroz-Castillo, J.M., Encinas-Encinas, J.C., Castillo-Ortega, M.M., et al. (2018) Accelerated weathering study of extruded polyethylene/poly (lactic acid)/chitosan films. *Polymer Degradation and Stability*. [Online] 155, 43–51. Available from: doi:10.1016/j.polymdegradstab.2018.06.007.

Lv, Y., Huang, Y., Kong, M., Yang, Q., et al. (2017) Multivariate correlation analysis of outdoor weathering behavior of polypropylene under diverse climate scenarios. *Polymer Testing*. [Online] 64, 65–76. Available from: doi:10.1016/j.polymertesting.2017.09.040.

Manfredi, M., Barberis, E. & Marengo, E. (2017) Prediction and classification of the degradation state of plastic materials used in modern and contemporary art. *Applied Physics A*. [Online] 123 (1), 35. Available from: doi:10.1007/s00339-016-0663-x.

Markic, A., Gaertner, J.-C., Gaertner-Mazouni, N. & Koelmans, A.A. (2020) Plastic ingestion by marine fish in the wild. *Critical Reviews in Environmental Science and Technology*. [Online] 50 (7), 657–697. Available from: doi:10.1080/10643389.2019.1631990.

Matsui, K., Hosaka, A., Watanabe, A., Teramae, N., et al. (2016) Development of a multi-sample micro UV irradiator for accelerated deterioration of polymers. *Polymer Testing*. [Online] 56, 54–57. Available from: doi:10.1016/j.polymertesting.2016.09.017.

Mellor, D.C., Moir, A.B. & Scott, G. (1973) The effect of processing conditions on the u.v. stability of polyolefins. *European Polymer Journal*. [Online] 9 (3), 219–225. Available from: doi:10.1016/0014-3057(73)90129-8.

Mirabella, F.M. (1993) *Internal reflection spectroscopy: theory and applications*. New York, Marcel Dekker.

Mohamed Nor, N.H. & Obbard, J.P. (2014) Microplastics in Singapore's coastal mangrove ecosystems. *Marine Pollution Bulletin*. [Online] 79 (1–2), 278–283. Available from: doi:10.1016/j.marpolbul.2013.11.025.

Moore, C.J. (2008) Synthetic polymers in the marine environment: A rapidly increasing, long-term threat. *Environmental Research*. [Online] 108 (2), 131–139. Available from: doi:10.1016/j.envres.2008.07.025.

Morrison, E., Shipman, A., Shrestha, S., Squier, E., et al. (2019) Evaluating The Ocean Cleanup, a Marine Debris Removal Project in the North Pacific Gyre, Using SWOT Analysis. *Case Studies in the Environment*. [Online] 3 (1), 1.10-6. Available from: doi:10.1525/cse.2018.001875.

Munno, K., De Frond, H., O'Donnell, B. & Rochman, C.M. (2020) Increasing the Accessibility for Characterizing Microplastics: Introducing New Application-Based and Spectral Libraries of Plastic Particles (SLoPP and SLoPP-E). *Analytical Chemistry*. 92 (3), 2443–2451.

Patti, A. & Acierno, D. (2019) The Puncture and Water Resistance of Polyurethane-Impregnated Fabrics after UV Weathering. *Polymers*. [Online] 12 (1), 15. Available from: doi:10.3390/polym12010015.

Pegram, J.E. & Andrady, A.L. (1989) Outdoor weathering of selected polymeric materials under marine exposure conditions. *Polymer Degradation and Stability*. [Online] 26 (4), 333–345. Available from: doi:10.1016/0141-3910(89)90112-2.

Pelegrini, K., Maraschin, T.G., Brandalise, R.N. & Piazza, D. (2019) Study of the degradation and recyclability of polyethylene and polypropylene present in the marine environment. *Journal of Applied Polymer Science*. [Online] 136 (48), 48215. Available from: doi:10.1002/app.48215.

Peng, Y., Li, X., Wang, W. & Cao, J. (2020) Photodegradation of wood flour/polypropylene composites incorporated with carbon materials with different morphologies. *Wood Material Science & Engineering*. [Online] 15 (2), 104–113. Available from: doi:10.1080/17480272.2018.1496359.

Philip, M. & Al-Azzawi, F. (2018) Effects of Natural and Artificial Weathering on the Physical Properties of Recycled Poly(ethylene terephthalate). *Journal of Polymers and the Environment*. [Online] 26 (8), 3139–3148. Available from: doi:10.1007/s10924-018-1191-x.

Potthoff, A., Oelschlägel, K., Schmitt-Jansen, M., Rummel, C.D., et al. (2017) From the sea to the laboratory: Characterization of microplastic as prerequisite for the assessment of ecotoxicological impact: Impact Assessment of Microplastics. *Integrated Environmental Assessment and Management*. [Online] 13 (3), 500–504. Available from: doi:10.1002/ieam.1902.

Q-LAB (2020) *QUV ACCELERATED WEATHERING TESTER*. [Online]. 2020. Q-LAB. Available from: https://www.q-lab.com/products/quv-weathering-tester/quv [Accessed: 11 September 2020].

Quill, J. & Fowler, S. (n.d.) *The essentials of laboratory weathering*. [Online]. Available from: http://www.pstc.org/files/public/Quill_Jeffrey.pdf.

Rajakumar, K., Sarasvathy, V., Thamarai Chelvan, A., Chitra, R., et al. (2009) Natural Weathering Studies of Polypropylene. *Journal of Polymers and the Environment*. [Online] 17 (3), 191–202. Available from: doi:10.1007/s10924-009-0138-7.

Rani, M., Shim, W.J., Jang, M., Han, G.M., et al. (2017) Releasing of hexabromocyclododecanes from expanded polystyrenes in seawater -field and laboratory experiments. *Chemosphere*. [Online] 185, 798–805. Available from: doi:10.1016/j.chemosphere.2017.07.042.

Renner, G., Schmidt, T.C. & Schram, J. (2017) A New Chemometric Approach for Automatic Identification of Microplastics from Environmental Compartments Based on FT-IR Spectroscopy. *Analytical Chemistry*. [Online] 89 (22), 12045–12053. Available from: doi:10.1021/acs.analchem.7b02472.

Richaud, E., Farcas, F., Bartoloméo, P., Fayolle, B., et al. (2006) Effect of oxygen pressure on the oxidation kinetics of unstabilised polypropylene. *Polymer Degradation and Stability*. [Online] 91 (2), 398–405. Available from: doi:10.1016/j.polymdegradstab.2005.04.043.

Romera-Castillo, C., Pinto, M., Langer, T.M., Álvarez-Salgado, X.A., et al. (2018) Dissolved organic carbon leaching from plastics stimulates microbial activity in the ocean. *Nature Communications*. [Online] 9 (1), 1430. Available from: doi:10.1038/s41467-018-03798-5.

Rouillon, C., Bussiere, P.-O., Desnoux, E., Collin, S., et al. (2016) Is carbonyl index a quantitative probe to monitor polypropylene photodegradation? *Polymer Degradation and Stability*. [Online] 128, 200–208. Available from: doi:10.1016/j.polymdegradstab.2015.12.011.

Rummel, C.D., Escher, B.I., Sandblom, O., Plassmann, M.M., et al. (2019) Effects of Leachates from UV-Weathered Microplastic in Cell-Based Bioassays. *Environmental Science & Technology*. [Online] Available from: doi:10.1021/acs.est.9b02400.

Sangeetha Devi, R., Rajesh Kannan, V., Nivas, D., Kannan, K., et al. (2015) Biodegradation of HDPE by Aspergillus spp. from marine ecosystem of Gulf of Mannar, India. *Marine Pollution Bulletin*. [Online] 96 (1–2), 32–40. Available from: doi:10.1016/j.marpolbul.2015.05.050.

Satoto, R., Subowo, W.S., Yusiasih, R., Takane, Y., et al. (1997) Weathering of high-density polyethylene in different latitudes. *Polymer Degradation and Stability*. [Online] 56 (3), 275–279. Available from: doi:10.1016/S0141-3910(96)00213-3.

Shah, A.A., Hasan, F., Hameed, A. & Ahmed, S. (2008) Biological degradation of plastics: A comprehensive review. *Biotechnology Advances*. [Online] 26 (3), 246–265. Available from: doi:10.1016/j.biotechadv.2007.12.005.

Shang, J., Chai, M. & Zhu, Y. (2003) Solid-phase photocatalytic degradation of polystyrene plastic with TiO2 as photocatalyst. *Journal of Solid State Chemistry*. [Online] 174 (1), 104–110. Available from: doi:10.1016/S0022-4596(03)00183-X.

Shim, W.J., Hong, S.H. & Eo, S.E. (2017) Identification methods in microplastic analysis: a review. *Analytical Methods*. [Online] 9 (9), 1384–1391. Available from: doi:10.1039/C6AY02558G.

Silverstein, R.M., Bassler, G.C. & Morrill, T.C. (1992) Spectrometric identification of organic compounds. *Magnetic Resonance in Chemistry*. [Online] 30 (4), 364–364. Available from: doi:10.1002/mrc.1260300417.

Song, Y.K., Hong, S.H., Jang, M., Han, G.M., et al. (2017) Combined Effects of UV Exposure Duration and Mechanical Abrasion on Microplastic Fragmentation by Polymer Type. *Environmental Science & Technology*. [Online] 51 (8), 4368–4376. Available from: doi:10.1021/acs.est.6b06155.

Tang, P.L., McCumskay, R., Rogerson, M., Waller, C., et al. (2019) Handheld FT-IR Spectroscopy for the Triage of Micro- and Meso-Sized Plastics in the Marine Environment Incorporating an Accelerated Weathering Study and an Aging Estimation. *Spectroscopy*. 34 (2), 54–60.

Thiele, C.J., Hudson, M.D. & Russell, A.E. (2019) Evaluation of existing methods to extract microplastics from bivalve tissue: Adapted KOH digestion protocol improves filtration at single-digit pore size. *Marine Pollution Bulletin*. [Online] 142, 384–393. Available from: doi:10.1016/j.marpolbul.2019.03.003.

Tian, L., Chen, Q., Jiang, W., Wang, L., et al. (2019) A carbon-14 radiotracer-based study on the phototransformation of polystyrene nanoplastics in water *versus* in air. *Environmental Science: Nano*. [Online] 6 (9), 2907–2917. Available from: doi:10.1039/C9EN00662A.

Tu, C., Chen, T., Zhou, Q., Liu, Y., et al. (2020) Biofilm formation and its influences on the properties of microplastics as affected by exposure time and depth in the seawater. *Science of The Total Environment*. [Online] 734, 139237. Available from: doi:10.1016/j.scitotenv.2020.139237.

Turner, A., Arnold, R. & Williams, T. (2020) Weathering and persistence of plastic in the marine environment: Lessons from LEGO. *Environmental Pollution*. [Online] 262, 114299. Available from: doi:10.1016/j.envpol.2020.114299.

Urbanek, A.K., Rymowicz, W. & Mirończuk, A.M. (2018) Degradation of plastics and plastic-degrading bacteria in cold marine habitats. *Applied Microbiology and Biotechnology*. [Online] 102 (18), 7669–7678. Available from: doi:10.1007/s00253-018-9195-y.

Valadez-Gonzalez, A., Cervantes-Uc, J.M. & Veleva, L. (1999) Mineral ®ller in¯uence on the photo-oxidation of high density polyethylene: I. Accelerated UV chamber exposure test. *Polymer Degradation and Stability*. 8.

Vaskuri, A., Kärhä, P., Heikkilä, A. & Ikonen, E. (2017) *Facility for determining action spectra of UV photodegradation*. In: [Online]. 2017 Auckland, New Zealand. p. 110011. Available from: doi:10.1063/1.4975573 [Accessed: 1 June 2020].

Vincent, T.A., Urasinska-Wojcik, B. & Gardner, J.W. (2015) Development of a Low-cost NDIR System for ppm Detection of Carbon Dioxide in Exhaled Breath Analysis. *Procedia Engineering*. [Online] 120, 388–391. Available from: doi:10.1016/j.proeng.2015.08.648.

Waldman, W.R. & De Paoli, M.-A. (2008) Photodegradation of polypropylene/polystyrene blends: Styrene–butadiene–styrene compatibilisation effect. *Polymer Degradation and Stability*. [Online] 93 (1), 273–280. Available from: doi:10.1016/j.polymdegradstab.2007.09.003.

Wang, F., Yang, W., Cheng, P., Zhang, S., et al. (2019) Adsorption characteristics of cadmium onto microplastics from aqueous solutions. *Chemosphere*. [Online] 235, 1073–1080. Available from: doi:10.1016/j.chemosphere.2019.06.196.

Wang, W., Ge, J., Yu, X. & Li, H. (2020) Environmental fate and impacts of microplastics in soil ecosystems: Progress and perspective. *Science of The Total Environment*. [Online] 708, 134841. Available from: doi:10.1016/j.scitotenv.2019.134841.

Wang, Z., Chen, M., Zhang, L., Wang, K., et al. (2018) Sorption behaviours of phenanthrene on the microplastics identified in a mariculture farm in Xiangshan Bay, southeastern China. *Science of The Total Environment*. [Online] 628–629, 1617–1626. Available from: doi:10.1016/j.scitotenv.2018.02.146.

Ward, C.P., Armstrong, C.J., Walsh, A.N., Jackson, J.H., et al. (2019) Sunlight Converts Polystyrene to Carbon Dioxide and Dissolved Organic Carbon. *Environmental Science & Technology Letters*. [Online] 6 (11), 669–674. Available from: doi:10.1021/acs.estlett.9b00532.

Welden, N.A. & Cowie, P.R. (2017) Degradation of common polymer ropes in a sublittoral marine environment. *Marine Pollution Bulletin*. [Online] 118 (1–2), 248–253. Available from: doi:10.1016/j.marpolbul.2017.02.072.

Wong, C.S., Green, D.R. & Cretney, W.J. (1974) Quantitative Tar and Plastic Waste Distributions in the Pacific Ocean. *Nature*. [Online] 247 (5435), 30–32. Available from: doi:10.1038/247030a0.

Wong, J.K.H., Lee, K.K., Tang, K.H.D. & Yap, P.-S. (2020) Microplastics in the freshwater and terrestrial environments: Prevalence, fates, impacts and sustainable solutions. *Science of The Total Environment*. [Online] 719, 137512. Available from: doi:10.1016/j.scitotenv.2020.137512.

Xu, X., Wong, C.Y., Tam, N.F.Y., Lo, H.-S., et al. (2020) Microplastics in invertebrates on soft shores in Hong Kong: Influence of habitat, taxa and feeding mode. *Science of The Total Environment*. [Online] 715, 136999. Available from: doi:10.1016/j.scitotenv.2020.136999.

Yamano, N., Kawasaki, N., Ida, S. & Nakayama, A. (2019) Biodegradation of polyamide 4 in seawater. *Polymer Degradation and Stability*. [Online] 166, 230–236. Available from: doi:10.1016/j.polymdegradstab.2019.05.032.

Yang, X., Jiang, X., Hu, J., Wang, F., et al. (2017) Relationship between physical and mechanical properties of accelerated weathering and outdoor weathering of PVC-coated membrane material under tensile stress. *Journal of Industrial Textiles*. [Online] 47 (2), 197–210. Available from: doi:10.1177/1528083716639062.

Yang, Z., Yin, T., Zhang, F., Wu, W., et al. (2020) Investigation on dispersion properties of CO2 and ester solvent mixtures using in situ FTIR spectroscopy. *RSC Advances*. [Online] 10 (31), 18192–18199. Available from: doi:10.1039/D0RA00326C.

Yin, W., Wang, Y., Liu, L. & He, J. (2019) Biofilms: The Microbial “Protective Clothing” in Extreme Environments. *International Journal of Molecular Sciences*. [Online] 20 (14), 3423. Available from: doi:10.3390/ijms20143423.

Zada, L., Leslie, H.A., Vethaak, A.D., Tinnevelt, G.H., et al. (2018) Fast microplastics identification with stimulated Raman scattering microscopy. *Journal of Raman Spectroscopy*. [Online] 49 (7), 1136–1144. Available from: doi:10.1002/jrs.5367.

Zettler, E.R., Mincer, T., Proskurowski, G. & Amaral-Zettler, L.A. (2011) *The 'plastisphere': a new and expanding habitat for marine protists*. In: September 2011 WILEY-BLACKWELL. pp. S45-S45 Supliment: 2 Special Issue: SI.

Zettler, E.R., Mincer, T.J. & Amaral-Zettler, L.A. (2013) Life in the "Plastisphere": Microbial Communities on Plastic Marine Debris. *Environmental Science & Technology*. [Online] 47 (13), 7137–7146. Available from: doi:10.1021/es401288x.

Zhu, L., Zhao, S., Bittar, T.B., Stubbins, A., et al. (2020) Photochemical dissolution of buoyant microplastics to dissolved organic carbon: Rates and microbial impacts. *Journal of Hazardous Materials*. [Online] 383, 121065. Available from: doi:10.1016/j.jhazmat.2019.121065.

Appendix 1

```
int in1 = 6;
int lvl = 9;
int in2 = 10;
int jam = 0;
unsigned long pre_time,cur_time = 0;
#include <LiquidCrystal.h>
LiquidCrystal lcd(12, 11, 5, 4, 3, 2);

void setup() {
  pinMode(in1, OUTPUT); /*Activates the raley that controles the Power to extention*/
  pinMode(in2, OUTPUT); /*Activates the raley that controles the ATO (Auto top Off)*/
  pinMode(lvl, INPUT);  /*Float switch in the weathering tank*/
  digitalWrite(in1, LOW); /*This turns Relay 1 on and powers the pump*/
  digitalWrite(in2, HIGH); /*This turns the ATO off*/
  lcd.begin(16, 2); // set up the LCD's number of columns and rows:
  lcd.print("Start-up...     "); // Print a message to the LCD.
  delay(500);

}

void loop()
{

if(digitalRead(lvl)== HIGH)/*When the water in the tank is HIGH it...*/
{
 digitalWrite(in1,HIGH);/*Turns rely 1 stopping the pump*/
 delay(100);

   jam=(cur_time/1000);
   lcd.setCursor(0, 1);
   lcd.print("                ");
   lcd.setCursor(0, 0);
   lcd.print("Pump Off        ");
   delay(2000);

    for(int i = 15; i >= 1; i--){

      lcd.setCursor(0, 0);
      lcd.print("Timer           ");
      lcd.setCursor(0, 1);
      lcd.print(i);
      lcd.println(" mins          ");
      delay(60000);
    }
```

```
 digitalWrite(in2,LOW); /*After empty the ATO can measure the water level and Top up if
        require. im expecting some evaporation of water and salinity must remain constant*/
 delay(100);

  lcd.setCursor(0, 0);
  lcd.print("Auto Top Off On");
  delay(1000);
  lcd.setCursor(0, 1);
  lcd.print("Timer Started...");
  delay(5000);

    for(int j = 54; j >= 1; j--){

      lcd.setCursor(0, 0);
      lcd.print("               ");
      lcd.setCursor(0, 1);
      lcd.print("               ");
      lcd.setCursor(0, 0);
      lcd.print("ATO Timer");
      lcd.setCursor(0, 1);
      lcd.print(j);
      delay(1000);

        if(j==1){
            lcd.setCursor(0, 1);
            lcd.print("Off");
            pre_time=millis();
        }
    }
}
else{

cur_time=millis()-pre_time;
  delay(100);
  digitalWrite(in1, LOW);   /*restarts the pump by opening relay 1*/
  digitalWrite(in2, HIGH);  /*stops the ATO by closiing relay 2*/
  delay(1000);

  lcd.setCursor(0, 0);
  lcd.print("               ");
  lcd.setCursor(0, 1);
  lcd.print("               ");
  lcd.setCursor(0, 0);
  lcd.print("Pumping Water ");
  lcd.setCursor(0, 1);
  lcd.print("               ");
  lcd.setCursor(0, 1);
  lcd.print(cur_time/1000);
  lcd.println(" =             ");
  lcd.setCursor(7, 1);
```

```
  lcd.println(jam);
  }
}
```